# MODELLING OF THE BINARY ALLOY SOLIDIFICATION PROCESS

by

**R L McAdie**

BSc (Eng), MSc (Eng), *Cape Town*, MSME, *Stanford*

A thesis submitted for the degree of Doctor of Philosophy in the Faculty of Engineering.

Department of Civil Engineering
University of Cape Town
Republic of South Africa

April 1992

# ABSTRACT

A thermodynamically consistent model capable of modelling a binary alloy undergoing solidification or melting is developed. The theory is continuum based, and the solid-liquid phase change system is described macroscopically by a single set of conservation equations. The model is an extension of that presented in the literature. The thermodynamic theories of this type in the current literature are based on the assumption of local equilibrium. This assumption is not representative of most alloy solidification processes where the solid-liquid phase region, termed the mushy region, is of dendritic nature with the rates of diffusion in the liquid being orders of magnitude faster than that in the solid. The propose model includes the assumption of local non-equilibrium where solute diffusion in the solid phase is assumed to be zero.

The thermodynamic formulation is expressed in terms of three thermodynamic variables: pressure, temperature and average solute concentration for both the equilbrium and non-equilbrium case. A generalized set of conservation equations of mass, energy, momentum and solute with the necessary constitutive equations is presented.

A Finite Element (FE) formulation of a simplified form of the governing equations is developed. The reduced set of equations implemented in the FE formulation consists of a fully coupled heat conduction and solute diffusion formulation, with solid-liquid phase change, where the effects of pressure and convection are neglected. The FE formulation is based on the fixed grid technique where the elements are two dimensional, four noded quadrilaterals with the primary variables being enthalpy and average solute concentration. Temperature and solid mass fraction are calculated on a local level at each integration point of an element.

A fully consistent Newton-Raphson method is used to solve the global coupled equations and an Euler backward difference scheme is used for the temporal discretization. The solution of the enthalpy-temperature relationship is carried out at the integration points using a Newton-Raphson method. A secant method employing the *regula falsi* technique takes into account sudden jumps or sharp changes in the enthalpy- temperature behaviour which occur at the phase zone interfaces. The Euler backward difference integration rule is used to calculate the solid mass fraction and its derivatives for the non-equilibrium case.

Two solidification examples, using both the local equilibrium and the local non-equilibrium cases, are analyzed. The finite element results obtained for the two cases are compared, and the accuracy of the finite element model is checked. Both dendritic and eutectic phase change are tackled. Even though the discrete eutectic phase change is approximated using the fixed grid approach, the results are considered to be reasonable approximations to what occurs in reality. Favorable comparisons of the results are obtained with that in the literature and convergence of the finite element results for different mesh sizes are shown. For dilute alloy solutions, the solidification results for the local equilibrium and the local non-equilibrium cases are shown to differ markedly, whereas for near eutectic solutions little difference is observed. The use of the local non-equilibrium assumption in the finite element solidification model is shown to effect the macro-segregation of solute.

# DECLARATION

I, Robert Leon McAdie, declare that this thesis is essentially my own work and that it has not been submitted for a degree at any other university.

Signed by candidate

R L McAdie

April 1992.

# DEDICATION

I would like to dedicate this thesis to my mother (1937-1989) who has been my inspiration and guide throughout my life.

# ACKNOWLEDGMENTS

I would express my gratitude to the following:

My supervisor, Professor J B Martin, for his encouragement, guidance and support during my postgraduate studies.

The Foundation for Research and Development and the Division for Material Science and Technology of the Council for Scientific and Industrial Research for their financial support.

Collin Mercer and Greg Mitchell for the many helpful comments and discussions.

Sidney Allen and Ewan Sellers for their assistance in proof reading the text.

To my family and friends for all their encouragement and support.

# TABLE OF CONTENTS


1 INTRODUCTION 1

2 THERMODYNAMIC DESCRIPTION OF LOCAL EFFECTS 4
2.1 Introduction . . . . . 4
2.1.1 Preliminaries . . . . . 7
2.2 Local equilibrium . . . . . 9
2.2.1 Free energy description . . . . . 10
2.2.2 Evaluation of thermodynamic coefficients . . . . . 14
2.3 Local non-equilibrium . . . . . 21
2.3.1 Free energy description . . . . . 24
2.3.2 Evaluation of thermodynamic coefficients . . . . . 27
2.4 Metallurgical examples . . . . . 30
2.4.1 Solidification of an Ag-Cu alloy . . . . . 31
2.4.2 Solidification of an Al-Si alloy . . . . . 37
2.5 Conclusions . . . . . 43

3 GOVERNING GLOBAL CONSERVATION EQUATIONS 46
3.1 Introduction . . . . . 46
3.2 Conservation of mass . . . . . 48
3.3 Conservation of solute . . . . . 49
3.4 Conservation of momentum . . . . . 51
3.5 Conservation of energy . . . . . 54
3.6 Entropy inequality . . . . . 54
3.7 Constitutive laws . . . . . 56
3.8 Evaluation of fluxes and expanded generalized conservation equations . . . . . 57
3.8.1 Conservation of energy . . . . . 59
3.8.2 Conservation of momentum . . . . . 59
3.8.3 Conservation of mass . . . . . 60
3.8.4 Conservation of solute . . . . . 60
3.9 Practical simplifying assumptions . . . . . 60
3.9.1 Conservation of mass . . . . . 61
3.9.2 Conservation of energy . . . . . 61
3.9.3 Conservation of solute . . . . . 62
3.9.4 Conservation of momentum . . . . . 63

3.10 Conclusions . . . . . 65

4 THE NUMERICAL MODEL 66
4.1 Introduction . . . . . 66
4.2 Finite element formulation . . . . . 69
4.3 Strong form of the initial boundary-value problem . . . . . 70
4.3.1 Problem domain . . . . . 70
4.3.2 Material Properties . . . . . 72
4.3.3 Boundary and initial conditions . . . . . 74
4.3.4 The Strong Form . . . . . 76
4.4 Weighted residual form of the initial boundary-value problem . . . . . 78
4.4.1 Solution and Variational Spaces . . . . . 78
4.4.2 The Weak Form . . . . . 79
4.5 Galerkin approximation of the initial boundary-value problem . . . . . 81
4.5.1 Galerkin spaces of approximation . . . . . 81
4.5.2 The Galerkin Form . . . . . 82
4.6 Finite element matrix approximation of the initial boundary-value problem . . . . 82
4.6.1 Spatial Discretization . . . . . 83
4.6.2 Approximation Spaces . . . . . 83
4.6.3 The Finite Element Matrix Form . . . . . 84
4.7 Temporal Algorithm . . . . . 88
4.7.1 Temporal Discretization . . . . . 88
4.7.2 Generalized Trapezoidal rule . . . . . 89
4.8 Nonlinear Solution Scheme . . . . . 90
4.8.1 Newton-Raphson Iteration Scheme . . . . . 90
4.8.2 Evaluation of the Jacobian Operator . . . . . 92
4.9 Predictor-Corrector Algorithm . . . . . 103
4.10 Numerical evaluation of the finite element equations . . . . . 105
4.11 Solution of state variables . . . . . 106
4.11.1 Predictor-corrector algorithm . . . . . 108
4.12 Conclusions . . . . . 112

5 NUMERICAL RESULTS AND DISCUSSION 114
5.1 Introduction . . . . . 114
5.2 Problem Description . . . . . 114
5.3 Results : Example I . . . . . 116
5.4 Results : Example II . . . . . 121
5.5 Conclusions . . . . . 122

6 CONCLUSION 127

# NOMENCLATURE

This is a list of symbols used in the main text of this thesis.

### Bold Uppercase symbols

| | |
|---|---|
| $\boldsymbol{A}$ | a (n × n) matrix |
| $\mathbf{D}$ | the deformation tensor |
| $\boldsymbol{D}$ | the solute diffusivity tensor |
| $\boldsymbol{D_h r}$ | the partial derivative of the residual $\boldsymbol{r}$ with respect to $\boldsymbol{h}$ |
| $\boldsymbol{D_c r}$ | the partial derivative of the residual $\boldsymbol{r}$ with respect to $\boldsymbol{c}$ |
| $\mathbf{F}$ | the body force vector |
| $\boldsymbol{F_C}$ | the finite element solute flux vector |
| $\boldsymbol{F_H}$ | the finite element heat flux vector |
| $\mathbf{I}$ | the identity matrix |
| $\mathbf{J}$ | the phase solute diffusion flux vector |
| $\boldsymbol{K_H}$ | the conductivity matrix |
| $\hat{\boldsymbol{K}}$ | the finite element reduced form of $\boldsymbol{K}$ |
| $\bar{\mathbf{K}}$ | the permeability tensor |
| $\boldsymbol{M}$ | the finite element mass matrix |
| $\boldsymbol{N_C}$ | the finite element solute diffusive flux vector |

### Uppercase symbols

| | |
|---|---|
| $C$ | the solute mass concentration |
| $\bar{C}$ | the average solute mass concentration |
| $\tilde{C}$ | the partial solute mass concentration |
| $\hat{C}$ | a dummy solute mass concentration |
| $C_*^S$ | the solid interface solute mass concentration |
| $C_P$ | the specific heat capacity |
| $C_{P_0}$ | the lever rule specific heat capacity contribution |
| $H$ | the enthalpy |
| $\tilde{H}$ | the predictor enthalpy |
| $L$ | the latent heat of fusion |
| $M$ | the mass |
| $N_a$ | a linear independent function of a shape function |
| $N_{EQ}$ | total number of equations |
| $N_{el}$ | total number of elements |
| $N_{np}$ | total number of nodal points |
| $N_{sd}$ | total number of space dimensions |
| $N_{STEP}$ | total number of time steps |
| P | the pressure |

# CHAPTER 1
# INTRODUCTION

Solidification or melting of binary alloys occurs over a varying temperature range exhibiting a two-phase zone, called the mushy region. The mushy region separates the pure solid and liquid regions of the domain with a solid-liquid zone consisting of dendritic crystals, which are either in the form of a dense matrix of columnar crystals or equiaxed crystals suspended in the liquid or both. The size, shape and spacing of the dendrite crystals, the concentrations of the alloy solute in and around the crystals, and inclusions between them, such as voids, effect the mechanical behaviour and microstructural soundness of the final solidified component.

These microscopic effects, which occur in the mushy region, are affected by the cooling rate and the temperature gradients, which in turn are affected by local (microscopic) and global (macroscopic) variations of solute. Variations in the solute, at a local level, result from solute being rejected from the solidifying dendrites due to poor solid solubility, and the excess solute being redistributed by diffusion into the liquid. Due to the fact that the temperature and solute concentration are coupled, the variation in liquid solute around the dendrites will effect the growth characteristics of the dendrites and resultant grain structure of the solid. These local variations in solute also set up interdendritic flow patterns which transport the solute rich, or depleted, liquid around the mushy region and in some cases out of the mushy region, where, in the pure fluid, the solute is convected away from the mushy region by thermal induced convection currents. This results in a macroscopic segregation of the alloy constituents which, as with grain structure variations, greatly influences the quality of final solidified product.

It is therefore clear that to model the solidification of a binary alloy, the relationship between it and temperature has to be a function of the local solute content. This thesis shall be concerned with developing local models to accurately simulate the effect of local solute redistribution on the solidification/melting process.

In most of the current literature [1-4] it assumed that on a local level both the liquid and the solid are assumed to be in thermodynamic equilibrium. This assumption is true for the case of solidification of small particles, where thermal and constitutional (chemical) equilibrium is established, in both phases, within the solidification time frame. In this thesis, this case is termed the local equilibrium case. When the particles are much larger the assumption of local thermodynamic equilibrium is not necessarily true; the reason being that the diffusion in the solid is orders of magnitude slower than in the liquid. Therefore when the solid particles are large, thermal phase equilibrium is established but the solid solute cannot attain constitutional equilibrium with the liquid within the solidification time. In this thesis, this case is termed the local non-equilibrium case. Models which assume local equilibrium throughout the dendritic region are therefore inaccurate and may incorrectly describe macroscopic solidification.

In this thesis, the phase change kinetics are described for both local equilibrium and local non-

equilibrium cases using a thermodynamic formulation expressed in terms of the Gibb's free energy of the system.

In order to model solidification macroscopically, and therefore to observe what global effect the local assumptions have on the phase change process, a set of conservation equations describing the transport of energy, mass, momentum and solute, in both the solid and liquid phases, has to be established.

Ideally, two sets of conservation equations have to be established for each phase, with appropriate boundary conditions at the phase interface to couple them. Methods which adopt this approach are often referred to as multiple region or multiple domain methods and are primarily used for discrete phase change problems (ie. solidification of pure or eutectic substances); [5-8]. The primary difficulty associated with the numerical implementation of the multiple domain method centers on tracking the phase interface, which is an unknown function of space and time. Therefore geometric regularity of the phase interface is imperative to ease the computational complexity.

In the mushy region dendrites grow naturally with a very large specific surface area and with dendrite arm spacings of the order of $10\mu m$. The specific nature of the dendrite formation in the mushy region is extremely complex, exhibiting preferred growth mechanisms and selective directionality that can depend on local temperatures and constituent concentrations or gradients thereof. In a macroscopic sense, such growth makes the liquid-solid interface highly irregular and virtually impossible to solve. Consequently the multiple domain method is impractical for the modelling of binary or multiconstituent solidification.

With the aid of classical mixture theory [2, 9-15] a single set of conservation equations can be developed which govern the solid, liquid and mushy region as a whole. The mushy region is not considered as a combination of distinct solid and liquid regions, but as a phase mixture of solid and liquid. This results in a continuum formulation where the mushy region is treated as a continuous transition between the solid and liquid phases.

A generalized description of the continuum conservation equations, taking into account the models for both local equilibrium and local non-equilibrium cases, is developed in this thesis. A constitutive law governing fluxes in the mushy region is also presented. The description follows closely that of Hills, Loper and Roberts [4] and Bennon and Incropera [1], the exception being the inclusion of the local non-equilibrium effects.

The continuum formulation lends itself to fixed numerical grid formulation unlike the multidomain formulation where moving numerical grids and/or coordinate mapping procedures are used to keep track of the moving phase change interface. In fixed grid formulations, the phase interfaces (ie. solid-mushy and mushy-liquid) are implicit and the positions of the phase interfaces are subsequently obtained from the resultant temperature fields.

In this thesis a fixed grid finite element formulation is used to solve the solidification problem. Due to the increased computational effort, convection is not included in the formulation. It is realized that convection plays a significant role in the process and therefore this numerical model is only a first step in the modelling process. The prime objective in developing this finite element

model is to observe whether the difference in the local equilibrium and local non-equilibrium descriptions significantly effect the global interpretation of the solidification process. The second objective is to develop a finite element model that is capable of modelling the full spectrum of diffusion dominated binary alloy solidification problems which include both continuous dendritic and discrete eutectic phase change.

The finite element formulation is expressed in terms of a set of coupled equations describing conservation of energy and solute for each element. The formulation is structured so that the field variables are enthalpy and solute concentration. Enthalpy is chosen as a field variable, instead of temperature, as this approach has several advantages. First, because the temperature-enthalpy relationship experiences no singularities, numerical difficulties resulting from abrupt variations of the heat capacity at the phase interfaces are eliminated. Second, energy conservation is ensured using the enthalpy approach, and third, any solidification is characterized by a strictly decreasing enthalpy.

The local phase change kinetics and temperature are calculated at the numerical integration points of each element, from the element enthalpy and solute fields. This model is implemented as a user element in a finite element code ABAQUS [16]. The global equations are solved using a fully consistent Newton Raphson method. The local temperature-enthalpy relationship, which includes jumps and sharp changes in slope due to phase transition, is solved using the Newton Raphson method together with a secant method employing the *regula falsi* technique.

The organization of this thesis is as follows: In Chapter 2, a thermodynamic formulation, expressed in terms of Gibb's free energy, is used to described phase change kinetics for both local equilibrium and local non-equilibrium cases. For both local equilibrium and local non-equilibrium cases, two metallurgical examples, describing local phase change, are chosen to illustrate the variations in free energy and thermodynamic coefficients of a binary alloy, at fixed solute concentration. In Chapter 3, the global continuum conservation equations of the phase change system are presented together with a constitutive law for the fluxes present in the phase change mixture. The equations are initially expressed in general format and then simplified using some practical metallurgical assumptions. The finite element implementation and solution procedures of the diffusion dominated solidification problem is given in Chapter 4. Two solidification examples, which include both dendritic and eutectic solidification, are analyzed in Chapter 5. The finite element results obtained from both local equilibrium, and local non-equilibrium cases are compared, and the accuracy of the finite element model is checked.

# CHAPTER 2
# THERMODYNAMIC DESCRIPTION OF LOCAL EFFECTS

## 2.1 Introduction

Binary alloy solidification is characterized by combination of discrete and non-discrete phase changes which take place over a region of varying temperature, pressure and solute concentration. This region, usually know as the mushy region, consists of a mixture of solid and liquid which varies in structure depending on the type of material and parameters such as temperature and pressure. The structure of this region can take on two forms; a zone of small equiaxed particles ( i.e. a slurry or to a lesser extent the equiaxed zone of a metal casting) or a matrix of solid crystals (i.e. the dendritic zone of a metal casting). For the former, the solid phase is in the form of fine particles in suspension which move around due to changing buoyancy forces. As they move they will either melt or accrete new material depending on the environment. For the latter, the dendritic region consists of solid growing as a porous matrix of crystals through which the liquid percolates. See Figure 2.1.

To model the evolution of the mushy region the global behaviour, such as heat transfer, diffusion of alloy constituents, pressure variations and fluid flow, has to be coupled into a model describing the local structure of the mushy region (ie. dendritic or equiaxed structure) and its growth. The local behaviour will affect what happens globally and vice versa. It is therefore important to develop an accurate description of the local structure and its growth as this will greatly influence the global evolution of the mushy region. In this chapter, therefore, the evolution of the local structure of the mushy region is described where the scale of the local description is in the order of the size of the sample volume element depicted in Figure 2.1.

On a scale of the order of the volume element depicted in Figure 2.1, the phase change process can be divided into an equilibrium phase change, or a non-equilibrium phase change. For the equilibrium phase change process the diffusion rates in both the solid and liquid phases are so rapid that the solute concentrations reach uniform equilibrium values within the time frame of the phase change process. This assumption is applicable to slurries and to a limited extent to the equiaxed region of a cast where the solid grains are so small that all diffusion processes are effectively instantaneous. In the non-equilibrium phase change process the liquid solute concentration reaches uniform equilibrium instantaneously, but by contrast, diffusion in the solid is so slow as to be effectively negligible. Thus, within the time frame of phase change, the solid in the phase mixture may not be in chemical equilibrium with the surrounding fluid at the same temperature. As stated by Hills and Roberts [21] the final equilibrium state reached by an isolated system is then not the maximum entropy state of complete chemical and thermal equilibrium, but is one of quasi-equilibrium in which there are variations in solid solute concentration. Only over a very long time (ie. well after the total domain has solidified), will maximum entropy be reached. As only the solid liquid phase change process is of interest here

| | |
|---|---|
| $P_0$ | a constant reference pressure |
| $\bar{\mathrm{P}}$ | the partial pressure |
| Q | the entropy production |
| $Q_H$ | a volumetric heat source |
| $Q_C$ | a volumetric solute source |
| $S$ | the entropy |
| T | the temperature |
| U | the internal energy per unit mass |
| $V$ | the volume |

**Bold lowercase symbols**

| | |
|---|---|
| $\boldsymbol{b}$ | a (n × 1) vector |
| $\boldsymbol{b}_g$ | the gravitational acceleration vector |
| $\boldsymbol{c}$ | the finite element solute concentration vector |
| $\tilde{\boldsymbol{c}}$ | the finite element predictor solute concentration vector |
| $\mathbf{f}$ | the phase interaction flux vector |
| $\boldsymbol{f}_C$ | the finite element solute flux vector |
| $\boldsymbol{f}_H$ | the finite element heat flux vector |
| $\boldsymbol{h}$ | the finite element enthalpy vector |
| $\tilde{\boldsymbol{h}}$ | the finite element predictor enthalpy vector |
| $\mathbf{i}$ | the total solute diffusion flux vector |
| $\mathbf{i}'$ | the sum of the phase solute diffusion flux vectors |
| $\mathbf{j}$ | the diffusive flux vector representing particle diffusion in the mushy region |
| $\mathbf{k}$ | the entropy flux vector |
| $\boldsymbol{k}_H$ | the finite element conductivity matrix |
| $\boldsymbol{m}_H$ | the finite element mass matrix |
| $\mathbf{n}$ | a unit normal vector |
| $\boldsymbol{n}_C$ | the finite element solute diffusion flux vector |
| $\mathbf{q}$ | the heat flux vector |
| $\boldsymbol{r}$ | the global residual vector |
| $\mathbf{r}$ | position vector |
| $\mathbf{u}$ | the mass averaged velocity vector |
| $\mathbf{w}$ | the relative phase velocity vector |
| $\boldsymbol{x}$ | the position vector |

**Lowercase symbols**

| | |
|---|---|
| $c_a$ | a component of the finite element solute concentration vector |
| $d_A$, $\hat{d}_A$ | constants |
| $f^S$ | solid mass fraction coordinate |
| $\{f_C\}_a$ | a component of the finite element solute flux vector |
| $\{f_H\}_a$ | a component of the finite element heat flux vector |
| $\mathrm{g}$ | the volume fraction |

| | |
|---|---|
| $g$ | the essential boundary condition |
| $h$ | the natural boundary condition |
| $h_a$ | a component of the finite element enthalpy vector |
| $i$ | the iteration counter |
| $k$, $k'$ | the equilibrium partition ratios |
| $\{k_H\}_{ab}$ | a component of the finite element conductivity matrix |
| $k_P$ | the barodiffusion ratio |
| $k_T$ | the Soret thermal diffusion ratio |
| $m_{ab}$ | a component of the finite element mass matrix |
| $m^L$ | the slope of the thermal liquidus |
| $m^{L'}$ | the slope of the pressure liquidus |
| $\dot{m}$ | the mass creation rate |
| $n$ | the total number of time steps |
| $\{n_C\}_a$ | a component of the finite element solute diffusion vector |
| r | the heat source per unit mass |
| $r$ | local state variable residual |
| $\bar{s}$ | specific entropy |
| $t$ | time |
| $v$ | a trail function |
| $w_1$ | the variational enthalpy field |
| $w_2$ | the variational solute concentration field |
| $x$ | the $x$ axis coordinate |
| $y$ | the $y$ axis coordinate |

## Bold Greek symbols

| | |
|---|---|
| $\boldsymbol{\mathcal{K}}$ | the conductivity tensor |
| $\boldsymbol{\sigma}$ | the stress tensor |
| $\boldsymbol{\psi}$ | a flux vector |
| $\boldsymbol{\Phi}$ | the Gibbs free energy per unit mass |
| $\tilde{\boldsymbol{\Phi}}$ | the partial phase Gibbs free energy per unit mass |

## Greek symbols

| | |
|---|---|
| $\alpha$ | the generalized trapezoidal time integration parameter |
| $\alpha_t$ | the thermal expansion coefficient |
| $\alpha_{t_0}$ | the lever rule contribution to the thermal expansion coefficient |
| $\beta$ | the isothermal compression coefficient |
| $\beta_0$ | the lever rule contribution to the isothermal compression coefficient |
| $\gamma$ | a flux coefficient |
| $\tilde{\gamma}$ | the square of a typical channel radius of a dendrite pore |
| $\Gamma$ | denotes the boundary of the domain |
| $\delta$ | the volumetric expansion coefficient |
| $\Delta$ | the increment in |

| | |
|---|---|
| $\bar{\delta}$ | the specific volumetric expansion coefficient |
| $\epsilon$ | the emissivity |
| $\bar{\eta}$ | the set of nodal points contained in the domain |
| $\mu$ | the chemical potential |
| $\bar{\mu}$ | the specific chemical potential |
| $\nu$ | the liquid viscosity |
| $\bar{\xi}$ | the numerical integration coordinate |
| $\rho$ | the density |
| $\bar{\rho}$ | the partial density |
| $\rho^{-1}$ | the volume per unit mass |
| $\sigma$ | the Stefan Boltzman constant |
| $\tau$ | a scalar representing value of time or a dummy integration variable |
| $\phi$ | the solid mass fraction |
| $\psi$ | the phase energy difference |
| $\Omega$ | denotes the spatial domain |
| $\bar{\Omega}$ | denotes the closed spatial domain ie. domain including boundaries |

**Bold calligraphic symbols**

| | |
|---|---|
| $\boldsymbol{\mathcal{F}}_C$ | the linear volumetric solute flux form |
| $\boldsymbol{\mathcal{F}}_{CC}$ | Jacobian contribution - partial derivative of the solute flux vector w.r.t. $\boldsymbol{c}$ |
| $\boldsymbol{\mathcal{F}}_H$ | the linear volumetric heat flux form |
| $\boldsymbol{\mathcal{F}}_{HH}$ | Jacobian contribution - partial derivative of the heat flux vector w.r.t. $\boldsymbol{h}$ |
| $\boldsymbol{\mathcal{H}}_C$ | the linear natural boundary solute flux form |
| $\boldsymbol{\mathcal{H}}_H$ | the linear natural boundary heat flux form |
| $\boldsymbol{\mathcal{K}}_C$ | the bilinear solute diffusion form |
| $\boldsymbol{\mathcal{K}}_{CC}$ | Jacobian contribution - partial derivative of the solute diffusion matrix w.r.t. $\boldsymbol{c}$ |
| $\boldsymbol{\mathcal{K}}_{CCL}$ | Liquid contribution to $\boldsymbol{\mathcal{K}}_{CC}$ |
| $\boldsymbol{\mathcal{K}}_{CCM}$ | Mushy contribution to $\boldsymbol{\mathcal{K}}_{CC}$ |
| $\boldsymbol{\mathcal{K}}_{CH}$ | Jacobian contribution - partial derivative of the solute diffusion matrix w.r.t. $\boldsymbol{h}$ |
| $\boldsymbol{\mathcal{K}}_{CHL}$ | Liquid contribution to $\boldsymbol{\mathcal{K}}_{CH}$ |
| $\boldsymbol{\mathcal{K}}_{CHM}$ | Mushy contribution to $\boldsymbol{\mathcal{K}}_{CH}$ |
| $\boldsymbol{\mathcal{K}}_H$ | the bilinear conductivity form |
| $\boldsymbol{\mathcal{K}}_{HC}$ | Jacobian contribution - partial derivative of the conductivity matrix w.r.t. $\boldsymbol{c}$ |
| $\boldsymbol{\mathcal{K}}_{HH}$ | Jacobian contribution - partial derivative of the conductivity matrix w.r.t. $\boldsymbol{h}$ |
| $\hat{\boldsymbol{\mathcal{K}}}$ | the reduced form of $\boldsymbol{\mathcal{K}}$ |
| $\boldsymbol{\mathcal{M}}_C$ | the bilinear solute concentration rate form |
| $\boldsymbol{\mathcal{M}}_{CC}$ | Jacobian contribution - partial derivative of the solute rate matrix w.r.t. $\boldsymbol{c}$ |
| $\boldsymbol{\mathcal{M}}_H$ | the bilinear enthalpy rate form |
| $\boldsymbol{\mathcal{M}}_{HH}$ | Jacobian contribution - partial derivative of the enthalpy rate matrix w.r.t. $\boldsymbol{h}$ |

**Calligraphic symbols**

| | |
|---|---|
| $\{\mathcal{F}^e_{CC}\}_{ac}$ | a component of $\boldsymbol{\mathcal{F}}_{CC}$ |

| | |
|---|---|
| $\{\mathcal{F}_{HH}\}_{ac}$ | a component of $\mathcal{F}_{HH}$ |
| $\{\mathcal{K}_{CC}\}_{ac}$ | a component of $\mathcal{K}_{CC}$ |
| $\{\mathcal{K}_{CCL}\}_{ac}$ | a component of $\mathcal{K}_{CCL}$ |
| $\{\mathcal{K}_{CCM}\}_{ac}$ | a component of $\mathcal{K}_{CCM}$ |
| $\{\mathcal{K}_{CH}\}_{ac}$ | a component of $\mathcal{K}_{CH}$ |
| $\{\mathcal{K}_{CHL}\}_{ac}$ | a component of $\mathcal{K}_{CHL}$ |
| $\{\mathcal{K}_{CHM}\}_{ac}$ | a component of $\mathcal{K}_{CHM}$ |
| $\{\mathcal{K}_{HC}\}_{ac}$ | a component of $\mathcal{K}_{HC}$ |
| $\{\mathcal{K}_{HH}\}_{ac}$ | a component of $\mathcal{K}_{HH}$ |
| $\{\mathcal{M}_{CC}\}_{ac}$ | a component of $\mathcal{M}_{CC}$ |
| $\{\mathcal{M}_{HH}\}_{ac}$ | a component of $\mathcal{M}_{HH}$ |
| $\mathcal{S}$ | the solution space |
| $\mathcal{V}$ | the variational space |

**Subscripts**

| | |
|---|---|
| $C$ | solute concentration |
| $CL$ | solute concentration, liquid |
| $CS$ | solute concentration, solid |
| $CM$ | solute concentration, mushy |
| $conv$ | convection |
| $e$ | eutectic |
| $EUT$ | eutectic |
| $f_1$ | function 1 |
| $f_2$ | function 2 |
| $g$ | essential boundary condition |
| $h$ | natural boundary condition |
| $H$ | enthalpy |
| $HL$ | enthalpy, liquid |
| $HS$ | enthalpy, solid |
| $HM$ | enthalpy, mushy |
| $i$ | alloy constituent i |
| $LIQ$ | liquidus |
| $n$ | time step n |
| $Q_H$ | volumetric heat flux |
| $rad$ | radiation |
| $ref$ | reference value |
| 0 | initial |
| 1 | alloy constituent 1 |
| 2 | alloy constituent 2 |
| * | intrinsic to |

**Right Superscripts**

| | |
|---|---|
| $e$ | element |

| | |
|---|---|
| $h$ | Galerkin form |
| $i$ | global iteration counter |
| $L$ | liquid |
| $M$ | mushy |
| $NSYM$ | non-symmetric |
| $N_{SD}$ | number of space dimensions |
| $SYM$ | symmetric |
| $S$ | solid |
| $T$ | transpose of a matrix or vector |
| $\cdot$ , $\bullet$ | differential with respect to time |
| $+$ | positive definiteness |

**Left Superscripts**

| | |
|---|---|
| $k$ | local iteration counter |

**Special Symbols**

| | |
|---|---|
| $\partial$ | partial differentiation with respect to |
| d | differential |
| D | the material derivative |
| $\Re$ | the set of real numbers |
| $Sym$ | the set symmetric two-tensors |
| $\triangle\beta$ | interphase contribution to the isothermal compression coefficient |
| $\triangle\alpha_t$ | interphase contribution to the thermal expansion coefficient |
| $\triangle C_p$ | interphase contribution to the specific heat capacity coefficient |
| $\cup$ | the union of |
| $\subset$ | the subset of |
| $\cap$ | the intersection of |
| $\forall$ | for all |
| $\mathsf{A}$ | finite element assembly operator |
| $(\cdot\,,\cdot\,)$ | inner product |
| $\in$ | an element of |
| ] [ | open set |
| [ ] | closed set |
| \|\| \|\| | the absolute value of |
| $\{\ \}_{P,T}$ | a function or variable at a fixed value of P and T |
| $\{\ \}_{ab}$ | a component of a two tensor or matrix |
| $\{\ \}_a$ | a component of a vector |
| $O$ | of the order of |
| $\emptyset$ | the empty set |
| § | Section |
| $\bullet$ | dot product |
| : | contraction |

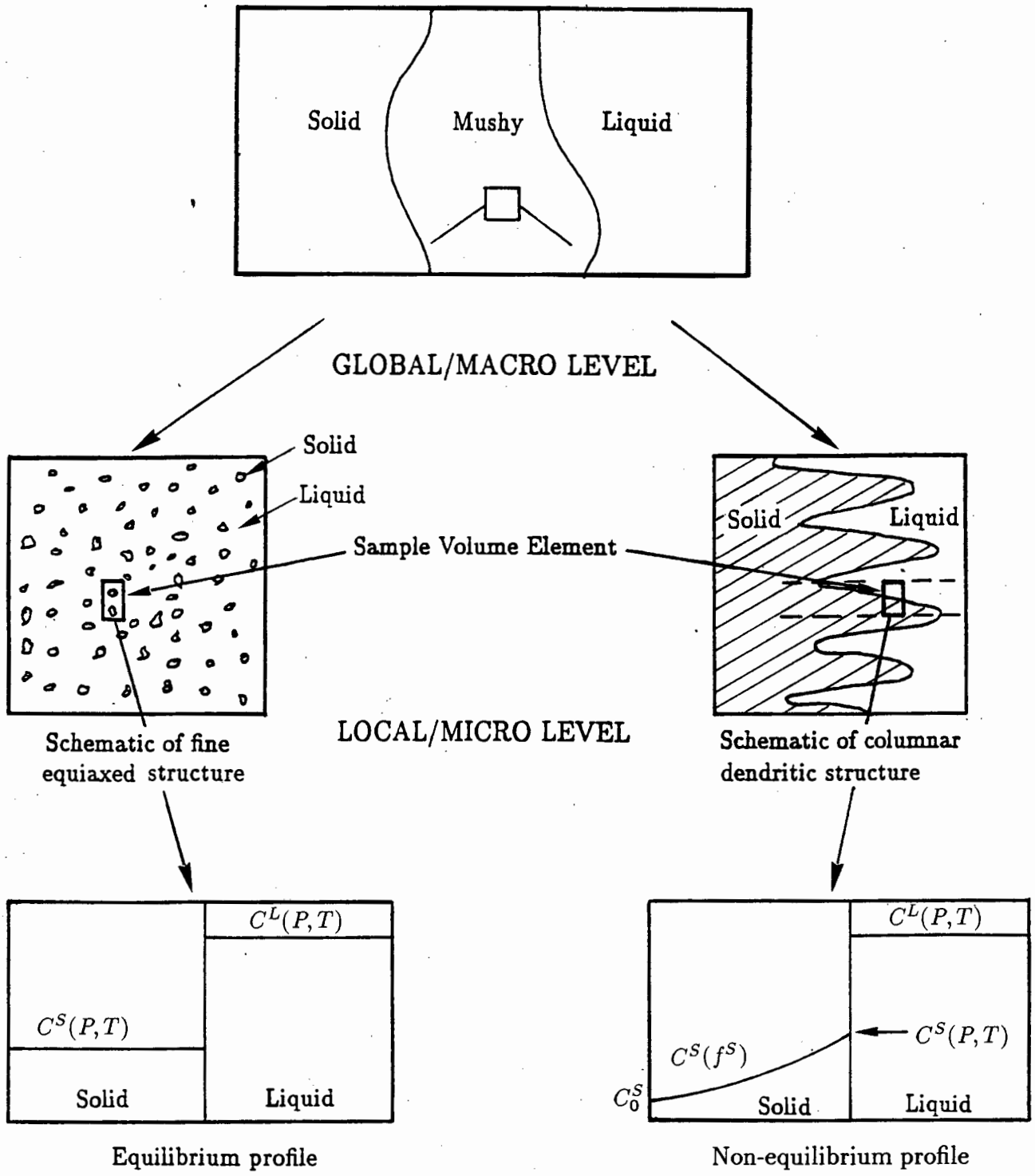


Figure 2.1: Local description of the mushy region

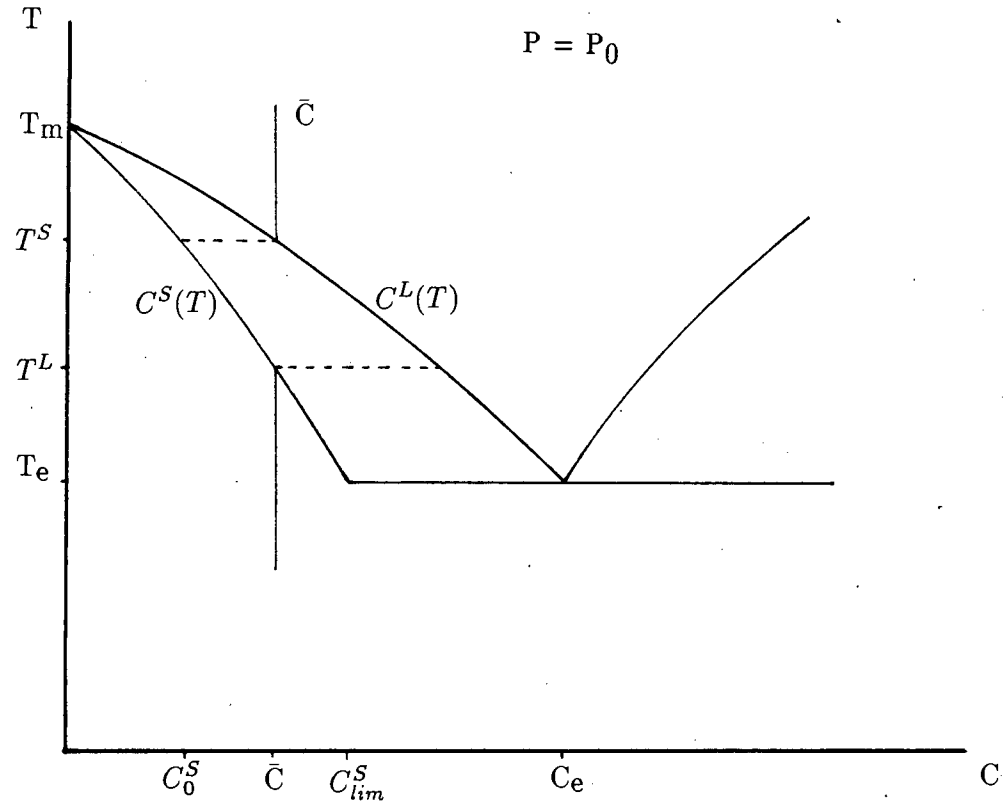


Figure 2.2: Phase diagram: Depiction of equilibrium solidification for fixed average solute concentration

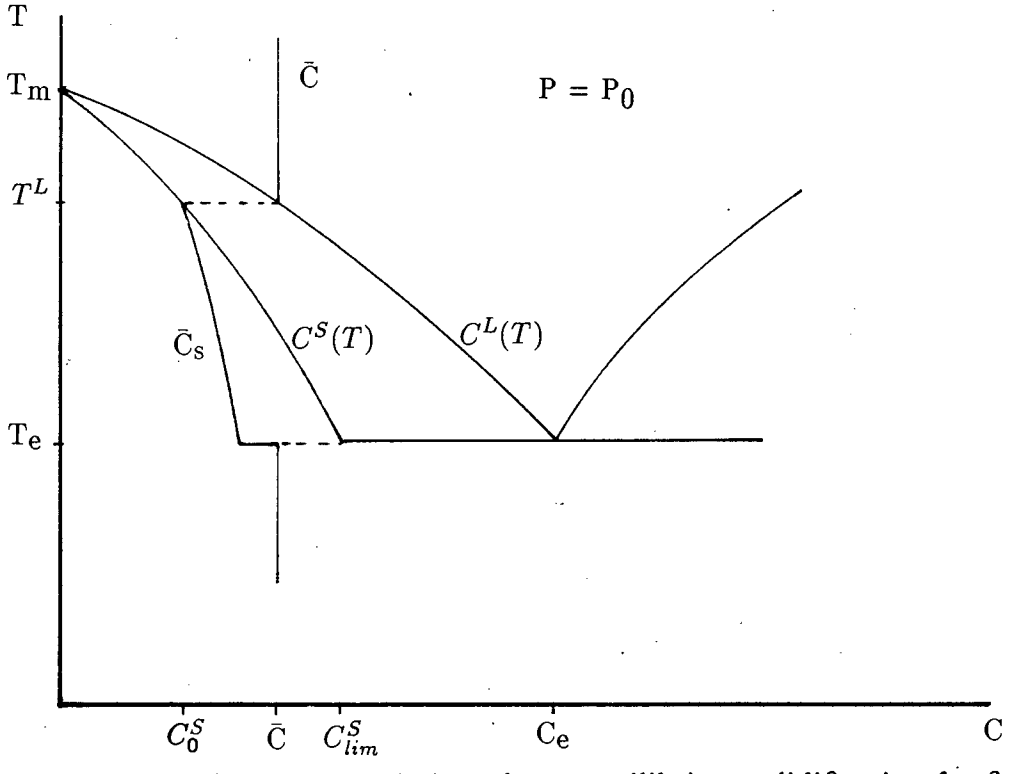


Figure 2.3: Phase diagram: Depiction of non-equilibrium solidification for fixed average solute concentration

the process from quasi to total equilibrium is ignored.

The equilibrium and non-equilibrium phase change systems can be described using the equilibrium phase diagram. Even though the phase diagram is only strictly relevant to a system in complete thermodynamic equilibrium, the non-equilibrium process can be described if equilibrium is assumed at the solid-liquid interface.

The solidification of a closed system, for both the equilibrium and non-equilibrium cases is described using the phase diagram, for the case of constant pressure, in Figures 2.2 and 2.3. A closed system is defined as a system in which no solute transport occurs, in or out of the system, thus the average solute concentration of the system (ie. $\bar{C}$ in Figures 2.3 and 2.3) remains constant. In contrast, an open system is defined as a system in which solute transport takes place, resulting in varying average solute concentration. It can be seen in Figures 2.1 and 2.2 that for the equilibrium process the average liquid and solid compositions lie on the liquidus and the solidus throughout solidification. For the non-equilibrium process, it can be seen from Figure 2.3 that the average solute concentration of the liquid lies on the liquidus with the solid interface solute concentration lying on the solidus and the average solid solute concentration lagging behind the solidus. For the volume element under non-equilibrium solidification, see Figure 2.1, the levels of solid solute concentration away from the interface exhibit a trace of the interface equilibrium values for different values of solid fraction. These solute concentration values, and therefore their average, will not be in equilibrium with the liquid except for the interface value. In the non-equilibrium case because of zero solid diffusion more solute is rejected into the liquid thus prolonging solidification and causing the final solidification to be eutectic.

In this chapter the local description of the solidification and remelting of an open system, of the order of the sample volume element, is described thermodynamically for both the equilibrium and local non-equilibrium cases.

### 2.1.1 Preliminaries

In order to model the solid-liquid phase change process in the mushy region basic preliminary definitions relating to the phase mixture have to defined. A binary mixture with constituents 1 and 2 is considered. The mass and volume of each constituent $i$ in phase $\alpha$ are designated as $\mathrm{M}_i^\alpha$ and $\mathrm{V}_i^\alpha$ where phase $\alpha$ can either be solid ($\alpha = S$) or liquid ($\alpha = L$). Note in this work, constituent 1 is termed the solute and constituent 2 is termed the solvent. It is assumed that the constituent mixture is inert where the mixture constituents are viewed as isolated subsystems and all properties of the mixture are mathematical consequences of the constituent properties, Bennon and Incropera [1]. Thus simple summation rules can be used to relate phase and constituent values. The actual density, volume fraction and mass fraction of constituent $i$ in phase $\alpha$ is defined as

$$\rho_i^\alpha = M_i^\alpha / V_i^\alpha \tag{2.1}$$

$$\mathrm{g}_i^\alpha = V_i^\alpha / V^\alpha \tag{2.2}$$

$$C_i^\alpha = M_i^\alpha / M^\alpha \tag{2.3}$$

where $V^\alpha$ and $M^\alpha$ are the volume and mass of phase $\alpha$. The term $C_i^\alpha$ is also termed the mass solute concentration or simply the concentration of constituent $i$ in phase $\alpha$.

Thus the actual density of phase $\alpha$ is

$$\rho_*^\alpha = \sum_{i=1,2} \mathrm{g}_i^\alpha \rho_{i_*}^\alpha \tag{2.4}$$

where $\mathrm{g}_i^\alpha \rho_{i_*}^\alpha = \bar{\rho}_i^\alpha$ is the partial density of $i$ in phase $\alpha$. Therefore the actual density of the phase is simply the summation of all the partial densities of the constituents contained in the phase.

Therefore, the total density of the binary phase mixture is

$$\rho = \sum_\alpha \mathrm{g}^\alpha \rho_*^\alpha \tag{2.5}$$

where $\mathrm{g}^\alpha = V^\alpha / V$ is the phase volume fraction and $\mathrm{g}^\alpha \rho_*^\alpha = \bar{\rho}^\alpha$ is the partial density of phase $\alpha$.

It also follows that the mass fractions can be defined as

$$C_i^\alpha = \bar{\rho}_i^\alpha / \rho_*^\alpha \tag{2.6}$$

and

$$\phi^\alpha = \bar{\rho}^\alpha / \rho = M^\alpha / M \tag{2.7}$$

where $\phi^\alpha$ is the mass fraction of phase $\alpha$.

It is assumed that no voids develop; that is

$$\sum_\alpha \mathrm{g}^\alpha = 1 \tag{2.8}$$

and from (2.6) and (2.7) it is seen that

$$\sum_\alpha \phi^\alpha = 1\,, \tag{2.9}$$

and

$$\sum_i C_i^\alpha = 1 \,, \tag{2.10}$$

From equation (2.10) the concentration of the first constituent $C_1^\alpha$ (ie. the solute concentration) will be defined as $C^\alpha$ and that of the second constituent $C_2^\alpha$ (ie. the solvent concentration) as $(1 - C^\alpha)$. From equation (2.9) the solid mass fraction $\phi^S$ will be defined as $\phi$ and the liquid mass fraction $\phi^L$ as $(1 - \phi)$.

In order to describe the structure and evolution of the region of mixed phase, the mass fraction of the solid phase $\phi(\boldsymbol{x})$ is used. On a microscale of crystal dimensions $\phi(\boldsymbol{x})$ can only be 0 or 1, but looking on the scale of the sample volume element $\phi(\boldsymbol{x})$ is considered as an average, varying smoothly between 0 and 1. Therefore $\phi$ is expressed as

$$\phi = \begin{cases} 1 & \text{solid region} \\ 0 < \phi < 1 & \text{mushy region} \\ 0 & \text{liquid region} \end{cases} .$$

The drawback to this assumption is that microstructural effects such as dendrite morphology (i.e. primary and secondary dendrite spacing, meniscus, curvature effects and interfacial energies etc.) are neglected. As only the broader macroscale (minimum scale being that of the sample element) of the solid-liquid phase change process is being considered in this work, it is assumed that these micro-effects are negligible.

The primary variables to be used to describe the phase change process are temperature T, pressure P and average solute concentration $\bar{C}$. It is realized that in a metallurgical context the dependence on pressure is weak and is usually ignored where pressure is set equal to a constant ($P = P_0$). However for the sake of generality subsequent discussions will include the effect of pressure. It is also assumed that the heat transfer process is so rapid that the temperatures of two co-existing phases $\alpha = S$ and $\alpha = L$ are equal (i.e. $T^S = T^L$).

## 2.2 Local equilibrium

As has been stated the local equilibrium assumption is applicable to the solidification of fine particles (Loper and Roberts [2] and [17]), amorphous materials (ie. waxes and glasses) and in a limited sense, the equiaxed zone of metal castings (Voller, Brent and Prakash [18]). The equilibrium assumption has also been used as a basis for dendritic solidification models (Hills, Loper and Roberts [4], Bennon and Incropera [1], [19]).

For the local equilibrium assumption, where the diffusion in the solid and liquid is assumed infinitely fast, see Figure 2.1, one can express the average solute concentration of the system as

$$\bar{C} = \frac{1}{\rho V} \left( \int_{V^S} \rho_*^S C^S \, dV^S + \int_{V^L} \rho_*^L C^L \, dV^L \right), \tag{2.11}$$

which results in a lever rule expression with respect to $\phi$, expressed as

$$\bar{C} = \phi \, C^S + (1 - \phi) \, C^L . \tag{2.12}$$

In equation (2.12) the average solid solute concentration $C^S$ is the solidus value, and the average liquid solute concentration $C^L$ is the liquidus value; see Figure 2.2.

### 2.2.1 Free energy description

To develop a consistent thermodynamic continuum description of the equilibrium solid-liquid phase change process, the Gibbs free energy is introduced. Gibbs free energy is used to describe the phase change process as its intensive variables pressure P and temperature T are the same variables used in thermostatics (i.e. phase equilibrium) to describe phase transitions. Hills, Loper and Roberts [4] use this description to develop a continuum based constitutive model for the mushy region.

The Gibbs Free Energy per unit mass of the system is described at a point in time by

$$\boldsymbol{\Phi} = \boldsymbol{\Phi}(P, T, \tilde{C}^S, \tilde{C}^L) , \tag{2.13}$$

where

$$\tilde{C}^S = M_1^S / M \quad \text{(partial solid solute concentration)} \tag{2.14}$$

and

(2.15)

$$\tilde{C}^L = M_1^L / M \quad \text{(partial liquid solute concentration)} . \tag{2.16}$$

Assuming that the solid and liquid phases do not interact chemically the additivity of the Gibbs free energy can be used to describe a system containing solid and liquid phases as follows

$$\boldsymbol{\Phi}(P, T, \tilde{C}^S, \tilde{C}^L) = \tilde{\boldsymbol{\Phi}}^S(P, T, \tilde{C}^S) + \tilde{\boldsymbol{\Phi}}^L(P, T, \tilde{C}^L) , \tag{2.17}$$

where $\tilde{\Phi}^{\alpha}$ is the Gibbs free energy of phase $\alpha$ per unit total mass (ie. partial phase Gibbs free energy).

To express the Gibbs free energy for each phase per unit mass of that phase we introduce the mass fraction $\phi$. The Gibbs free energy of the system can thus be re-expressed in the form of a lever rule in terms of $\phi$ as

$$\Phi(P,T,C^S,C^L,\phi) \;=\; \phi\,\Phi^S(P,T,C^S) + (1-\phi)\,\Phi^L(P,T,C^L)\,, \tag{2.18}$$

where $\Phi^{\alpha}$ is the phase free energy defined per unit mass of phase $\alpha$ and $C^{\alpha} = M_{\mathrm{I}}^{\alpha}/M^{\alpha}$ is the intrinsic solute concentration for phase $\alpha$.

The differential form of the Gibbs free energy is expressed as

$$\mathrm{d}\Phi = \rho^{-1}\mathrm{d}P - S\mathrm{d}T + (1-\phi)\mu^L\mathrm{d}C^L + \phi\mu^S\mathrm{d}C^S + \psi\mathrm{d}\phi\,, \tag{2.19}$$

where :

a) $\rho^{-1}$ is the volume of the phase mixture and is defined as

$$\rho^{-1}(P,T,C^L,C^S,\phi) = \phi\,\rho_*^{S^{-1}}(P,T,C^S) + (1-\phi)\,\rho_*^{L^{-1}}(P,T,C^L)\,, \tag{2.20}$$

b) S is the entropy of the phase mixture and is defined as

$$S(P,T,C^L,C^S,\phi) = \phi\,S_*^S(P,T,C^S) + (1-\phi)\,S_*^L(P,T,C^L)\,, \tag{2.21}$$

c) $\mu^{\alpha}$ is the phase chemical potential and is defined as

$$\mu^{\alpha}(P,T,C^{\alpha}) = \left\{\frac{\partial\Phi^{\alpha}}{\partial C^{\alpha}}(P,T,C^{\alpha})\right\}_{P,T} \quad \text{for } \alpha = \text{S or L}\,, \tag{2.22}$$

d) $\psi$ is the phase energy difference and is defined as

$$\psi(P,T,C^S,C^L) = \Phi^S(P,T,C^S) - \Phi^L(P,T,C^L)\,, \tag{2.23}$$

e) $\rho_*^{\alpha^{-1}}$ is the intrinsic phase volume and is defined as

$$\rho_*^{\alpha-1}(P,T,C^\alpha) = \left\{\frac{\partial \Phi^\alpha}{\partial P}(P,T,C^\alpha)\right\}_{T,C^\alpha} \quad \text{for } \alpha = \text{S or L , and} \tag{2.24}$$

f) $S_*^\alpha$ is the intrinsic phase entropy and is defined as

$$S_*^\alpha(P,T,C^\alpha) = -\left\{\frac{\partial \Phi^\alpha}{\partial T}(P,T,C^\alpha)\right\}_{P,C^\alpha} \quad \text{for } \alpha = \text{S or L .} \tag{2.25}$$

Note the subscript * denotes per unit mass of the intrinsic phase $\alpha$.

From the differential form of the lever rule expression for average solute concentration equation (2.12), expressed as

$$\mathrm{d}\bar{C} = \phi \mathrm{d}C^S + (1-\phi)\mathrm{d}C^L + (C^S - C^L)\mathrm{d}\phi\,, \tag{2.26}$$

the expression for $\mathrm{d}\phi$ is substituted into the differential form of the Gibbs free energy of the system, equation (2.19), resulting in

$$\begin{aligned}\mathrm{d}\phi &= \rho^{-1}\mathrm{d}P - S\mathrm{d}T + \frac{\psi}{C^S - C^L}\mathrm{d}\bar{C} + (1-\phi)\left\{\mu^L - \frac{\psi}{C^S - C^L}\right\}\mathrm{d}C^L \\ &+ \phi\left\{\mu^S - \frac{\psi}{C^S - C^L}\right\}\mathrm{d}C^S\,.\end{aligned} \tag{2.27}$$

The free energy is thus expressed in terms of three externally controlled variables P,T and $\bar{C}$ and two internal variables $C^S$ and $C^L$ which are controlled by their conjugate forces $\left\{\mu^L - \psi/(C^S - C^L)\right\}$ and $\left\{\mu^S - \psi/(C^S - C^L)\right\}$.

For a system where infinite diffusion in the solid and liquid is assumed, $C^S$ and $C^L$ are brought to their equilibrium values instantaneously by their conjugate forces which relax infinitely fast. Therefore, for local equilibrium, the resultant conjugate forces become

$$\mu^L - \frac{\psi}{C^S - C^L} = 0 \tag{2.28}$$

and

$$\mu^S - \frac{\psi}{C^S - C^L} = 0\,. \tag{2.29}$$

Thus at any one point along the equilibrium path of the system, the free energy can be described by three external variables P, T and $\bar{C}$ where local equilibrium with respect to $C^S$ and $C^L$ is maintained, viz.

$$\boldsymbol{\Phi} = \boldsymbol{\Phi}(P, T, \bar{C}) \,. \tag{2.30}$$

Thus as derived by Hills, Loper and Roberts [4] a constitutive law for the mushy region can be expressed in terms of general functions of P, T and $\bar{C}$. From (2.28) and (2.29) two conditions for local equilibrium are obtained

$$\mu^S = \mu^L = \mu \tag{2.31}$$

and

$$\mu = \frac{\psi}{C^S - C^L} \,, \tag{2.32}$$

where $\mu$ is the chemical potential of the phase mixture.

For the equilibrium phase mixture the differential of the free energy is thus expressed as

$$\mathrm{d}\boldsymbol{\Phi} = \rho^{-1}\mathrm{dP} - \mathrm{SdT} + \mu \mathrm{d}\bar{C} \,. \tag{2.33}$$

From equation (2.33) it is seen that $\mu = \mu(P, T, \bar{C})$ where $\bar{C} = \bar{C}(C^S, C^L, \phi)$.

From the definitions of $\mu^S$ and $\mu^L$ given in equation (2.22) we get $\mu^S = \mu^S(P, T, C^S)$ and $\mu^L = \mu^L(P, T, C^L)$, thus $\mu^S$ and $\mu^L$ are independent $\phi$. For the equilibrium condition equation (2.31) to hold, it follows that

$$\mu = \mu(P, T) \,, \tag{2.34}$$

$$C^S = C^S(P, T) \tag{2.35}$$

and

$$C^L = C^L(P, T) \,, \tag{2.36}$$

where $C^S(P, T)$ and $C^L(P, T)$ are expressions for the solidus and liquidus, respectively.

From equations (2.33) and (2.34) and the first order homogeneous approximation to the binary mixture given as

$$\Phi^{\alpha} = \mu_1 (1 - C^{\alpha}) + \mu_2 (C^{\alpha}) , \tag{2.37}$$

the free energy $\Phi$, volume $\rho^{-1}$, and entropy S of the phase mixture under local equilibrium conditions can be expressed as linear functions of $\bar{C}$ as:

$$\Phi = \mu \bar{C} + \mu_2 , \tag{2.38}$$

$$\rho^{-1} = \bar{\delta} \bar{C} + \delta_2, \tag{2.39}$$

and

$$\mathrm{S} = \bar{s} \bar{C} + s_2 , \tag{2.40}$$

where $\mu = \mu_1 - \mu_2$ is the chemical potential of the binary mixture of solute concentration $\bar{C}$ , $\mu_i$ is the chemical potential of pure constituent $i$ , $\bar{\delta} = \partial\mu/\partial P$ is the change in specific volume of the phase mixture of solute concentration $\bar{C}$ , $\delta_2 = \partial\mu_2/\partial P$ is the change in specific volume for pure constituent 2 , $\bar{s} = \partial\mu/\partial T$ is the change in specific entropy for the phase mixture with solute concentration $\bar{C}$ and $s_2 = \partial\mu_2/\partial T$ is the change in specific entropy of pure constituent 2.

### 2.2.2 Evaluation of thermodynamic coefficients

In order to describe the change in thermodynamic coefficients due to the phase change process the differential forms of the solidus and liquidus are presented. These expressions are obtained by taking the total differentials of equations (2.28) and (2.29).

The differential form of (2.28) is given as

$$\begin{aligned} &\left[\rho_*^{S-1} - \rho_*^{L-1} - \frac{\partial\mu^L}{\partial P}(C^S - C^L)\right]_{T,C^S,C^L} dP + \\ &\left[S_*^L - S_*^L - \frac{\partial\mu^L}{\partial T}(C^S - C^L)\right]_{P,C^S,C^L} dT + \\ &\left[\mu^S - \mu^L\right]_{T,P,C^L} dC^S + \left[-\frac{\partial\mu^L}{\partial C^L}(C^S - C^L)\right]_{T,P,C^S} dC^L = 0 . \end{aligned} \tag{2.41}$$

By applying the equilibrium condition, $\mu^S = \mu^L$, the differential form of the liquidus is obtained as follows

$$dC^L = \frac{1}{\bar{\mu}^L(C^L - C^S)}\left\{\delta^L dP - L^L/T\, dT\right\}, \tag{2.42}$$

where

$$-\delta^L = \left\{(\rho_*^S)^{-1} - (\rho_*^L)^{-1} - (\frac{\partial \mu^L}{\partial P})(C^S - C^L)\right\}, \tag{2.43}$$

$$L^L/T = \left\{S_*^L - S_*^S - (\frac{\partial \mu^L}{\partial T})(C^S - C^L)\right\} \tag{2.44}$$

and

$$\bar{\mu}^L = \partial \mu^L / \partial C^L . \tag{2.45}$$

Similarly the differential form of the solidus is obtained from the full differential of (2.29) and applying the equilibrium condition $\mu^S = \mu^L$ we obtain

$$dC^S = \frac{1}{\bar{\mu}^S(C^L - C^S)}\left\{\delta^S dP - L^S/T dT\right\}, \tag{2.46}$$

where

$$-\delta^S = \left\{(\rho_*^S)^{-1} - (\rho_*^L)^{-1} - (\frac{\partial \mu^S}{\partial P})(C^S - C^L)\right\}, \tag{2.47}$$

$$L^S/T = \left\{S_*^L - S_*^S - (\frac{\partial \mu^S}{\partial T})(C^S - C^L)\right\} \tag{2.48}$$

and

$$\bar{\mu}^S = \partial \mu^S / \partial C^S . \tag{2.49}$$

It must be noted that $\delta^\alpha$ is the volumetric expansion that takes place on phase change and can be written as

$$\delta^\alpha = \left[\frac{(\rho_*^S)^{-1} - (\rho_*^L)^{-1}}{C^S - C^L} - \bar{\delta}^\alpha\right](C^L - C^S), \tag{2.50}$$

where :

a ) $\bar{\delta}^\alpha$ is the specific volume change of the phase $\alpha$ for the composition $C^\alpha$ which is either constrained to the liquidus, or solidus, depending on that phase, and is defined by

$$\bar{\delta}^\alpha = \partial \mu^\alpha / \partial p \text{ , and} \tag{2.51}$$

b ) $\bar{\delta}$ is the specific volume change of the mixture of solid and liquid of composition $\bar{C}$ in phase equilibrium and is defined by

$$\frac{\rho_*^{S-1} - \rho_*^{L-1}}{C^S - C^L} = \{\partial\mu/\partial p\}_{T,C^S,C^L} = \bar{\delta} . \tag{2.52}$$

Therefore $\delta^\alpha$ is defined as

$$\delta^\alpha = [\bar{\delta} - \bar{\delta}^\alpha] (C^L - C^S) , \tag{2.53}$$

which describes a change in specific volume during phase change from solid to the mushy region or from liquid to the mushy region or vice versa.

The term $L^\alpha$ is the latent heat that is either liberated or absorbed upon phase change and is defined as

$$L^\alpha = T \left[ \frac{S_*^L - S_*^S}{C^L - C^S} - \bar{s}^\alpha \right] (C^L - C^S) , \tag{2.54}$$

where :

a ) $\bar{s}^\alpha$ describes the specific entropy of the phase $\alpha$ of composition $C^\alpha$, which is constrained to lie on the liquidus, or solidus depending on the phase $\alpha$, and is defined as

$$\bar{s}^\alpha = -\partial\mu^\alpha/\partial T , \text{ and} \tag{2.55}$$

b ) $\bar{s}$ describes the change in specific entropy of the phase mixture (mushy region) for a composition $\bar{C}$ in phase equilibrium, and is defined as

$$\frac{S_*^L - S_*^S}{C^L - C^S} = -\{\partial\mu/\partial T\}_{P,C^S,C^L} = \bar{s} . \tag{2.56}$$

Therefore $L^\alpha/T$ represents a change in specific entropy when going from liquid to the mushy region or solid to the mushy region, and is defined as

$$L^\alpha/T = [\bar{s} - \bar{s}^\alpha](C^L - C^S) . \tag{2.57}$$

Note that $\delta^L$ can be re-expressed as, Loper and Roberts [2],

$$\rho_*^{S^{-1}} - (C^S \rho_{1_*}^{L^{-1}} + (1 - C^S)\rho_{2_*}^{L^{-1}}) \;=\; -\delta^L \,, \tag{2.58}$$

which represents a change in specific volume that occurs when a unit mass of solid of composition $C^S$ melts to form a liquid of the same composition. From equation (2.58) it is seen that the volumetric expansion coefficient $\delta^L$ will be positive if expansion occurs upon melting.

The latent heat $L^L$ can be re-expressed as, Loper and Roberts [2],

$$(C^S S_{1_*}^L + (1 - C^S) S_{2_*}^L) - S_*^S \;=\; L^L/T \,, \tag{2.59}$$

which represents the latent heat released per unit mass when the solid of composition $C^S$ melts to form liquid of the same composition. Note that if the solid state is more ordered than the liquid the latent heat $L$ will be positive, [2].

Using the expressions for latent heat (equations 2.44 and 2.48), volumetric expansion (equations 2.43 and 2.47) and the partial derivative of chemical potential with respect to solute concentration (equations 2.45 and 2.49) the differential forms, of the expressions for volume (equation 2.20) and entropy (equation 2.21), can therefore be expressed in terms of P, T and $\bar{C}$.

The differential form of the expression for the volume (equation 2.20) expressed in terms of P, T and $\bar{C}$ for the mushy region is

$$\mathrm{d}\rho^{-1} \;=\; -\beta/\rho \;\mathrm{dP} + \alpha_t/\rho \;\mathrm{dT} + \bar{\delta}\;\mathrm{d}\bar{C} \,. \tag{2.60}$$

Similarly the differential form of the expression for the entropy (equation 2.21) expressed in terms of P, T and $\bar{C}$ for the mushy region is

$$\mathrm{dS} \;=\; -\alpha_t/\rho \;\mathrm{dP} + C_p/T \;\mathrm{dT} + \bar{s}\;\mathrm{d}\bar{C} \,. \tag{2.61}$$

The expressions for the isothermal compression coefficient $\beta$, the thermal expansion coefficient $\alpha_t$ and the specific heat capacity $C_p$, of the phase mixture, are described as

$$\beta \;=\; \mathrm{g}^S\,\beta^S + \mathrm{g}^L\,\beta^L \,, \tag{2.62}$$

$$\alpha_t \;=\; \mathrm{g}^S\,\alpha_t^S + \mathrm{g}^L\,\alpha_t^L \tag{2.63}$$

and

$$C_p = \phi\, C_p^S + (1-\phi)\, C_p^L \,. \tag{2.64}$$

The terms in equations (2.62) - (2.64) are defined as

$$\mathrm{g}^S = \phi\, \rho/\rho_*^S \tag{2.65}$$

$$\mathrm{g}^L = (1-\phi)\, \rho/\rho_*^L \,, \tag{2.66}$$

$$\beta^\alpha = \beta_*^\alpha + \frac{\rho_*^\alpha}{\bar{\mu}^\alpha} \left[\frac{\delta^\alpha}{C^L - C^S}\right]^2 \,, \tag{2.67}$$

$$\alpha_t^\alpha = \alpha_{t_*}^\alpha + \frac{\rho_*^\alpha \delta^\alpha L^\alpha}{\bar{\mu}^\alpha\, T\, (C^L - C^S)^2} \tag{2.68}$$

and

$$C_p^\alpha = C_{p_*}^\alpha + \frac{(L^\alpha)^2}{\bar{\mu}^\alpha\, T\, (C^L - C^S)^2} \,, \tag{2.69}$$

where $g^\alpha$, $\alpha_t^\alpha$, $\beta^\alpha$ and $C_p^\alpha$ are defined as the volume fraction, thermal expansion coefficient, isothermal compression coefficient and the specific heat capacity of the specific phase $\alpha$.

In the regions of pure liquid or pure solid $\beta^\alpha = \beta_*^\alpha$, $\alpha_t^\alpha = \alpha_{t_*}^\alpha$ and $C_p^\alpha = C_{p_*}^\alpha$. The coefficients representing the pure phase are small in comparison to the interphase terms (i.e. the second righthand terms in equations (2.67 - 2.69). Thus, in the mixed phase region, $\beta^\alpha, \alpha_t^\alpha$ and $C_p^\alpha$ greatly exceed $\beta_*^\alpha$, $\alpha_{t_*}^\alpha$ and $C_{p_*}$ in magnitude and $\alpha$, $\beta$ and $C_p$ are far larger than in the adjacent pure solid and pure liquid regions. As a result these coefficients exhibit large discontinuities across the interfaces between the solid and mushy region and between the liquid and mushy region.

Note $\alpha_{t_*}^\alpha$, $\beta_*^\alpha$ and $C_{p_*}^\alpha$ are evaluated as :

$$\alpha_{t_*}^\alpha = \rho_*^\alpha \left\{ \left(\frac{\partial (\rho_*^\alpha)^{-1}}{\partial T}\right)_{P,C^\alpha} \right\}_{C^\alpha = C^\alpha(P,T)} \,, \tag{2.70}$$

$$\beta_*^\alpha = \rho_*^\alpha \left\{ \left(\frac{\partial (\rho_*^\alpha)^{-1}}{\partial P}\right)_{T,C^\alpha} \right\}_{C^\alpha = C^\alpha(P,T)} \,, \tag{2.71}$$

and

$$C_{p_*} = T \left\{ \left(\frac{\partial S_*^\alpha}{\partial T}\right)_{P,C^\alpha} \right\}_{C^\alpha = C^\alpha(P,T)} \,. \tag{2.72}$$

It can be seen from equations (2.70 - 2.72) that the derivatives are evaluated outside the equi-

librium zone (i.e. $C^\alpha \neq C^\alpha(P,T)$). Once the derivatives have been obtained they are then evaluated for $C^\alpha = C^\alpha(P,T)$. This is in keeping with experimentally obtained values of $\alpha^\alpha_{t_*}$, $\beta^\alpha_*$ and $C^\alpha_{p_*}$ which are usually measured from samples of fixed composition. Note that if the derivatives of $\rho^{\alpha\,-1}_*$ and $S^\alpha_*$ with respect to T and P where evaluated in the equilibrium region, it would mean that T and P would only change if the composition changed to maintain local equilibrium (i.e. $C^\alpha = C^\alpha(P,T)$) which would be inconsistent with experimental values [4].

A reasonable approximation for many metal alloy systems is that the left-hand solidus and liquidus branches are in constant ratio, i.e.

$$\frac{C^S(P,T)}{C^L(P,T)} = k = constant \tag{2.73}$$

and the analogue for the right-hand branches is

$$\frac{1 - C^S(P,T)}{1 - C^L(P,T)} = k' = constant\ , \tag{2.74}$$

where $k$ and $k'$ are usually termed the equilibrium partition coefficients.

If equation (2.73) is applied to the differential forms of the solidus and liquidus (equations 2.42 and 2.46), it turns out that the following ratios are equal;

$$\delta^S/\delta^L \;=\; L^S/L^L \;=\; k\bar{\mu}^S/\bar{\mu}^L\ . \tag{2.75}$$

If it is assumed that the ratios equal unity (Hills, Loper and Roberts [4]), then

$$\delta^L \;=\; \delta^S \;=\; \delta\ , \tag{2.76}$$

$$L^L \;=\; L^S \;=\; L\ , \tag{2.77}$$

and

$$\bar{\mu}^L \;=\; k\bar{\mu}^S \;=\; \bar{\mu}\ . \tag{2.78}$$

Thus from equations (2.53) and (2.57)

$$\bar{\delta}^L \;=\; \bar{\delta}^S \tag{2.79}$$

and

$$\bar{s}^L = \bar{s}^S . \tag{2.80}$$

If these assumptions are then applied to the expressions for $\alpha, \beta$ and $C_p$, in equations (2.62) - (2.64), the following are obtained:

$$\beta = \beta_0 + \Delta\beta , \tag{2.81}$$

$$\alpha_t = \alpha_{t_0} + \Delta\alpha_t \tag{2.82}$$

and

$$C_p = C_{p_0} + \Delta C_p , \tag{2.83}$$

where

$$\beta_0 = g^S \beta_*^S + g^L \beta_*^L , \tag{2.84}$$

$$\alpha_{t_0} = g^S \alpha_{t_*}^S + g^L \alpha_{t_*}^L , \tag{2.85}$$

$$C_{p_0} = \phi C_{p_*}^S + (1-\phi) C_{p_*}^L , \tag{2.86}$$

$$\Delta\beta = \frac{\rho\delta^2(1-(1-k)\phi)}{\bar{\mu}(1-k)^2 C^{L^2}} , \tag{2.87}$$

$$\Delta\alpha_t = \frac{\rho\delta L(1-(1-k)\phi)}{\bar{\mu}T(1-k)^2 C^{L^2}} \tag{2.88}$$

and

$$\Delta C_p = \frac{L^2(1-(1-k)\phi)}{\bar{\mu}T(1-k)^2 C^{L^2}} . \tag{2.89}$$

From equations (2.42) and (2.46), and the metallurgical assumptions given in equations (2.73) and (2.76-2.80), the volumetric expansion $\delta$ and latent heat of fusion $L$ can be defined as

$$L = -\frac{T\bar{\mu}(1-k)C^L}{m^L} \tag{2.90}$$

and

$$\delta = \frac{\bar{\mu}(1-k)C^L}{m^{L'}} , \tag{2.91}$$

where $m^L = \partial C^L/\partial T$ (the thermal liquidus slope) and $m^{L'} = \partial C^L/\partial P$ (the pressure liquidus

Using the lever rule expression for $\bar{C}$, equation (2.12), and equations (2.90) and (2.91) it can be shown that

$$\Delta\beta = \rho\delta\, \partial\phi/\partial p\,, \tag{2.92}$$

$$\Delta\alpha_t = -\rho\delta\, \partial\phi/\partial T \tag{2.93}$$

and

$$\Delta C_p = -L\, \partial\phi/\partial T\,. \tag{2.94}$$

Therefore equations (2.62-2.64) can be re-expressed in terms of the derivatives of the solid mass fraction $\phi$ as

$$\beta = \beta_0 + \rho\delta\, \partial\phi/\partial P\,, \tag{2.95}$$

$$\alpha_t = \alpha_{t_0} - \rho\delta\, \partial\phi/\partial T \tag{2.96}$$

and

$$C_p = C_{p_0} - L\, \partial\phi/\partial T\,. \tag{2.97}$$

These equations for $\alpha_t$, $\beta$ and $C_p$ are identical to that derived in the metallurgical literature where, for example, $C_p$ is defined as the effective specific heat of the phase mixture and $C_{p_0}$ is the lever rule specific heat of the phase mixture.

The variations of $\alpha_t, C_p$ and $\beta$ from the pure solid and liquid zones to the phase change region, as discussed for the thermodynamic formulation, are clearly shown in Section 2.4.2 for an Al-Si alloy.

## 2.3 Local non-equilibrium

Under the non-equilibrium assumption the solid solute does not vary with time and exhibits a profile which is a function of the interface solid solute values for a particular solid mass fraction varying from zero to the value of solid mass fraction $\phi$ at time $t$. This is defined in Figure 2.1 for a representative volume element on the scale of a dendrite arm.

The solidification of the representative volume element, depicted in Figure 2.1, is illustrated using the phase diagram in Figure 2.3, for a closed system. It can be seen that as temperature T reaches the liquidus the first solid to form will have the solidus solute concentration $C_0^S$ and as the T decreases, the new solid formed at the interface will have a solute concentration corresponding to a solidus value that moves from $C_0^S$ to $C_{lim}^S$. As a result of zero solid diffusion the solid solute concentration levels will not change resulting in a trace of the solidus values throughout the solid portion of the volume element. The innermost core of the dendrite will

therefore have the composition $C_0^S$ with the outer regions of the solid becoming successively richer in solute. Once the eutectic temperature is reached (i.e. $T = T_e$) the final solid formed will have a constant eutectic solute concentration $C_e$. Thus at the onset of eutectic phase change the profile will exhibit a jump from $C_{lim}^S$ to $C_e$. If remelting occurs the process is simply reversed with the interface equilibrium being maintained.

In contrast with the description of the phase change process of the closed system, the solid solute profile for the open system may not be a monotonically increasing function and interface equilibrium may not necessarily be maintained in the open system. For example, the solid solute profile may exhibit a hump if at some time solute-rich liquid flowed into the solidifying volume element, see Figure 2.4. If for some reason remelting occurs the solute content of the solid will be released into the liquid and the interface will retreat with the solid solute interface value no longer exhibiting the equilibrium value but the interface value from the previous solidification. Therefore in order to model this phenomenon the non-equilibrium model must be developed such that, on solidification, a record of the history of the dendrite growth can be kept. It is clear that this is not necessary for a closed system with no solid diffusion as the solute balance is such that after remelting the interface equilibrium condition is maintained. If some solid back diffusion occurred in the closed system the remelting case would be the same as that for the open system. In order to avoid the difficulty Rappaz and Voller [20] propose that with zero solid diffusion the solute diffusion layer within the solid can be assumed to be zero resulting in a singularity at the interface which has the equilibrium solute concentration $C^S(P,T)$ while the rest of the solid solute profile remains unchanged. Interface equilibrium is therefore satisfied while the solute balance is maintained during melting, see Figure 2.4.

As has been stated in the introduction to this chapter, the assumption of local non-equilibrium is applicable to dendritic solidification or the solidification of large equiaxed particles. This assumption, commonly known as the Schiel model, has been used as basis for continuum models of dendritic solidification. Voller, Brent and Prakash [18] use this model to predict the micro-macrosegregation process for the solidification case only. Later Rappaz and Voller [20] considered the melting case as well and showed the differences and complexities when modelling an open system as opposed to a closed system. Hills and Roberts [21] have developed a dynamic theory of the mushy region using the Schiel model as a basis. Their theory is based on the average solute concentration of the solid particle thus neglecting any history effects so making the theory incapable of modelling the remelting process.

The thermodynamic description of the non-equilibrium phase change process developed in this section is different to that presented by Hills and Roberts [21]. It is formulated to include the solidification history thus enabling the remelting process to be described. The formulation presented in this section is not based on the average solid solute concentration in the particle (ie. sample volume element), as in [21], but instead on the solid solute profile history. The equation for the solid solute profile is expressed in terms of a functional which is a function of $f^S$ where $0 \leq f^S \leq \phi(t)$, with $\phi(t)$ being the solid mass fraction at time $t$, see Figures (2.1 and 2.4) .

Thus

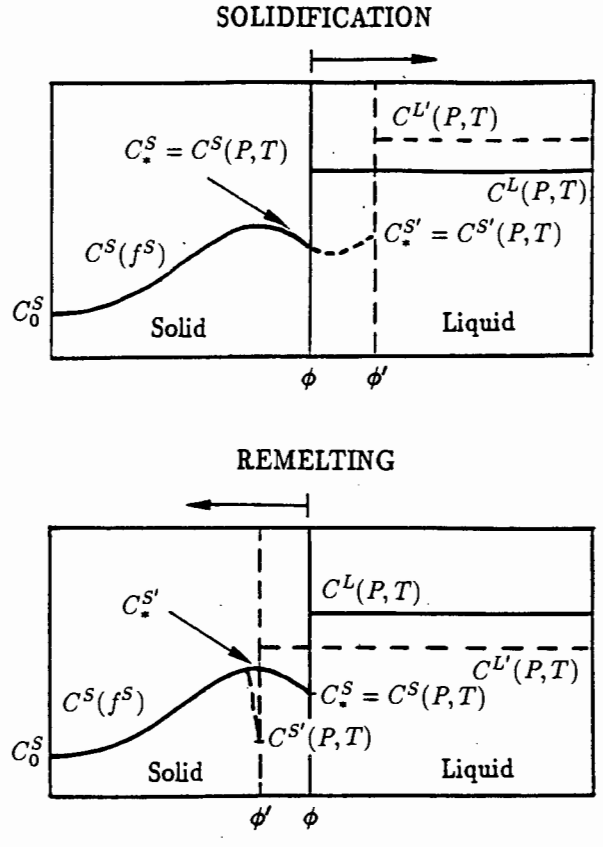


Figure 2.4: Schematic of solute profiles for the non-equilibrium model of an open system, Rappaz and Voller [20].

$$C^S = C^S(f^S) \quad \text{for} \quad 0 \leq f^S \leq \phi(t)\,, \tag{2.98}$$

where

$$C^S(0) = C^S_0 \tag{2.99}$$

and

$$C^S(\phi(t)) = C^S_*\,. \tag{2.100}$$

The value of the solid solute concentration at the interface at time $t$ is $C^S_*$ and $C^S_0$ is the initial solid interface value at the onset of solidification. For solidification, local equilibrium at the interface is assumed, thus $C^S_*$ is in equilibrium with $C^L$ but $C^S(f^S)$ for $f^S < \phi(t)$ is not in equilibrium with the liquid. Therefore, for a particular pressure and temperature, local equilibrium at the interface implies

$$C^S_* = C^S(P,T) \tag{2.101}$$

and

$$C^L = C^L(P,T)\,. \tag{2.102}$$

It follows that the solid volume and its solute profile grows by accretion of material with different values of $C^S_* = C^S(P,T)$. The solid solute profile $C^S(f^S)$, for $0 \leq f^S \leq \phi(t)$, is thus the trace of the interface solute values from time $t = 0$ to time $t = \tau$.

The average solute concentration of the system can now be defined as

$$\bar{C} = \frac{1}{\rho V}\left(\int_{V^S} \rho^S_* C^S(f^S)\, dV^S + \int_{V^L} \rho^L_* C^L\, dV^L\right) \tag{2.103}$$

and in terms of a linear expression in $\phi$ we get

$$\bar{C} = \int_0^\phi C^S(f^S)\, df^S + (1-\phi)\, C^L\,, \tag{2.104}$$

$$= \phi\, \bar{C}^S + (1-\phi)\, C^L\,, \tag{2.105}$$

where $\bar{C}^S$ is the average concentration of solute in the solid region given as

$$\bar{C}^S = \frac{1}{\phi}\int_0^\phi C^S(f^S)\, dV^S. \tag{2.106}$$

### 2.3.1 Free energy description

The Gibbs free energy for a system with zero solid diffusion is expressed per unit mass as

$$\boldsymbol{\Phi} = \boldsymbol{\Phi}(P,T,\hat{C}^S(f^S),\hat{C}^L)\,. \tag{2.107}$$

As it is assumed that the solid and liquid phases do not interact chemically additivity of the free energy is used to express $\boldsymbol{\Phi}$ in the form of a lever rule in terms of $\phi$ as

$$\boldsymbol{\Phi}(P,T,C^S(f^S),C^L,\phi) = \phi\, \boldsymbol{\Phi}^S(P,T,C^S(f^S)) + (1-\phi)\, \boldsymbol{\Phi}^L(P,T,C^L)\,. \tag{2.108}$$

Note this description of the free energy, in particular that of the solid phase, is different from

that presented by Hills and Roberts [21] who use the average solid solute to describe $\Phi^S$ (i.e. $\Phi^S = \Phi^S(P, T, \bar{C}^S)$). The description presented in this work which includes the solid solute history brought about by zero solid diffusion is a more accurate description of the energy of the system, thus enabling remelting to be considered.

The differential form of (2.108) is given as .

$$d\Phi = \rho^{-1}\, dP - S\, dT + \phi\, \mu^S(f^S)\, dC^S(f^S) + (1-\phi)\, \mu^L\, dC^L + \psi\, d\phi\,, \tag{2.109}$$

where $\rho^{-1}$, $S$, $\mu^\alpha$ and $\psi$ are the volume, entropy, phase chemical potential and phase energy difference of the phase mixture.

The volume of the phase mixture $\rho^{-1}$ is defined as

$$\rho^{-1} = \phi\, (\rho_*^S)^{-1} + (1-\phi)\, (\rho_*^L)^{-1}\,, \tag{2.110}$$

where

$$(\rho_*^S)^{-1} = (\frac{\partial \Phi^S}{\partial P})_{T, C^S(f^S)} \tag{2.111}$$

and

$$(\rho_*^L)^{-1} = (\frac{\partial \Phi^L}{\partial P})_{T, C^L}\,. \tag{2.112}$$

The entropy of the phase mixture S is defined as

$$S = \phi\, S_*^S - (1-\phi)\, S_*^L\,, \tag{2.113}$$

where

$$S_*^S = -(\frac{\partial \Phi^S}{\partial T})_{P, C^S(f^S)} \tag{2.114}$$

and

$$S_*^L = -(\frac{\partial \Phi^L}{\partial T})_{P, C^L}\,. \tag{2.115}$$

The phase chemical potential of the phase mixture $\mu^\alpha$ is defined as

$$\mu^S(f^S) = (\frac{\partial \Phi^S}{\partial C^S(f^S)})_{P,T} \tag{2.116}$$

and

$$\mu^L = (\frac{\partial \Phi^L}{\partial C^L})_{P,T} . \tag{2.117}$$

The phase energy difference of the phase mixture $\psi$ is defined as

$$\psi = \Phi^S(P,T,C^S(f^S)) - \Phi^L(P,T,C^L) . \tag{2.118}$$

The differential form of the lever rule expression for $\bar{C}$ , equation ( 2.105), is thus expressed as

$$\mathrm{d}\bar{C} = C^S(\phi)\mathrm{d}\phi + (1-\phi)\mathrm{d}C^L - C^L\mathrm{d}\phi , \tag{2.119}$$

$$= (1-\phi)\mathrm{d}C^L + (C^S(\phi) - C^L)\mathrm{d}\phi , \tag{2.120}$$

where $C^S(\phi) = C^S_*$ the equilibrium solid solute concentration interface value.

From (2.120) $d\phi$ is substituted into (2.109) resulting in

$$\mathrm{d}\Phi = \rho^{-1}\mathrm{d}P - S\mathrm{d}T + \frac{\psi}{C^S_* - C^L}\mathrm{d}\bar{C} + \phi\mu^S(f^S)\mathrm{d}C^S(f^S)$$

$$+ (1-\phi)\left\{\mu^L - \frac{\psi}{C^S_* - C^L}\right\}\mathrm{d}C^L . \tag{2.121}$$

From the assumption of zero solid solute diffusion, $dC^S(f^S) = 0$ and from the assumption of infinite diffusion in the liquid we assume that there is an infinitely fast relaxation of the conjugate force to $C^L$, resulting in

$$\mu^L - \frac{\psi}{C^S_* - C^L} = 0 . \tag{2.122}$$

The resulting system can be described, at any point along the equilibrium path, by three thermodynamic variables P, T and $\bar{C}$, where local equilibrium with respect to the liquid and the solid interface solute concentration is maintained and there is no variation in the solid solute profile. The differential form the Gibbs free energy system is then expressed as

$$\mathrm{d}\Phi = \rho^{-1}\mathrm{dP} - \mathrm{SdT} + \mu\mathrm{d}\bar{C} , \tag{2.123}$$

where

$$\Phi = \Phi(P, T, \bar{C}) \tag{2.124}$$

and

$$\mu = \frac{\psi}{C_*^S - C^L} \,. \tag{2.125}$$

From (2.122) and thus (2.125) $\mu = \mu^L$ and, as for the equilibrium case, $\mu \neq \mu(P, T, \bar{C})$ but $\mu = \mu(P, T)$ where $C^L = C^L(P, T)$.

### 2.3.2 Evaluation of thermodynamic coefficients

From equation (2.122) it is seen that the condition to be satisfied in order to describe the system in terms of $P, T$ and $\bar{C}$ is that of local equilibrium with respect to the liquid. This condition is expressed in terms of the solid interface solute concentration and if interface equilibrium is assumed then $C_*^S = C^S(P, T)$. With this assumption the differential form of (2.122) is the same as that of the liquidus for the equilibrium case. Thus the differential form of (2.122) used to describe the change in the thermodynamic coefficients is expressed as

$$\mathrm{d}C^L = \frac{1}{\bar{\mu}^L(C^L - C_*^S)} \left\{ \delta^L \mathrm{dP} - L^L/T \mathrm{dT} \right\} , \tag{2.126}$$

where $C_*^S = C^S(P, T)$ and $C^L = C^L(P, T)$ .

The expression for the volumetric expansion $\delta^L$ the liberation of latent heat $L^L$ and $\bar{\mu}^L$ are expressed as :

$$\delta^L = -\left\{ (\rho_*^S)^{-1} - (\rho_*^L)^{-1} - \bar{\delta}^L(C_*^S - C^L) \right\} , \tag{2.127}$$

$$L^L/T = \left\{ S_*^L - S_*^S + \bar{s}^L(C_*^S - C^L) \right\} \tag{2.128}$$

and

$$\bar{\mu}^L = \partial \mu^L / \partial C^L \,. \tag{2.129}$$

The expressions for the differential form of the volume $\rho^{-1}$ and entropy S can now also be expressed in terms of P, T and $\bar{C}$ using the expressions (2.127) and (2.128) for volumetric

expansion $\delta^\alpha$ and latent heat $L^\alpha$.

The differential forms of $\rho^{-1}$ and S are the same as that for the equilibrium case except where the coefficients for the solid phase do not have a phase change contribution. Therefore

$$\mathrm{d}\rho^{-1} = -\beta/\rho \,\mathrm{dP} + \alpha_t/\rho \,\mathrm{dT} + \bar{\delta} \,\mathrm{d}\bar{C} \tag{2.130}$$

and

$$\mathrm{dS} = -\alpha_t/\rho \,\mathrm{dP} + C_p/T \,\mathrm{dT} + \bar{S} \,\mathrm{d}\bar{C} \,, \tag{2.131}$$

where

$$\beta = \mathrm{g}^S \beta^S + \mathrm{g}^L \beta^L \,, \tag{2.132}$$

$$\alpha_t = \mathrm{g}^S \alpha_t^S + \mathrm{g}^L \alpha_t^L \tag{2.133}$$

and

$$C_p = \phi \, C_p^S + (1-\phi) \, C_p^L \,. \tag{2.134}$$

The coefficients of each phase in the phase change zone are expressed as :

$$\beta^S = \beta_*^S \,, \tag{2.135}$$

$$\beta^L = \beta_*^L + \frac{\rho_*^L}{\bar{\mu}^L} \left[ \frac{\delta^L}{C^L - C_*^S} \right]^2 \,, \tag{2.136}$$

$$\alpha_t^S = \alpha_{t_*}^S \,, \tag{2.137}$$

$$\alpha_t^L = \alpha_{t_*}^L + \frac{\rho_*^L \delta^L L^L}{\bar{\mu}^L \, T \, (C^L - C_*^S)^2} \,, \tag{2.138}$$

$$C_p^S = C_{p_*}^S \tag{2.139}$$

and

$$C_p^L = C_{p_*}^L + \frac{(L^L)^2}{\bar{\mu}^L \, T \, (C^L - C_*^S)^2} \,. \tag{2.140}$$

It is clear from equations (2.135), (2.137) and (2.139) that the isothermal compression coefficient $\beta^S$, the thermal expansion coefficient $\alpha_t^S$ and the specific heat $C_p^S$ remain fixed at their pure solid phase values in the phase change region, due to the zero solid diffusion (ie. $\mathrm{d}C^S(f^S) = 0$). The thermodynamic coefficients defined for the pure phase regions are expressed as:

a) the isothermal compression coefficient

$$\beta_*^S = \left\{ \frac{\partial(\rho_*^S)^{-1}}{\partial P} \right\}_{T,C^S(f^S)} \tag{2.141}$$

and

$$\beta_*^L = \left\{ \frac{\partial(\rho_*^L)^{-1}}{\partial P} \right\}_{T,C^L} , \tag{2.142}$$

b) the thermal expansion co-efficient

$$\alpha_{t_*}^S = \left\{ \frac{\partial(\rho_*^S)^{-1}}{\partial T} \right\}_{P,C^S(f^S)} \tag{2.143}$$

and

$$\alpha_{t_*}^L = \left\{ \frac{\partial(\rho_*^L)^{-1}}{\partial T} \right\}_{P,C^L} , \text{ and} \tag{2.144}$$

c) the specific heat capacity

$$C_{P_*}^S = \left\{ \frac{\partial S_*^S}{\partial T} \right\}_{P,C^S(f^S)} \tag{2.145}$$

and

$$C_{P_*}^L = \left\{ \frac{\partial S_*^L}{\partial T} \right\}_{P,C^L} . \tag{2.146}$$

Note that as discussed for the equilibrium case (ie. equations 2.70 - 2.72), the evaluation of the thermodynamic coefficients expressed in equations (2.142 - 2.146) are evaluated outside the phase change region (ie. $C^L \neq C^L(P,T)$).

Using the metallurgical approximations given in Section 2.2.2 (ie. $C^S(P,T) = kC^L(P,T)$) the local interface equilibrium condition is expressed as $C_*^S = kC^L(P,T)$. Therefore as in the equilibrium case

$$\beta = \beta_0 + \Delta\beta , \tag{2.147}$$

$$\alpha_t = \alpha_{t_0} + \Delta\alpha_t \tag{2.148}$$

and

$$C_p = C_{p_0} + \Delta C_p \,, \tag{2.149}$$

where :

$$\beta_0 = g^S \beta_*^S + g^L \beta_*^L \,, \tag{2.150}$$

$$\alpha_{t_0} = g^S \alpha_{t_*}^S + g^L \alpha_{t_*}^L \,, \tag{2.151}$$

$$C_{p_0} = \phi C_{p_*}^S + (1-\phi) C_{p_*}^L \,, \tag{2.152}$$

$$\Delta\beta = \frac{\rho\delta^2(1-\phi)}{\bar{\mu}(1-k)^2 C^{L^2}} \,, \tag{2.153}$$

$$\Delta\alpha_t = \frac{\rho\delta L(1-\phi)}{\bar{\mu}T(1-k)^2 C^{L^2}} \tag{2.154}$$

and

$$\Delta C_P = \frac{L^2(1-\phi)}{\bar{\mu}T(1-k)^2 C^{L^2}} \,. \tag{2.155}$$

Note that in equations (2.153 - 2.156) $L^L = L$, $\delta^L = \delta$ and $\bar{\mu}^L = \bar{\mu}$.

Using equation (2.66) it can be shown that for the non-equilibrium case

$$\Delta\beta = \rho\delta \, \partial\phi/\partial P \,, \tag{2.156}$$

$$\Delta\alpha_t = -\rho\delta \, \partial\phi/\partial T \tag{2.157}$$

and

$$\Delta C_P = -L \, \partial\phi/\partial T \,, \tag{2.158}$$

which is equivalent to that obtained in the metallurgical literature.

## 2.4 Metallurgical examples

Two metallurgical examples are chosen to illustrate the differences between the local equilibrium and local non-equilibrium assumptions and the effects these assumptions have on the thermodynamic data. As only the local effects are being studied; macro effects, such as diffusion and convection, are ignored. An isolated system is studied where the average solute concentration and pressure are kept constant but where the temperature is lowered externally for solidification

to occur. The first example, solidification of an Ag-Cu alloy, was chosen as the differences between the equilibrium and the non-equilibrium phase change processes can be clearly illustrated. Due to the lack of metallurgical and thermodynamic data for the Ag-Cu alloy at high pressures, an Al-Si system was chosen to illustrate the effect of pressure on the solidification process. As has been previously stated in Section 2.1, in most metallurgical processes the solidification or melting process is conducted at pressures of the order of atmospheric pressure. At these pressures the effects on the thermodynamic characteristics of the process are negligible and pressure is thus ignored. At very high pressures this is not the case as the thermodynamic characteristics are considerably influenced. This is illustrated in the Al-Si example.

### 2.4.1 Solidification of an Ag-Cu alloy

The solidification of an isolated Ag-Cu alloy system, under constant pressure and constant average solute concentration, is described. The pressure is fixed at atmospheric pressure and the average solute concentration is fixed at $\bar{C} = 0.05$ (ie. 5% wt Cu).

The solidification process is illustrated with the use of a linear approximation to the equilibrium phase diagram, Figure 2.5. For the local equilibrium assumption, the sample is totally solidified at $T = T^S$, whereas when the local non-equilibrium assumption is used, total solidification only occurs once the eutectic has been reached (ie. $T = T_e$). For the equilibrium case the average solute concentration of the solid lies on the solidus (ie. $\bar{C}^S = C^S(T)$) whereas for the non-equilibrium case the average solid solute concentration is lower in composition than the solidus value for the same temperature (ie. $\bar{C}^S < C^S(T)$).

In Figure 2.6 the evolution of solid mass fraction for both the equilibrium and the non-equilibrium cases are shown. For the equilibrium case, the sample element is 100% solidified at $T = T^S$ whereas for the non-equilibrium case the sample element is only 80% solidified at $T = T^S$. Solidification, under the non-equilibrium assumption, continues on into the eutectic region where approximately 8% of the solid solidifies at the eutectic. The solid mass fraction values for the equilibrium case are obtained by solving equation (2.12) and that for the non-equilibrium case are found by integrating equation (2.120) with $\bar{C}$ kept constant, resulting in the standard Schiel equation. Thus the values of the average solid solute concentration, see Figures 2.6 and 2.8, are obtained by substituting the value of solid mass fraction, obtained from the Schiel equation, into equation (2.105) and solving.

Figures 2.7 and 2.8 depict the variation in the solute profiles in the sample element during solidification and after total solidification, for the non-equilibrium assumption. Figure 2.7 illustrates equilibrium with respect to the interface and liquid. The solid solute exhibits a profile which is a trace of the equilibrium interface values for different values of solid mass fraction. In Figure 2.8 the variation in the solid solute concentration in the solidified form is shown. It is clearly shown that the profile takes an immediate jump at $T = T_e$ with the remaining solid solidifying at a constant eutectic solute concentration $C_e$ (ie. see Figure 2.3).

Figures 2.9 and 2.10 illustrate the variation in the Gibbs free energy $\Phi$ and the enthalpy H of the system for both the equilibrium and non-equilibrium cases. The Gibbs free energy of the

system is expressed for the phase mixture for the equilibrium case by equation (2.18) and for the non-equilibrium case by equation (2.108). The enthalpy of the phase mixture is expressed using a Legendre transformation of Gibbs free energy as

$$H = \Phi + TS \, . \tag{2.159}$$

The free energy for each phase $\alpha$ is thus calculated as

$$\Phi^{\alpha} = H^{\alpha} - TS^{\alpha} \, , \tag{2.160}$$

where the enthalpy $H^{\alpha}$ and entropy $S^{\alpha}$ for the phase $\alpha$ are calculated using the ideal mixture approximation and are expressed as

$$H^{\alpha} = C^{\alpha} H^{\alpha}_{Cu} + (1 - C^{\alpha}) H^{\alpha}_{Ag} \tag{2.161}$$

and

$$S^{\alpha} = C^{\alpha} S^{\alpha}_{Cu} + (1 - C^{\alpha}) S^{\alpha}_{Ag} \, . \tag{2.162}$$

The enthalpy for each constituent $i$ of phase $\alpha$ is evaluated as

$$H^{\alpha}_{i} = \Delta H^{f}_{298} + \int_{298}^{T} C^{\alpha}_{p_i}(\tau) \, d\tau \, , \tag{2.163}$$

where $\Delta H^{f}_{298}$ is the heat of formation of the component at the reference temperature 298 K .

The entropy for each constituent $i$ of phase $\alpha$ is evaluated as

$$S^{\alpha}_{i} = S^{0}_{298} + \int_{298}^{T} \frac{C^{\alpha}_{p_i}(\tau)}{\tau} \, d\tau \, , \tag{2.164}$$

where $S^{0}_{298}$ is the standard entropy of the component at the reference temperature 298 K .

The values of the heats of formation, standard entropies and heat capacities are given for Ag and Cu in Table 2.1, Rao [22].

In Figures 2.9 and 2.10 it can be seen that the free energy and enthalpy of the phase mixture reach their solid values at far higher temperatures (ie. $T = T^{S}$) for the equilibrium case than for the non-equilibrium case. This is consistent with the evolution of solid mass fraction, see

| Component | $\Delta H^f_{298}$ KJ/mol | $S^0_{298}$ J/mol K | $C_p$ J/mol K |
|---|---|---|---|
| $Ag^S$ | 0.000 | 42.550 | $21.297 + (8.535 \times 10^{-3}T) + (1.506 \times 10^5 T^{-2})$ |
| $Ag^L$ | 8.936 | 47.187 | 30.543 |
| $Cu^S$ | 0.000 | 33.150 | $22.635 + (6.276 \times 10^{-3}$ T) |
| $Cu^L$ | 9.305 | 36.246 | 31.380 |

Table 2.1: Heats of formation, Standard entropies and Specific heats for $Ag^\alpha$ and $Cu^\alpha$

Figure 2.6. Once the eutectic region is reached (ie. $T = T_e$) both the Gibbs free energy and the enthalpy exhibit a jump from their respective values in the mushy region to their respective solid values.

The specific heat of the phase mixture is shown in Figure 2.11 for both the equilibrium and non-equilibrium cases. As discussed in Section 2.2, it is clearly illustrated in Figure 2.11 that the specific heat is far larger in the mushy zone than in the adjacent regions of pure phase resulting in discontinuities between the mushy and pure phase regions. At the eutectic (ie. $T = T_e$) the specific heat, for the non-equilibrium case, becomes infinite (some very large value). The reason for this is that $C_p \propto \partial\phi/\partial T$ (ie. see equations 2.97 and 2.158) where $\partial\phi/\partial T$ is infinite (has a very large value) at the eutectic. Expressions for the specific heat are given for the equilibrium case by equation (2.83) and for the non-equilibrium case by equation (2.149) where the latent heat is defined as

$$L = H^L - H^S \tag{2.165}$$

and the chemical potential $\bar{\mu}$ is found by substituting the latent heat expressed in equation (2.165) into equation (2.90). Note it can also be shown that the specific heat can be derived from the enthalpy expression of the phase mixture as

$$C_p = \partial H/\partial T\,, \tag{2.166}$$

where the enthalpy of the phase mixture is expressed as

$$H = \phi H^S + (1-\phi) H^L. \tag{2.167}$$

Thus, where the enthalpy curve exhibits a jump at the eutectic temperature the specific heat must tend to infinity. As with the evolution of solid mass fraction the temperature range for the variation of specific heat in the mushy region is far smaller for the equilibrium case than that for the non-equilibrium case.

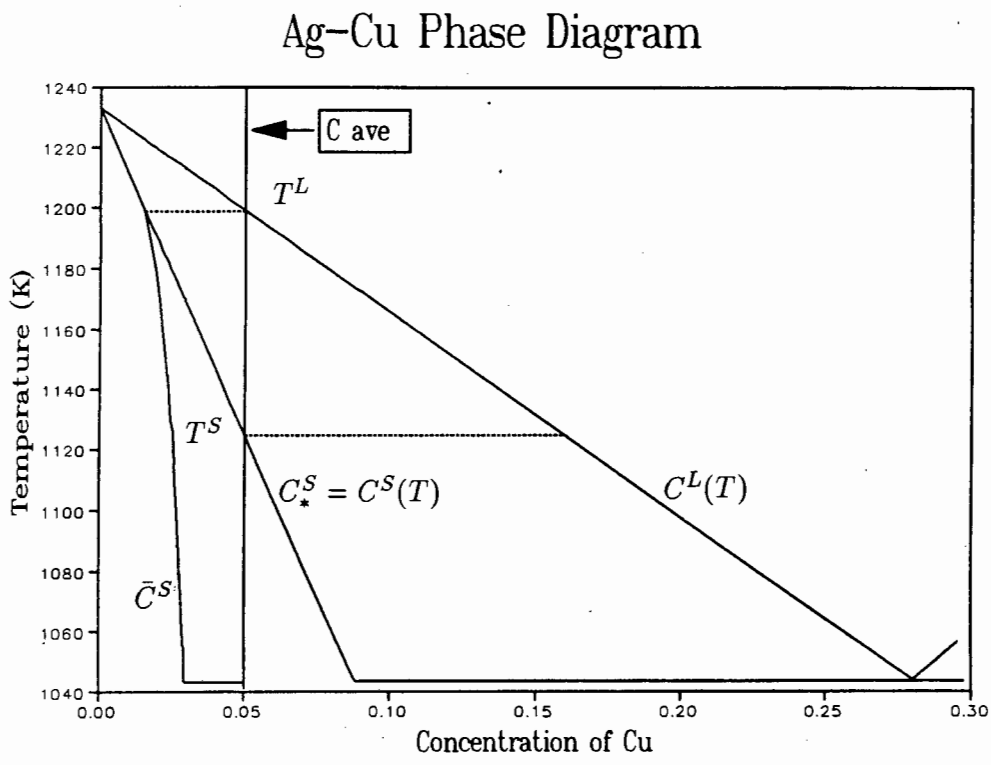


Figure 2.5: Ag-Cu phase diagram depicting equilibrium and non-equilibrium solidification for $\bar{C} = 0.05$

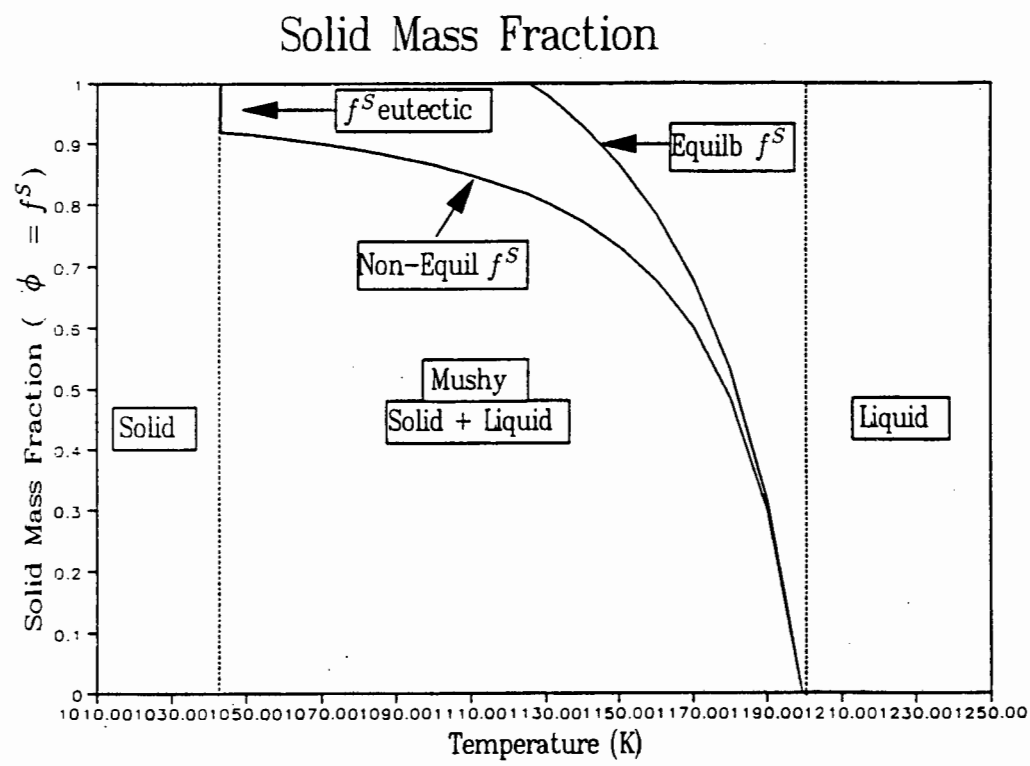


Figure 2.6: A plot of the solid mass fraction versus temperature for equilibrium and non-equilibrium solidification of an Ag-Cu alloy where $\bar{C} = 0.05$ .

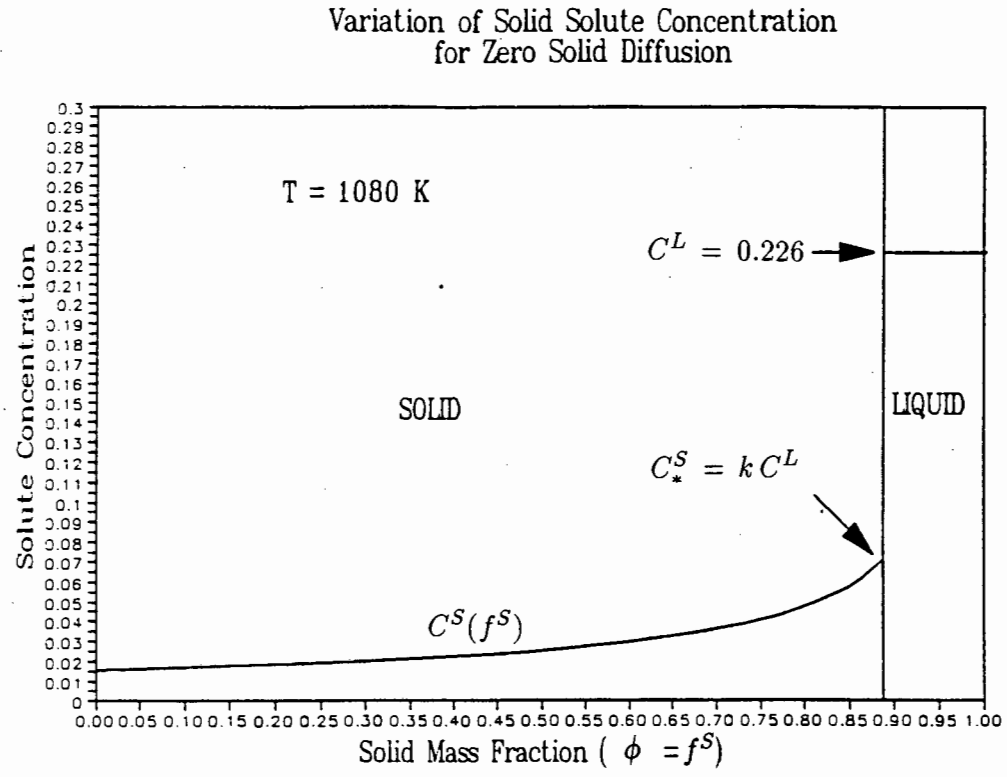


Figure 2.7: Schematic of the Ag-Cu volume element illustrating the solute profiles during non-equilibrium solidification.

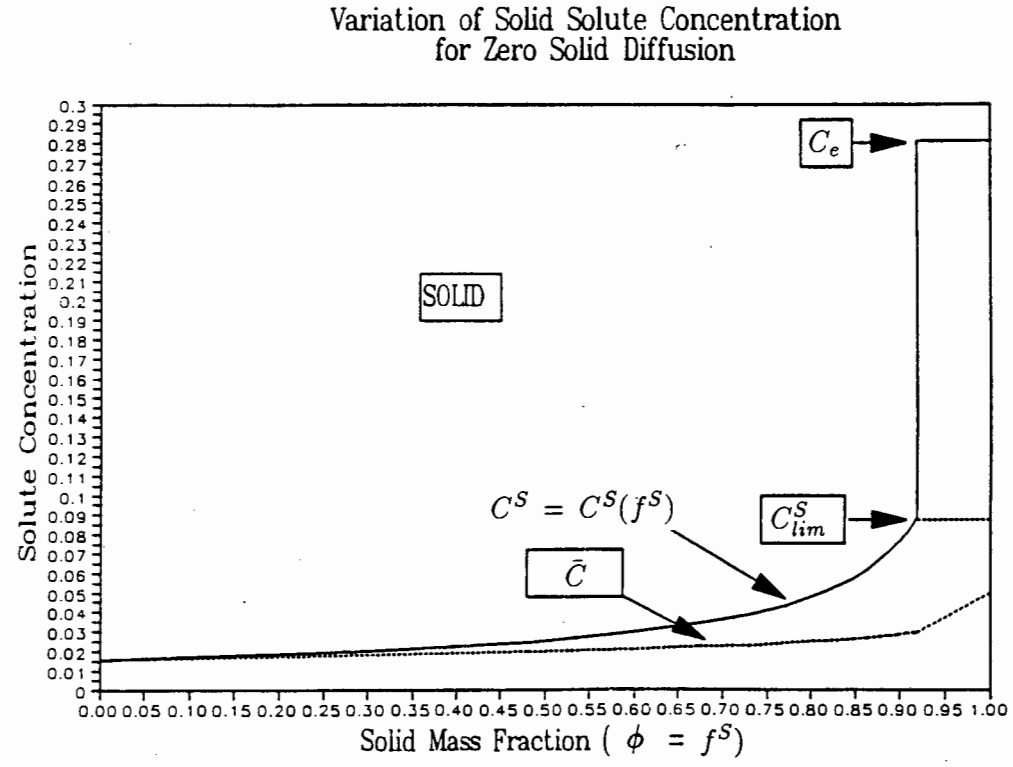


Figure 2.8: Schematic of the solidified Ag-Cu volume element illustrating the solute profile obtained by non-equilibrium solidification.

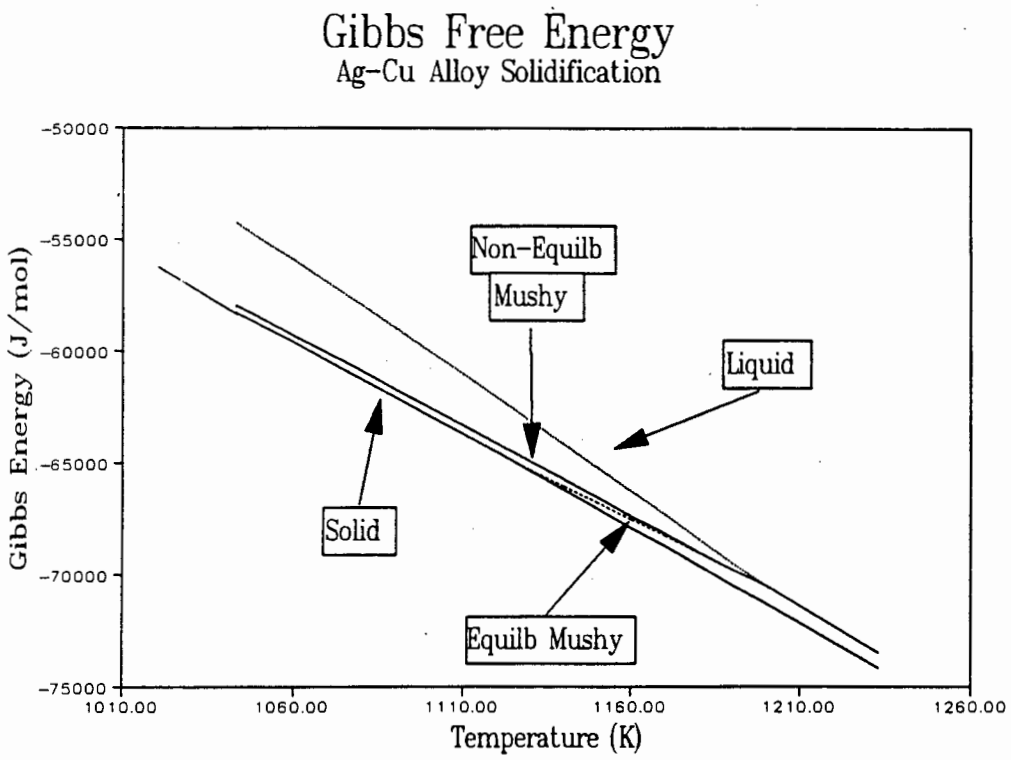


Figure 2.9: A plot of Gibbs free energy versus temperature for equilibrium and non-equilibrium solidification of an Ag-Cu alloy where $\bar{C} = 0.05$.

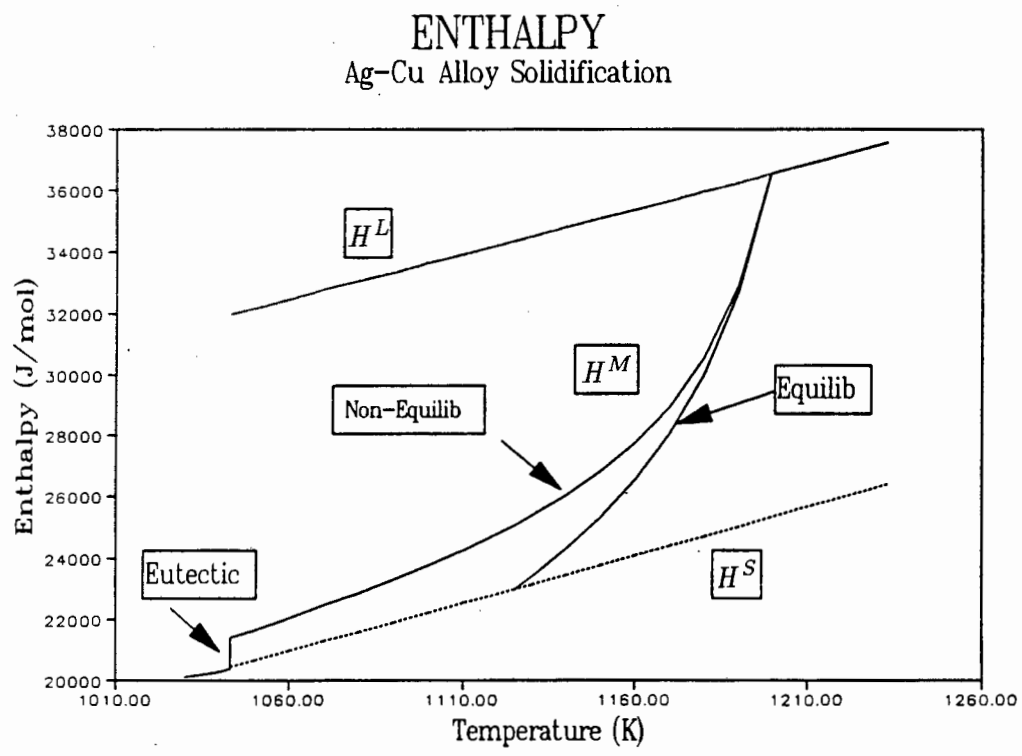


Figure 2.10: A plot of enthalpy versus temperature for equilibrium and non-equilibrium solidification of an Ag-Cu alloy where $\bar{C} = 0.05$.

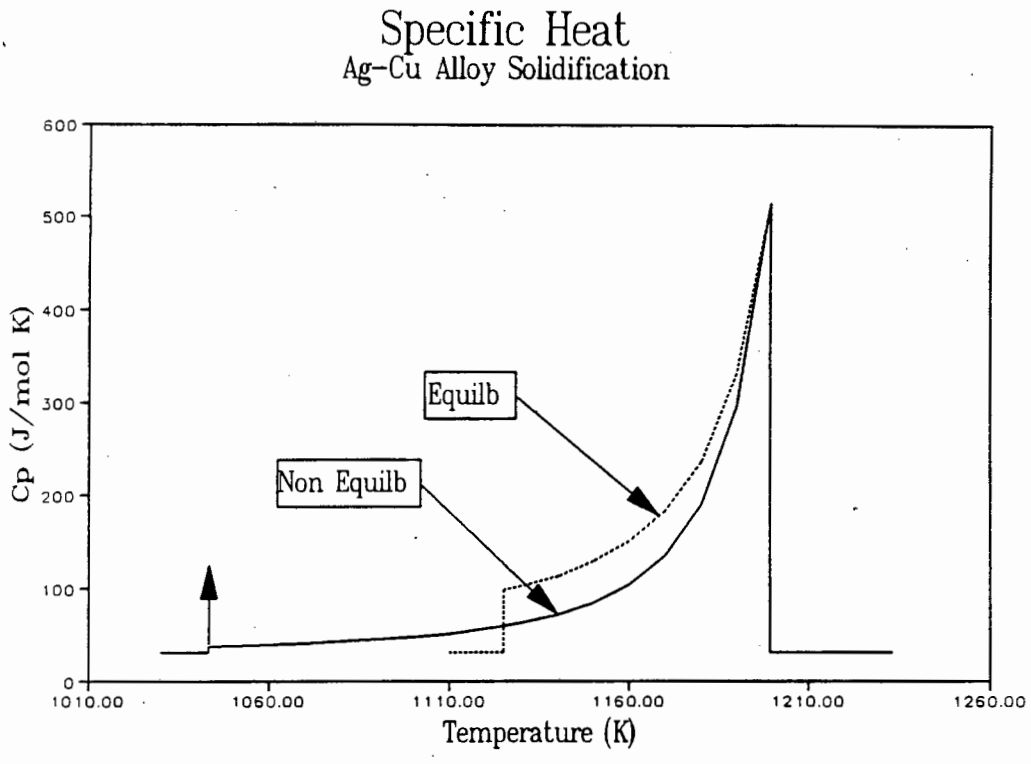


Figure 2.11: A plot of the specific heat capacity versus temperature for equilibrium and non-equilibrium solidification of an Ag-Cu alloy where $\bar{C} = 0.05$.

### 2.4.2 Solidification of an Al-Si alloy

As stated at the beginning of this section, this example is used to illustrate the effect of pressure on the solidification process. The reason for choosing the Al-Si alloy for this example was solely due to the availability of data at high pressures, Thomas [23]. The solidification of a sample under different pressures for a fixed average solute concentration, $\bar{C} = 0.05$ (ie. 5% wt Si), is described. The phase diagram of the Al-Si system at atmospheric pressure is shown in Figure 2.12. In Figure 2.13 the variation of the eutectic temperature with respect to pressure is shown. It can be seen that for an increase in pressure up to 4GPa the phase diagram is shifted 'upwards' with respect to temperature. Figures 2.13 and 2.14 clearly illustrate the increase in the liquidus temperatures with the increase in the pressure, especially from 0 - 4GPa.

The Gibbs free energy, enthalpy and thermodynamic coefficients are calculated and plotted at atmospheric pressure and at 2GPa where the slope of the temperature pressure curve is assumed linear. As behaviour of the energy and thermodynamic coefficients in the mushy region are dependent on the solid mass fraction, the solid mass fraction of the system is illustrated in Figure 2.15.

In Figures 2.16 and 2.17 the Gibbs free energy $\Phi$ and enthalpy H of the phase change system show a marked shift to higher temperatures for an increased pressure of 2Gpa. The effect of the equilibrium and non-equilibrium assumptions on the Gibbs free energy and enthalpy are not significant. This is because for $\bar{C} = 0.05$, eutectic solidification will occur for both cases. The temperature range for solidification is thus the same for both cases. From Figures 2.16

and 2.17 it can be seen that the system solidifies at a lower enthalpy and free energy for the equilibrium case than for the non-equilibrium case. This is consistent with the evolution of solid mass fraction, see Figure 2.15. The equations used to plot the Gibbs free energy and enthalpy are the same as that presented for the Ag-Cu example in Section 2.4.1 but where the enthalpy and entropy for Al and Si of the phase $\alpha$ is expressed using the ideal mixture approximation as

$$H^{\alpha} = C^{\alpha} H^{\alpha}_{Si} + (1 - C^{\alpha}) H^{\alpha}_{Al} \tag{2.168}$$

and

$$S^{\alpha} = C^{\alpha} S^{\alpha}_{Si} + (1 - C^{\alpha}) S^{\alpha}_{Al} \, . \tag{2.169}$$

The values of the heats of formation, standard entropies and heat capacities for Al and Si are given in Table 2.2, Rao [22].

| Component | $\Delta H^{f}_{298}$ KJ/mol | $S^{0}_{298}$ J/mol K | $C_p$ J/mol K |
|---|---|---|---|
| $Si^S$ | 0.000 | 18.810 | $23.933 + (2.469 \times 10^{-3} T) - (4.142 \times 10^{5} T^{-2})$ |
| $Si^L$ | 48.472 | 44.459 | 27.196 |
| $Al^S$ | 0.000 | 28.350 | $20.669 + (12.385 \times 10^{-3}$ T) |
| $Al^L$ | 8.233 | 34.735 | 31.798 |

Table 2.2: Heats of formation, Standard entropies and Specific heats for $Si^{\alpha}$ and $Al^{\alpha}$

In Figures 2.16 - 2.19 plots of the variations in specific heat $C_p$ thermal expansion coefficient $\alpha_t$ and isothermal compression coefficient $\beta$ are shown at atmospheric pressure and at 2GPa. Variations in the coefficients using the equilibrium and the non-equilibrium assumption are also shown. The equations used to plot the variations in $C_p$, $\alpha_t$ and $\beta$ are expressed for the equilibrium case by equations (2.81 - 2.83) and for the non-equilibrium case by (2.147 - 2.149). Where the latent heat L, given by equation (2.165), the volumetric expansion $\delta$ and chemical potential $\bar{\mu}$ obtained from equations (2.90) and (2.91) respectively, are used to solve equations (2.81 - 2.83) and (2.147 - 2.149).

The solid and liquid values for $C_p$ are given in Table 2.2 and the solid and liquid values of $\rho$ and $\alpha_t$ were obtained from Smithells [24]. Solid and liquid values for $\beta$ for Al and Si could not be found. As proven in Sections 2.1 and 2.2 (ie. equations 2.95 - 2.97 and equations 2.156 - 2.158) the coefficients are functions of derivatives of the solid mass fraction $\phi$. Thus at the eutectic $C_p, \alpha_t$ and $\beta$ all infinite (some large value). It is clear in Figures 2.16 - 2.19 that the values of $C_p, \alpha_t$ and $\beta$ are far larger in the mushy region than in the regions of pure phase resulting in discontinuities at the boundaries of the mushy region. The difference in the values for the non-equilibrium and equilibrium assumptions are not significant, with the non-equilibrium values being lower than the equilibrium values.

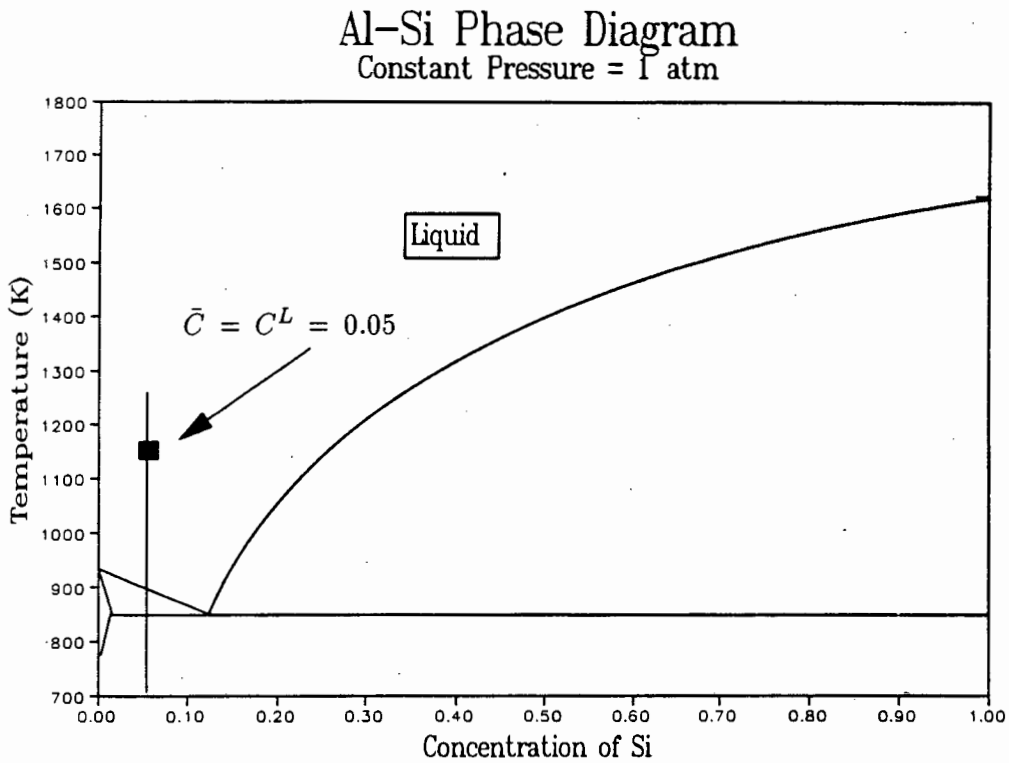


Figure 2.12: Al-Si phase diagram

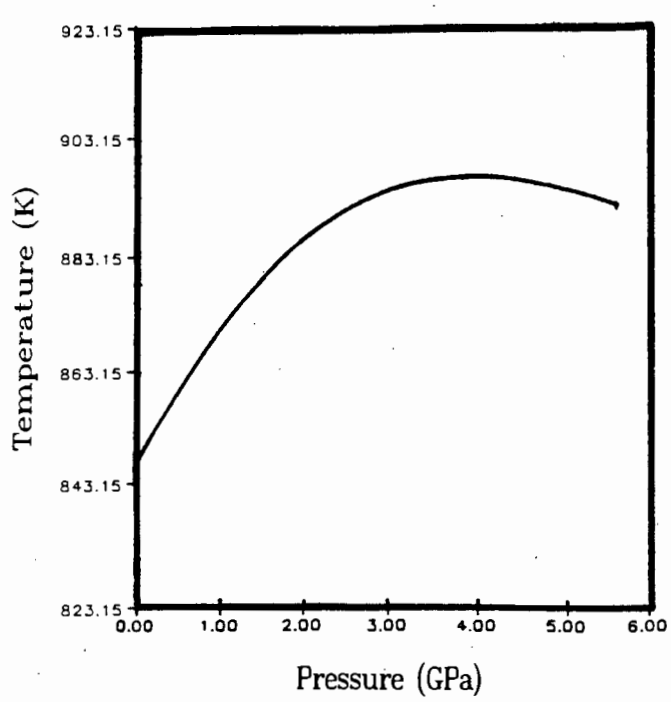


Figure 2.13: A plot of the eutectic temperature versus pressure for an Al-Si alloy.

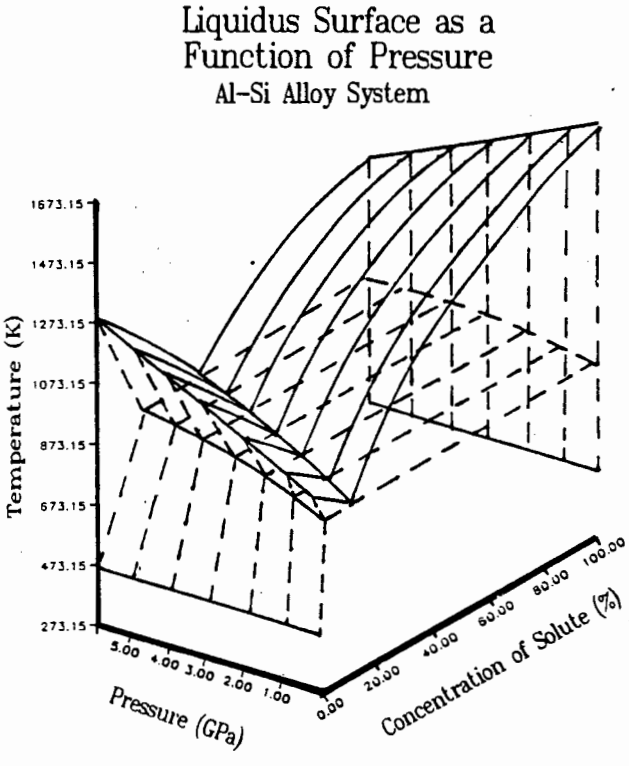


Figure 2.14: A plot showing the variation of the liquidus at different pressures for an Al-Si alloy.

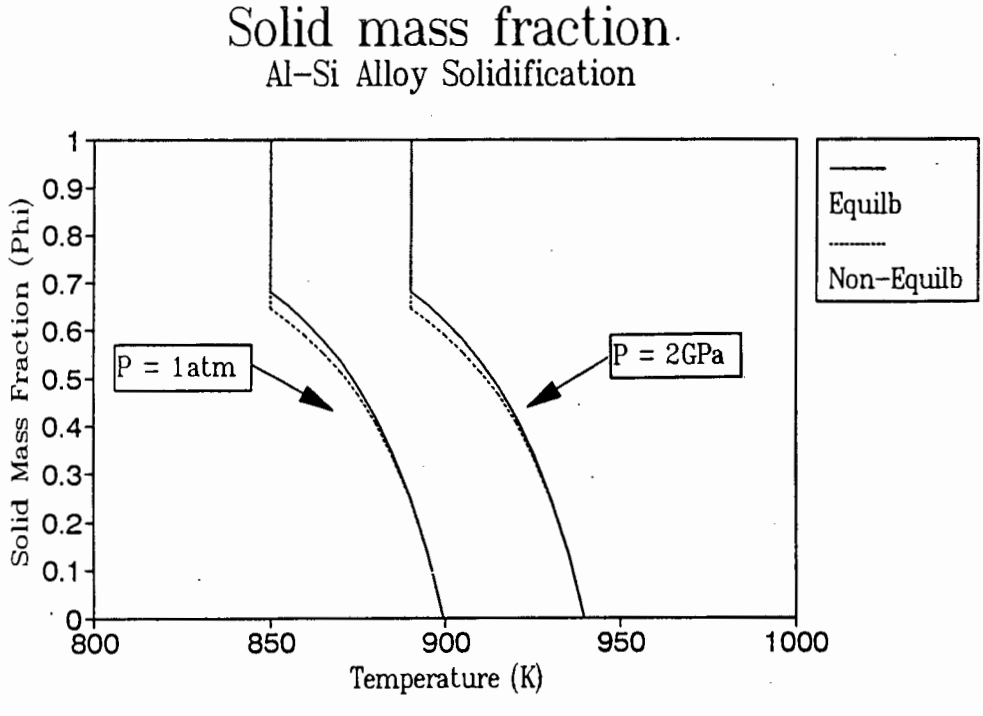


Figure 2.15: A plot of solid mass fraction versus temperature at atmospheric pressure and at 2GPa for the solidification of an Al-Si alloy where $\bar{C} = 0.05$.

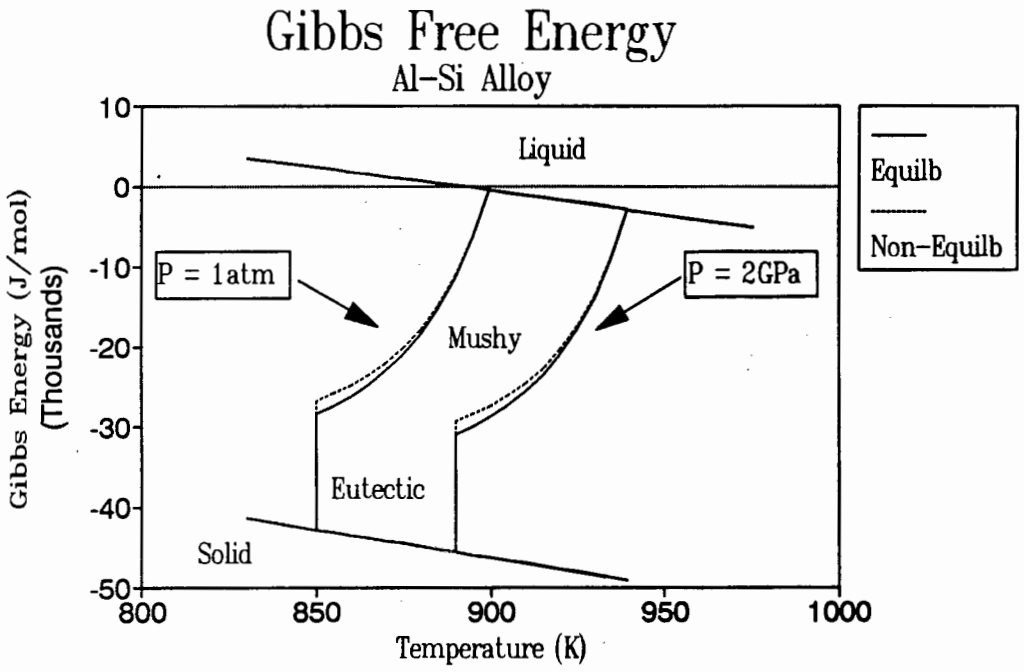


Figure 2.16: A plot of Gibbs free energy versus temperature at atmospheric pressure and at 2GPa for the solidification of an Al-Si alloy where $\bar{C} = 0.05$.

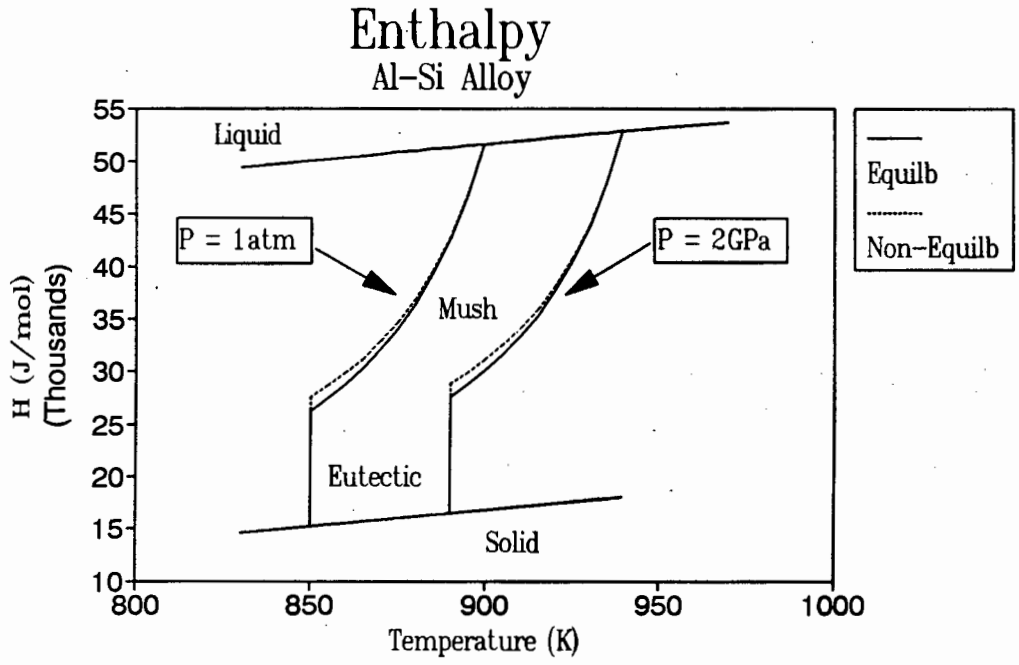


Figure 2.17: A plot of enthalpy versus temperature at atmospheric pressure and at 2GPa for the solidification of an Al-Si alloy where $\bar{C} = 0.05$.

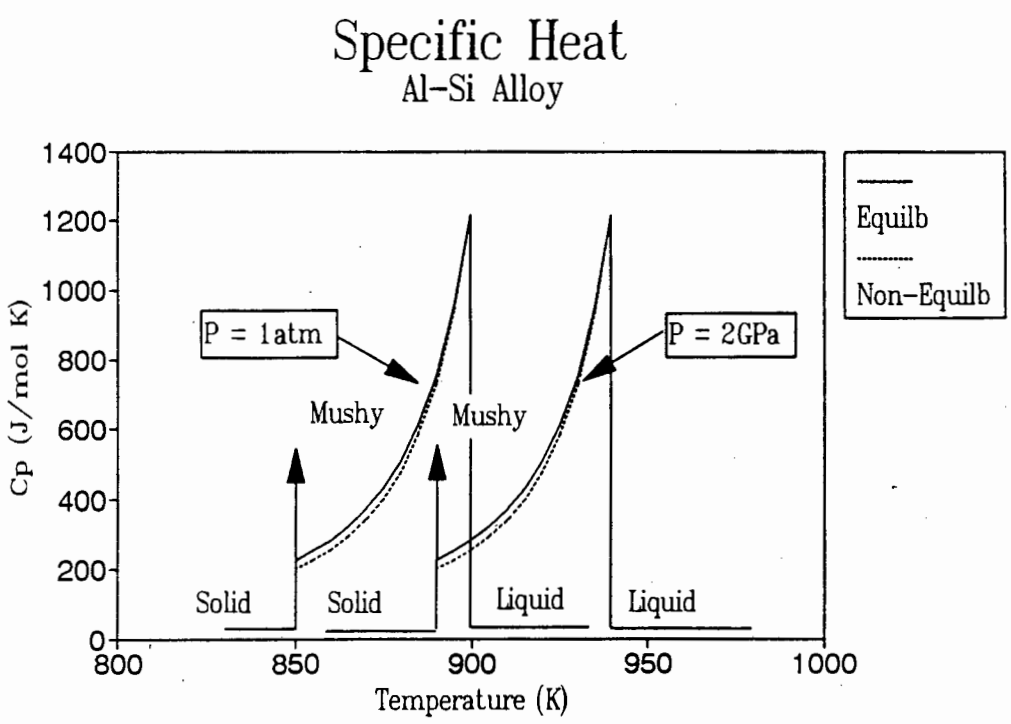


Figure 2.18: A plot of the specific heat capacity versus temperature at atmospheric pressure and at 2GPa for the solidification of an Al-Si alloy where $\bar{C} = 0.05$.

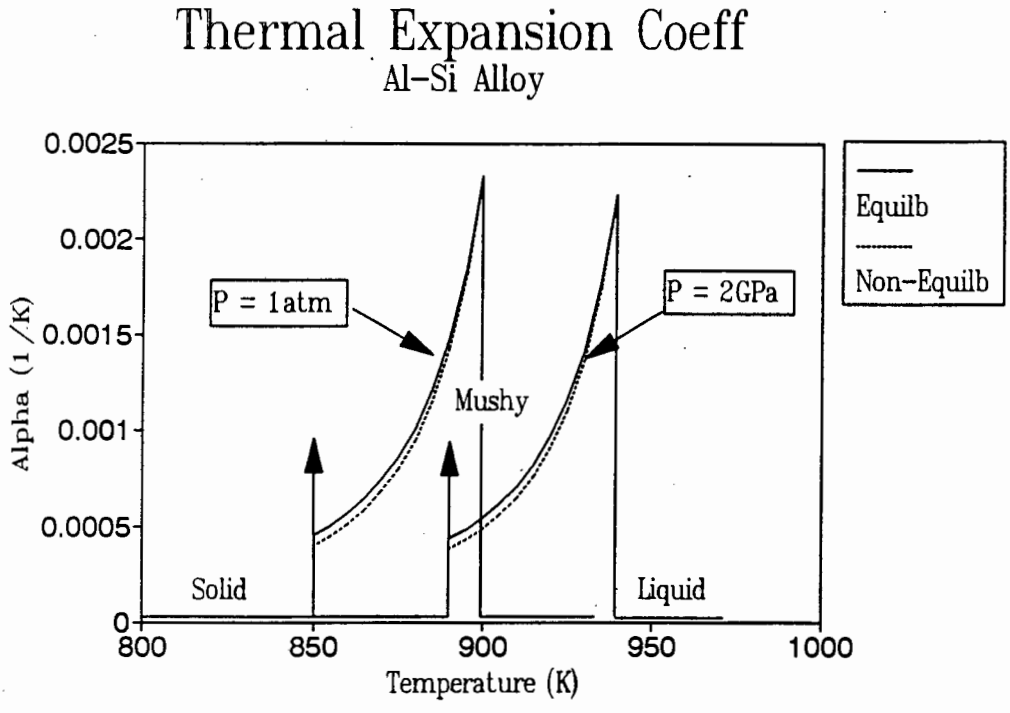


Figure 2.19: A plot of the thermal expansion coefficient versus temperature at atmospheric pressure and at 2GPa for the solidification of an Al-Si alloy where $\bar{C} = 0.05$.

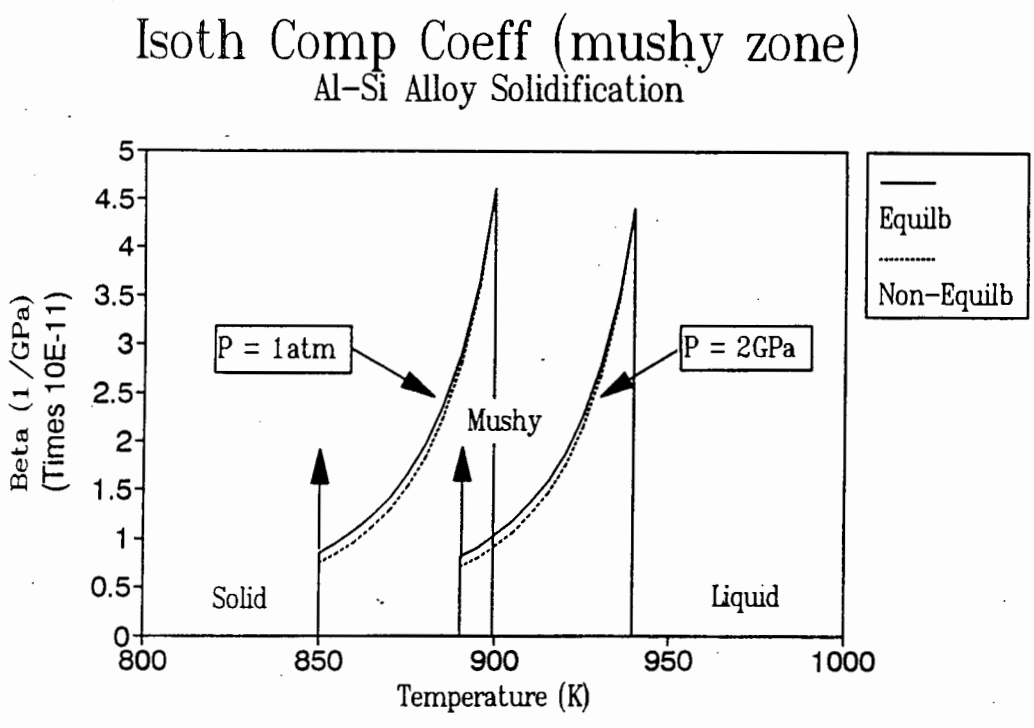


Figure 2.20: A plot of the change in isothermal compression coefficient versus temperature, in the mushy region, at atmospheric pressure and at 2GPa for the solidification of an Al-Si alloy where $\bar{C} = 0.05$.

## 2.5 Conclusions

In this chapter, a free energy description of the local evolution of the mushy region has been described. The local description was defined on the scale of a dendrite or equiaxed crystal. Two cases were considered: local equilibrium and local non-equilibrium.

For the local equilibrium case, the solute concentration levels in the solid crystal are in equilibrium with the surrounding liquid throughout the solidification/melting process. For the local non-equilibrium case, the solute concentration levels in the solid crystal are not in equilibrium with the surrounding liquid throughout the solidification/melting process. The equilibrium case is representative of the solidification/melting of small particles where the time taken for equilibrium to be attained, especially in the solid, is within the time of the phase change. The non-equilibrium case is representative of the solidification/melting of large particles where the diffusion rate within the solid is too slow to attain uniform equilibrium with the surrounding liquid, within the time of phase change. It is assumed, therefore, that the local diffusion rates for the equilibrium case are infinite in both the solid and the liquid, whereas for the non-equilibrium case, the diffusion rate in the liquid is assumed infinite and that in the solid is assumed to be zero. For the non-equilibrium case, interface equilibrium is maintained for solidification but cannot be guaranteed for remelting. Using the assumption of Rappaz and Voller [20], interface equilibrium is maintained for the non-equilibrium case when remelting occurs.

The thermodynamic description of the equilibrium case is similar to that of Hills, Loper and Roberts [4] where the free energy of the phase mixture is described in terms of three independent variables; pressure P, temperature T and average solute concentration $\bar{C}$. Similarly, the entropy S and the volume $\rho^{-1}$ of the phase mixture are described in terms of P,T and $\bar{C}$. Phase equilibrium is obtained when the chemical potentials of each phase are equal (ie. $\mu^S = \mu^L$) and from this equilibrium condition, expressions for the solidus and liquidus are derived. Therefore, using the expressions obtained for the solidus and liquidus, expressions for the thermodynamic coefficients are derived. When using the linear phase diagram assumption, the interphase terms of the thermal expansion coefficient $\alpha_t$ and the specific heat capacity $C_p$ are shown to be directly proportional to the derivatives of the solid mass fraction with respect to temperature. Similarly, the interphase term of the isothermal compression coefficient $\beta$ is shown to be the directly proportional to the derivatives of the solid mass fraction with respect to pressure.

For the non-equilibrium case the thermodynamic formulation differs from that of Hills and Roberts [21] in that the free energy is expressed in terms of a functional of the solid solute concentration, instead of the average solid solute concentration. The free energy description presented in this work, therefore, is able to account for the solidification history thus enabling remelting to be described. Therefore, together with the assumption of local interface equilibrium, the free energy can be expressed in terms of the three variables; temperature T, pressure P and average solute concentration $\bar{C}$. The volume $\rho^{-1}$ and entropy S are also described as functions of P, T and $\bar{C}$. The thermodynamic coefficients that are subsequently derived from the differential forms of entropy and volume are expressed in terms of a lever rule of their respective solid and liquid values. The expressions for the solid phase coefficients in the mushy region maintain their pure solid phase values whereas the corresponding liquid coefficients include interphase terms. The chemical potential $\mu$ of the phase mixture is expressed in terms of the interface solute concentrations which in turn is equal to the liquid chemical potential $\mu^L$. This illustrates equilibrium with respect to the interface and the liquid. The chemical potential values in the rest of the solid are not equal to $\mu$, except at the interface, thus illustrating non-equilibrium with respect to the remaining solid. As for the equilibrium case, when using the linear phase diagram assumption, the interphase terms of the thermal expansion coefficient $\alpha_t$ and the specific heat capacity $C_p$ are shown to be the directly proportional to the derivatives of the solid mass fraction with respect to temperature. Similarly, the interphase term of the isothermal compression coefficient $\beta$, is shown to be the directly proportional to the derivatives of the solid mass fraction with respect to pressure.

To illustrate the differences between local equilibrium and local non-equilibrium two metallurgical examples were chosen. For both examples the solidification of a closed sample volume element, was studied. The first example considered the solidification of an Ag-Cu binary alloy at atmospheric pressure and the second example considered the solidification of an Al-Si binary alloy at atmospheric pressure and at 2GPa. These examples show the variations in the Gibb's free energy, enthalpy, solid mass fraction and the thermodynamic coefficients as a function of temperature. In the first example there are distinct differences in the results between the equilibrium and non-equilibrium cases. For the equilibrium case the element is totally solidified once the solidus is reached whereas for the non-equilibrium case final solidification occurs at the eutectic . This is to be expected, as in the non-equilibrium case, due to zero solid diffusion, solute is rejected into the liquid delaying solidification, whereas for the equilibrium case, the solute is

diffused completely into the solid with no solute rejection into the liquid and therefore no delay in solidification. In the second example little difference between the results for the equilibrium and non-equilibrium cases occur as in both cases the final solidification will be eutectic. The effect of increasing the pressure uniformly to 2GPa does not change the trend in the results but shifts the solidification to a higher temperature. The net effect is to shift the phase diagram upwards.

# CHAPTER 3
# GOVERNING GLOBAL CONSERVATION EQUATIONS

## 3.1 Introduction

The global behavior of the solid-liquid phase change process is now discussed. The evolution of the solidification or melting process is governed by a set of globally defined conservation equations. These equations model the behavior of the temperature, pressure and solute concentration of solute on a macroscopic scale and the variation in these variables in turn effect the solid-liquid phase change process on a local level. Conversely the assumptions used in the local models effect the form of the global conservation equations. The conservation equations are usually defined for both the solid and liquid phase and are coupled through interphase boundary conditions. In alloy solidification/melting the phase change process takes place over a temperature range where the region is made up of a crystal (dendritic) matrix and interspersed solid particles surrounded with liquid. The two phase formulation would be impractical in this circumstance. Therefore, the idea would be to have a single set of equations which can account for the whole region. Models of this kind, usually termed continuum models, have been formulated by a number of authors, Bennon and Incropera [1], Voller, Brent and Prakash [18] and Hills, Loper and Roberts [4]. The formulations for these models are generally based on classical mixture theory [10 - 13] but can also be developed from volume-averaging techniques [25 - 27].

The conservation equations which are used to describe the solidification/melting process macroscopically are the equations of mass, solute, momentum and energy, where the driving forces in the liquid and mushy region are convection and diffusion and in the solid region diffusion only. Depending on the process the system may be convection dominated or diffusion dominated or both.

The continuum formulation presented in this work is based on general mixture theory where the assumptions of local non-equilibrium and local equilibrium are included. Most of the continuum formulations presented in the literature are based local equilibrium assumptions [1], [18], [4] and [28], except Voller, Brent and Prakash [18] who include local non-equilibrium assumptions for the solidification case only.

The development of conservation equations from general mixture theory is based on the following principles, Bennon and Incropera [1]: firstly, mixture components may be viewed as isolated subsystems, if interactions with other mixture components are properly treated; secondly all properties of the mixture are mathematical consequences of the component properties; and thirdly, the mean collective mixture behaviour is governed by equations similar to those governing the individual components. Since these principles presume an inert mixture, application to multiphase, multiconstituent mixtures requires special care. While the phases can generally be considered as isolated, their constituents are often inseparable due to intimate bonding on

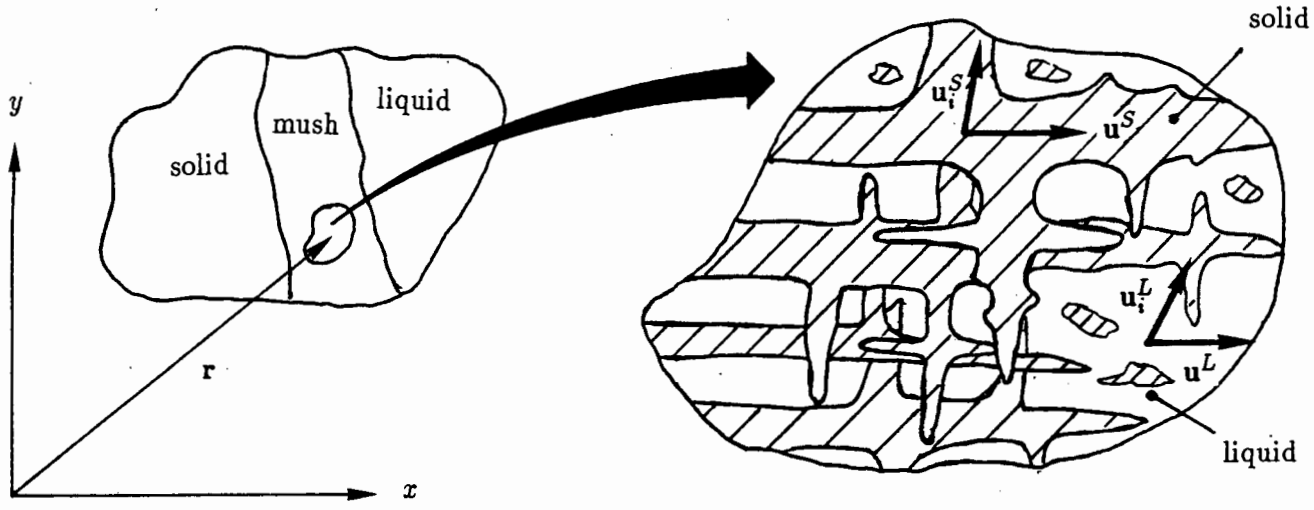


Figure 3.1: A 2D representation of the continuum.

an atomic level. Furthermore, since the properties of a non-inert mixture are not direct mathematical consequences of the component properties, application of mixture theory to non-inert systems requires additional information concerning the behaviour of the mixture constituents on an atomic scale. For many applications this information is obtained using phase diagrams, or empirical relationships.

In the present formulation a constituent represents a basic chemical element or compound in a binary mixture, and a phase represents a quantity of matter which is homogeneous in physical structure and comprises one or more of the constituents. Phases are assumed to be distinct and separable components of the continuum, although they need not be homogeneous in chemical composition. The system comprised of two (in this case) or more constituents, and two distinct separable phases of solid and liquid, is viewed as a continuum in which any location $\mathbf{r}$ can be simultaneously occupied by all constituents and all phases, see Figure 3.1. The mean velocity of the constituents comprising phase $\alpha$, relative to fixed reference frame, see Figure 3.1, is $\mathbf{u}^\alpha$ which is termed the mass averaged phase velocity. Therefore for each phase $\alpha$ the mass averaged velocity for that phase is defined as

$$\mathbf{u}^\alpha = C^\alpha \mathbf{u}_1^\alpha + (1 - C^\alpha)\mathbf{u}_2^\alpha , \tag{3.1}$$

where $\mathbf{u}_1^\alpha$ and $\mathbf{u}_2^\alpha$ are the intrinsic velocities of each constituents 1 and 2, relative to a fixed reference frame and $C^\alpha$ is the mass concentration of solute (constituent 1), see equation (2.3). The diffusion velocity of constituent $i$ in phase $\alpha$ is therefore described as $\mathbf{u}_i^\alpha - \mathbf{u}^\alpha$.

For the continuum the mass averaged velocity is therefore expressed as

$$\mathbf{u} = \phi \mathbf{u}^S + (1 - \phi)\mathbf{u}^L. \tag{3.2}$$

In the following sections general descriptions of the conservation equations of mass, solute, momentum and energy including the entropy growth and a constitutive model of the dendritic phase change process are discussed.

## 3.2 Conservation of mass

For an arbitrary fixed control volume V, of surface area A, which is larger than the sample element but smaller than the dimensions of the domain, the conservation of mass for the phase $\alpha$ is given as

$$\int_V \dot{m}^\alpha \mathrm{d}V^\alpha = \frac{\partial}{\partial t} \int_V \rho_*^\alpha \mathrm{d}V^\alpha + \int_A \rho_*^\alpha \mathbf{u}^\alpha \bullet \mathbf{n}\, \mathrm{d}A^\alpha , \tag{3.3}$$

where $\dot{m}^\alpha$ is the rate of creation of phase $\alpha$, $\rho_*^\alpha$ is the intrinsic density of phase $\alpha$ and $\mathbf{u}^\alpha$ is the mass averaged velocity of phase $\alpha$. Note that the differential surface area $\mathrm{d}A^\alpha$ is assumed to be equal to $\mathrm{g}^\alpha\, \mathrm{d}A$. Since $\mathrm{g}^\alpha$ is assumed to be continuous and $\sum_\alpha \mathrm{g}^\alpha = 1$, the integrands of equation (3.3) are continuous and differentiable functions. Thus since the control volume is arbitrary, equation (3.3) can be expressed as

$$\mathrm{g}^\alpha \dot{m}^\alpha = \frac{\partial \bar{\rho}^\alpha}{\partial t} + \nabla \bullet (\bar{\rho}^\alpha \mathbf{u}^\alpha) . \tag{3.4}$$

To conserve mass during solidification or melting, one phase has to be created at the expense of the other, therefore

$$\mathrm{g}^S \dot{m}^S + \mathrm{g}^L \dot{m}^L = 0 , \tag{3.5}$$

which results in the standard equation for the conservation of mass;

$$\frac{\partial \rho}{\partial t} + \nabla \bullet (\rho \mathbf{u}) = 0 . \tag{3.6}$$

Equation (3.6) can be re-expressed in the Lagrangian description as

$$\frac{D\rho}{Dt} + \rho \nabla \bullet \mathbf{u} = 0 , \tag{3.7}$$

where

$$\frac{D}{Dt} = \frac{\partial}{\partial t} + \mathbf{u} \bullet \nabla . \tag{3.8}$$

## 3.3 Conservation of solute

For an arbitrary fixed control volume described in section (3.2) one can denote the rate at which solute appears in a unit volume of phase $\alpha$ as

$$\int_V \dot{m}_1^\alpha \mathrm{dV}^\alpha = \frac{\partial}{\partial t}\int_V \rho_{*_1}^\alpha \mathrm{dV}^\alpha + \int_A \rho_{*_1}^\alpha \mathbf{u}_1^\alpha \bullet \mathbf{n}\, \mathrm{dA}^\alpha , \tag{3.9}$$

$$= \frac{\partial}{\partial t}\int_V \rho_{*_1}^\alpha \mathrm{dV}^\alpha + \int_A \rho_{*_1}^\alpha \mathbf{u} \bullet \mathbf{n}\, \mathrm{dA}^\alpha + \int_A \rho_{*_1}^\alpha (\mathbf{u}_1^\alpha - \mathbf{u}^\alpha)\, \mathrm{dA}^\alpha , \tag{3.10}$$

where $\dot{m}_1^\alpha$ is the rate at which solute (constituent 1) appears in phase $\alpha$, $\rho_{*_1}^\alpha$ is the intrinsic density of constituent 1 in phase $\alpha$, $\mathbf{u}_1^\alpha$ is the intrinsic velocity of solute in phase $\alpha$ and $\mathbf{u}^\alpha$ the mass averaged velocity of phase $\alpha$.

Equation (3.10) can be re-written for any arbitrary volume in terms of the mass concentration of solute in phase $\alpha$. Thus for the liquid phase the conservation of solute is

$$\mathrm{g}^L \dot{m}_1^L = \frac{\partial}{\partial t}(\rho(1-\phi)\bar{C}^L) + \nabla \bullet (\rho(1-\phi)\bar{C}^L \mathbf{u}^L) + \nabla \bullet \mathbf{J}_1^L , \tag{3.11}$$

where $\mathbf{J}_1^L$ is the liquid solute diffusion flux expressed as $\mathbf{J}_1^L = \bar{\rho}_1^L(\mathbf{u}_1^L - \mathbf{u}^L)$, with $\bar{\rho}_1^L$ being the partial liquid density of solute, where $\bar{\rho}_1^L = \mathrm{g}^L \rho_{*_1}^L$. The term $\bar{C}^L$ is the average liquid solute concentration in the control volume. For both the equilibrium and non-equilibrium cases $\bar{C}^L = C^L$.

Similarly, for the solid phase,

$$\mathrm{g}^S \dot{m}_1^S = \frac{\partial}{\partial t}(\rho\phi\bar{C}^S) + \nabla \bullet (\rho\phi\bar{C}^S \mathbf{u}^S) + \nabla \bullet \mathbf{J}_1^S , \tag{3.12}$$

where $\mathbf{J}_1^S$ is the solid solute diffusion flux expressed as $\mathbf{J}_1^S = \bar{\rho}_1^S(\mathbf{u}_1^S - \mathbf{u}^S)$, with $\bar{\rho}_1^S$ being the partial solid density of solute, where $\bar{\rho}_1^S = \mathrm{g}^S \rho_{*_1}^S$. The term $\bar{C}^S$ is the average solid solute concentration in the control volume. For the equilibrium case $\bar{C}^S = C^S$ and for the non-equilibrium case $\bar{C}^S$ is expressed in equation (2.106).

Solute is conserved in the solidifying or melting volume by the appearance of solute in one phase at the expense of the other phase. The conservation of solute can thus be expressed as

$$\mathrm{g}^S \dot{m}_1^S + \mathrm{g}^L \dot{m}_1^L = 0 , \tag{3.13}$$

which in turn is expressed as

$$\frac{\partial}{\partial t}\rho(\phi\bar{C}^S + (1-\phi)C^L) + \nabla \bullet \rho(\phi\bar{C}^S\mathbf{u}^S + (1-\phi)C^L\mathbf{u}^L) = -\nabla \bullet \mathbf{J}_1^S - \nabla \bullet \mathbf{J}_1^L . \quad (3.14)$$

It is assumed that the diffusion in the solid phase on the global level is so small, in comparison with the liquid, that it is assumed to be zero. Therefore $\mathbf{u}_1^S = \mathbf{u}^S$, making $\mathbf{J}_1^S = 0$.

The average concentration of solute of the phase mixture as a whole is expressed using the lever rule as $\bar{C} = \phi\bar{C}^S + (1-\phi)C^L$ where the differential forms of $\bar{C}$ are expressed for the local equilibrium case by equation (2.26) and for the local non-equilibrium by equation (2.120). Therefore the conservation of solute for the mixture as a whole can be expressed in terms of $\bar{C}$, as

$$\frac{\partial}{\partial t}\rho\bar{C} + \nabla \bullet \rho(\phi\bar{C}^S\mathbf{u}^S + (1-\phi)C^L\mathbf{u}^L) = \nabla \bullet \mathbf{J}_1^L , \quad (3.15)$$

and in terms of the Lagrangian description, equation (3.15) is expressed as

$$\rho\frac{D\bar{C}}{Dt} = -\nabla \bullet \mathbf{i} , \quad (3.16)$$

where

$$\mathbf{i} = \mathbf{i}' + (\hat{C}^S - C^L)\mathbf{j} \quad (3.17)$$

and

$$\mathbf{i}' = \mathbf{J}_1^S + \mathbf{J}_1^L . \quad (3.18)$$

Note that as zero solid diffusion is assumed, $\mathbf{J}_1^S = 0$. For the local equilibrium case $\hat{C}^S = C^S$, where $C^S$ is the average solid solute concentration. For the local non-equilibrium case $\hat{C}^S = C_*^S$, where $C_*^S$ is the solid solute concentration at the solid-liquid interface. The flux $\mathbf{j}$ accounts for the diffusive movement of particles in the mushy region which is expressed as

$$\mathbf{j} = -\rho\phi(1-\phi)\mathbf{w} , \quad (3.19)$$

where $\mathbf{w} = \mathbf{u}^L - \mathbf{u}^S$, the relative phase velocity.

For a mushy region, consisting of very fine particles, it is assumed that $\mathbf{u}^S = \mathbf{u}^L = \mathbf{u}$ and therefore $\mathbf{j} = 0$. Note also, that for a mushy region of dendritic structure it is commonly assumed that $\mathbf{u}^S = 0$.

which in turn is expressed as

$$\frac{\partial}{\partial t}\rho(\phi\bar{C}^S + (1-\phi)C^L) + \nabla \bullet \rho(\phi\bar{C}^S\mathbf{u}^S + (1-\phi)C^L\mathbf{u}^L) = \nabla \bullet \mathbf{J}_1^S - \nabla \bullet \mathbf{J}_1^L . \quad (3.14)$$

It is assumed that the diffusion in the solid phase on the global level is so small, in comparison with the liquid, that it is assumed to be zero. Therefore $\mathbf{u}_1^S = \mathbf{u}^S$, making $\mathbf{J}_1^S = 0$.

The average concentration of solute of the phase mixture as a whole is expressed using the lever rule as $\bar{C} = \phi\bar{C}^S + (1-\phi)C^L$ where the differential forms of $\bar{C}$ are expressed for the local equilibrium case by equation (2.26) and for the local non-equilibrium by equation (2.120). Therefore the conservation of solute for the mixture as a whole can be expressed in terms of $\bar{C}$ as

$$\frac{\partial}{\partial t}\rho\bar{C} + \nabla \bullet \rho(\phi\bar{C}^S\mathbf{u}^S + (1-\phi)C^L\mathbf{u}^L) = \nabla \bullet \mathbf{J}_1^L , \quad (3.15)$$

and in terms of the Lagrangian description, equation (3.15) is expressed as

$$\rho\frac{D\bar{C}}{Dt} = -\nabla \bullet \mathbf{i} , \quad (3.16)$$

where

$$\mathbf{i} = \mathbf{i}' + (\hat{C}^S - C^L)\mathbf{j} \quad (3.17)$$

and

$$\mathbf{i}' = \mathbf{J}_1^S + \mathbf{J}_1^L . \quad (3.18)$$

Note that as zero solid diffusion is assumed, $\mathbf{J}_1^S = 0$. For the local equilibrium case $\hat{C}^S = C^S$, where $C^S$ is the average solid solute concentration. For the local non-equilibrium case $\hat{C}^S = C_*^S$, where $C_*^S$ is the solid solute concentration at the solid-liquid interface. The flux $\mathbf{j}$ accounts for the diffusive movement of particles in the mushy region which is expressed as

$$\mathbf{j} = -\rho\phi(1-\phi)\mathbf{w} , \quad (3.19)$$

where $\mathbf{w} = \mathbf{u}^L - \mathbf{u}^S$, the relative phase velocity.

For a mushy region, consisting of very fine particles, it is assumed that $\mathbf{u}^S = \mathbf{u}^L = \mathbf{u}$ and therefore $\mathbf{j} = 0$. Note also, that for a mushy region of dendritic structure it is commonly assumed that $\mathbf{u}^S = 0$.

The diffusive flux of the solute in the phase mixture $\mathbf{i}'$ is expressed using diffusive mixture theory by Landau and Liftshitz [29] as

$$\mathbf{i}' = -\rho\left(\boldsymbol{D}\nabla C^L + (k_P/P)\nabla P + (k_T/T)\nabla T\right), \tag{3.20}$$

where $\boldsymbol{D}$ is the material diffusion coefficient tensor of the phase mixture, $k_P$ is the barodiffusion ratio and $k_T$ the thermal diffusion ratio associated with the Soret effect. As no solid diffusion is considered $\nabla C^S$ is not considered in equation (3.20). The material diffusion coefficient of the solid-liquid mixture is expressed as $\boldsymbol{D} = \phi\ \boldsymbol{D}^S + (1-\phi)\,\boldsymbol{D}^L$. As zero solid diffusion is assumed, $\boldsymbol{D}^S = 0$, and therefore $\boldsymbol{D} = (1-\phi)\,\boldsymbol{D}^L$ for the phase mixture.

Note that the diffusive flux for the phase mixture is expressed in terms of a $\nabla C^L$ instead of $\nabla \bar{C}$. This is because the inclusion of $\nabla \bar{C}$ would cause $\bar{C}$, in an isolated mixed phase system, to become uniform with respect to $\boldsymbol{x}$ when total equilibrium is attained. This is not consistent with the lever rule description of $\bar{C}$, where for an isolated mixed phase system in equilibrium the solid mass fraction $\phi$ varies arbitrarily with respect to $\boldsymbol{x}$ from 0 in the pure liquid to 1 in the pure solid, resulting in the average solute concentration $\bar{C}$ taking any value from $\bar{C}^S$ to $C^L$ for any $\boldsymbol{x}$. A detailed discussion of this point, for the local equilibrium case, is presented by Hills and Roberts [30].

The barodiffusion term in equation (3.20) need only be taken into account where there are considerable pressure gradients induced by an external pressure field. Thus, for most metallurgical applications where the applied pressure fields are mainly uniform and of the order of atmospheric pressure, this term is neglected. Similarly, the Soret effect is usually ignored in most metallurgical applications as its effect, within the time frame of solidification/melting, is negligibly small in comparison to the material diffusion.

## 3.4 Conservation of momentum

For an arbitrary fixed control volume described in Section (3.2) the conservation of momentum for the phase $\alpha$ is described as

$$\begin{aligned}\frac{\partial}{\partial t}\int_V \rho_*^\alpha \mathbf{u}^\alpha \,\mathrm{dV}^\alpha + \int_A (\rho_*^\alpha \mathbf{u}^\alpha \mathbf{u}^\alpha)\bullet \mathbf{n}\,\mathrm{dA}^\alpha &= \int_V \rho_*^\alpha \mathbf{F}^\alpha \,\mathrm{dV}^\alpha + \int_A \sigma_*^\alpha \bullet \mathbf{n}\,\mathrm{dA}^\alpha \\ &+ \int_V \mathbf{f}_*^\alpha \,\mathrm{dV}^\alpha,\end{aligned} \tag{3.21}$$

where $\rho_*^\alpha$ is the intrinsic density of phase $\alpha$, $\mathbf{u}^\alpha$ is the mass averaged velocity of phase $\alpha$, $\mathbf{F}^\alpha$ is the body force vector of phase $\alpha$, $\boldsymbol{\sigma}_*^\alpha$ is the intrinsic mean stress tensor of phase $\alpha$ and $\mathbf{f}_*^\alpha$ is the intrinsic flux which accounts for the momentum production due to phase interactions such as drag and lift.

In this formulation $\boldsymbol{\sigma}_*^\alpha$ represents the macroscopic state of stress within phase $\alpha$ with respect to the local phase volume. The vector $\mathbf{f}_*^\alpha$ represents the direct momentum exchange due to phase change and phase interaction forces; the phase interaction forces represent the macroscopic state of stress occurring at the microscopic interfaces between phases. Hills et al [4] postulate a linear constitutive law for the phase interaction flux, expressed with respect to the total volume, which includes normal (partial pressures) and shear (viscous) forces imparted on the solid by the liquid or visa versa, as well as momentum exchange through phase change. The phase interaction flux expressed with respect to the total volume is $\mathbf{f}^\alpha = \mathrm{g}^\alpha \mathbf{f}_*^\alpha$ and is termed the partial phase interaction flux.

Since the control volume is arbitrary, equation (3.21) can be expressed as

$$\frac{\partial}{\partial t}(\bar{\rho}^\alpha \mathbf{u}^\alpha) + \nabla \bullet (\bar{\rho}^\alpha \mathbf{u}^\alpha \mathbf{u}^\alpha) = \bar{\rho}^\alpha \mathbf{F}^\alpha + \nabla \bullet (\mathrm{g}^\alpha \boldsymbol{\sigma}_*^\alpha) + \mathrm{g}^\alpha \mathbf{f}_*^\alpha \,, \tag{3.22}$$

where $\bar{\rho}^\alpha$ is the partial density of phase $\alpha$.

The continuum equation governing the conservation of momentum of the phase mixture is obtained by summing the individual phase momentum equations and imposing Newton's third law (ie. $\mathrm{g}^S \mathbf{f}_*^S + \mathrm{g}^L \mathbf{f}_*^L = 0$), yielding

$$\frac{\partial}{\partial t}(\bar{\rho}^S \mathbf{u}^S + \bar{\rho}^L \mathbf{u}^L) + \nabla \bullet (\bar{\rho}^S \mathbf{u}^S \mathbf{u}^S + \bar{\rho}^L \mathbf{u}^L \mathbf{u}^L) = \rho \mathbf{F} + \nabla \bullet (\mathrm{g}^S \boldsymbol{\sigma}_*^S + \mathrm{g}^L \boldsymbol{\sigma}_*^L) \,, \tag{3.23}$$

where

$$\rho \mathbf{F} = \bar{\rho}^S \mathbf{F}^S + \bar{\rho}^L \mathbf{F}^L \,. \tag{3.24}$$

To define the phase stress tensors it is assumed that the liquid is Newtonian and the solid is perfectly rigid. As stated by Bennon and Incropera [1] appropriate averaging of the classical Newtonian constitutive equations for the liquid is necessary due to the spatial variations in the phase volume fractions. Thus the intrinsic mean liquid stress tensor $\boldsymbol{\sigma}_*^L$ as defined by Bennon and Incropera [1], Prescott et al [31] and Ganesan and Poirier [31] is

$$\boldsymbol{\sigma}_*^L = -\mathrm{P}_*^L \mathbf{I} + \frac{2}{3}\frac{\nu^L}{g^L} \mathrm{tr}\, \mathbf{D}^L \mathbf{I} + 2\frac{\nu^L}{g^L} \mathbf{D}^L \,, \tag{3.25}$$

where $\mathrm{P}_*^L$ is the intrinsic liquid pressure, $\nu^L$ the liquid viscosity, $\mathbf{I}$ is the identity matrix and $\mathbf{D}^L$ the liquid deformation tensor, [32], expressed as

$$\mathbf{D}^L = \frac{1}{2}[\nabla(g^L \mathbf{u}^L) + \nabla(g^L \mathbf{u}^L)^T] \,, \tag{3.26}$$

with $\mathbf{u}^L$ being the mass averaged velocity.

If one describes the conservation of momentum equation using the Lagrangian description it becomes evident what momentum transfer occurs during the phase change process. Thus equation (3.23) can be expressed using the Lagrangian formulation as

$$\bar{\rho}^S \frac{D^S \mathbf{u}^S}{Dt} + \bar{\rho}^L \frac{D^L \mathbf{u}^L}{Dt} + \mathrm{g}^L \dot{m}^L \mathbf{w} = \rho \mathbf{F} + \nabla \bullet (\mathrm{g}^S \boldsymbol{\sigma}_*^S + \mathrm{g}^L \boldsymbol{\sigma}_*^L) , \tag{3.27}$$

where

$$\mathrm{g}^S \dot{m}^S = -\mathrm{g}^L \dot{m}^L , \tag{3.28}$$

$$\frac{D^\alpha}{Dt} = \frac{\partial}{\partial t} + \mathbf{u}^\alpha \bullet \nabla \tag{3.29}$$

and

$$\frac{\partial}{\partial t}(\bar{\rho}^\alpha \mathbf{u}^\alpha) + \nabla \bullet (\bar{\rho}^\alpha \mathbf{u}^\alpha \mathbf{u}^\alpha) = \bar{\rho}^\alpha \frac{D^\alpha \mathbf{u}^\alpha}{Dt} + \mathrm{g}^\alpha \dot{m}^\alpha \mathbf{u}^\alpha . \tag{3.30}$$

The first two terms on the left hand side of equation (3.27) represent the rates of increase in momentum of the solid and liquid phases following their motion. The last term on the left hand side of equation (3.27) represents the momentum transfer from the liquid to the solid as it freezes or from solid to liquid as it melts.

Note that equation (3.25) can be expressed with respect to the total volume as

$$\boldsymbol{\sigma}^L = -\bar{\mathrm{P}}^L \mathbf{I} + \frac{2}{3} \nu^L \mathrm{tr} \mathbf{D}^L \mathbf{I} + 2 \nu^L \mathbf{D}^L , \tag{3.31}$$

where $\boldsymbol{\sigma}^L$ is termed the partial mean liquid stress and expressed as $\boldsymbol{\sigma}^L = g^L \boldsymbol{\sigma}_*^L$, and $\bar{\mathrm{P}}^L$ is the partial pressure of the liquid which is expressed as $\bar{\mathrm{P}}^L = \mathrm{g}^L \mathrm{P}_*^L$.

As the solid phase is assumed perfectly rigid (ie. $\mathbf{D}^S = 0$), the solid stress tensor can only be expressed using the conservation of momentum equation of the solid phase. Therefore the solid stress tensor, expressed with respect to the total volume, is

$$\nabla \bullet \boldsymbol{\sigma}^S = \frac{\partial}{\partial t}(\bar{\rho}^S \mathbf{u}^S) + \nabla \bullet (\bar{\rho}^S \mathbf{u}^S \mathbf{u}^S) - \bar{\rho}^S \mathbf{F}^S - \mathbf{f}^S . \tag{3.32}$$

As the phase interaction effects are assumed negligible, and the phase interactions on the solid are equal and opposite to those on the liquid, $\mathbf{f}^S = -\mathbf{f}^L$. Therefore, substituting in the expressions for the solid phase stress tensor into the conservation of total momentum equation, the following is obtained:

$$\frac{\partial}{\partial t}(\bar{\rho}^L \mathbf{u}^L) + \nabla \bullet (\bar{\rho}^L \mathbf{u}^L \mathbf{u}^L) = \bar{\rho}^L \mathbf{F}^L + \mathbf{f}^L + \nabla \bullet (-\bar{\mathrm{P}}^L \mathbf{I} + [\frac{2}{3}\nu^L \operatorname{tr} \mathbf{D}^L \mathbf{I} + 2\nu^L \mathbf{D}^L]). \quad (3.33)$$

Using the Lagrangian description equation (3.33) is expressed as

$$\bar{\rho}^L \frac{D^L \mathbf{u}^L}{Dt} + \mathrm{g}^L \dot{m}^L \mathbf{u}^L = \bar{\rho}^L \mathbf{F}^L + \mathbf{f}^L + \nabla \bullet (-\bar{\mathrm{P}}^L \mathbf{I} + [\frac{2}{3}\nu^L \operatorname{tr} \mathbf{D}^L \mathbf{I} + 2\nu^L \mathbf{D}^L]) . \quad (3.34)$$

## 3.5 Conservation of energy

To discuss the conservation of energy and entropy production of the solid-liquid phase change system, it is assumed that thermal equilibrium between the phases exists, such that the temperature of the two coexisting phases are equal. The description of the conservation of energy presented here will be approached in a similar fashion to that presented by Hills et al [4]. Thus the energy balance of the phase change system is described using the thermodynamic variables of the mixture, as a whole, as

$$\rho \frac{DU}{Dt} + \nabla \bullet \mathbf{q} - \rho \mathrm{r} + \mathbf{f} \bullet \mathbf{w} + \boldsymbol{\sigma}^L : \mathbf{D}^L = 0 , \quad (3.35)$$

where $U$ is the internal energy per unit mass of the phase mixture, r is the heat source per unit mass and time, $\mathbf{q}$ is the heat flux vector, $\mathbf{f} = \mathbf{f}^L = -\mathbf{f}^S$ is the partial phase interaction force defined in Section (3.4), $\mathbf{w}$ is the relative velocity in the mushy region defined in Section (3.4), $\boldsymbol{\sigma}^L$ is the partial mean liquid stress tensor defined in Section (3.4) and $\mathbf{D}^L$ is the liquid deformation tensor described in Section (3.4). The solid is assumed to be perfectly rigid, $\mathbf{D}^S = 0$, thus the strain energy contribution of the solid is not included in the energy equation. Note that for a solid-liquid mixture of very small solid particles in liquid suspension, the strain energy contribution of each phase to the conservation of energy expression is combined into a single total strain energy contribution.

## 3.6 Entropy inequality

To define the laws which govern the progression to total equilibrium or maximum entropy, the entropy growth has to be defined. This is done using the entropy inequality postulated by Muller [9], which is given as

$$\rho \frac{DS}{Dt} + \nabla \bullet \mathbf{k} - \rho \mathrm{r}/T \geq 0 , \quad (3.36)$$

where **k** is the entropy flux and S the entropy of the phase mixture per unit mass. As the Gibbs free energy per unit mass $\boldsymbol{\Phi}$ is being used to describe the phase change process, the expression for the entropy inequality can be rephrased in terms of $\boldsymbol{\Phi}$ where $\boldsymbol{\Phi}$ = U - ST + P/$\rho$. Thus using equation (3.35) the entropy inequality becomes

$$\rho[\frac{D\boldsymbol{\Phi}}{Dt} + S\frac{DT}{Dt} - \frac{1}{\rho}\frac{DP}{DT} + \frac{P}{\rho^2}\frac{D\rho}{Dt}] + T\nabla\bullet\mathbf{k} - \nabla\bullet\mathbf{q} - \mathbf{f}\bullet\mathbf{w} + \boldsymbol{\sigma}^L\!:\mathbf{D}^L \geq 0\,. \tag{3.37}$$

Note that as described in detail, in Chapter 2, the Gibbs free energy can be expressed as a function of P, T and $\bar{C}$, for solid-liquid phase change systems based on local equilibrium and local non-equilibrium assumptions. Thus equation (3.37) can be re-expressed using the conservation of mass expression, viz.

$$\frac{D\rho}{Dt} = -\bar{\rho}^L\nabla\bullet\mathbf{u}^L - \bar{\rho}^S\nabla\mathbf{u}^S + \rho\mathbf{w}\bullet\nabla\phi\,, \tag{3.38}$$

and the conservation of solute expression, viz.

$$\frac{D\bar{C}}{Dt} = -\nabla\bullet\mathbf{i}\,, \tag{3.39}$$

as follows

$$Q \equiv T\nabla\bullet\mathbf{k} - \nabla\bullet\mathbf{q} - \mu\nabla\bullet\mathbf{i} - \mathbf{f}\bullet\mathbf{w} - P\mathbf{w}\bullet\nabla\phi + [\boldsymbol{\sigma}^L + P(1-\phi)\,\mathbf{I}]\!:\mathbf{D}^L \geq 0\,, \tag{3.40}$$

where

$$\{\frac{\partial\boldsymbol{\Phi}}{\partial T}\}_{P,\bar{C}} = -S\,,\quad \{\frac{\partial\boldsymbol{\Phi}}{\partial P}\}_{T,\bar{C}} = \frac{1}{\rho}\quad\text{and}\quad \{\frac{\partial\boldsymbol{\Phi}}{\partial\bar{C}}\}_{P,T} = \mu\,. \tag{3.41}$$

The entropy inequality as defined in equation (3.40) will be used to restrict the constitutive class used to define the flux vectors $\mathbf{k}, \mathbf{q}, \mathbf{i}$ and $\mathbf{f}$ for both the local equilibrium based system and the local non-equilibrium based system. For an isolated solid-liquid system where phase change is based on the local equilibrium assumption, as described in Chapter 2, maximum entropy is attained when Q = 0. For an isolated solid-liquid system where the phase change is based on the local non-equilibrium assumption, as described in Chapter 2, maximum entropy is not reached when Q = 0. In fact when Q = 0 a 'quasi-equilibrium' state will be reached, which, although not at maximum entropy, is static. In reality this assumption is not correct as diffusion in the solid *does* exist but is very small in comparison to that of the liquid. In terms of the time

scales of the metallurgical process, maximum entropy will only be reached after an very long time. It is thus feasible, in this context, to assume that the 'quasi-equilibrium' state is static to all intents and purposes. Hills and Roberts [21] develop a formulation which includes the slow diffusion and show how the parameters relating to solid diffusion eventually relax to obtain equilibrium with the inequality becoming zero. They also show that a 'quasi-equilibrium' state is reached far short of full equilibrium where the inequality, reflecting the contributions from the parameters related to solid diffusion, is insignificant. Consequently, Hills and Roberts [21] assumed these parameters to be zero and accordingly the inequality is assumed to be zero at 'quasi-equilibrium'. Note that the 'quasi-equilibrium' state is termed the local non-equilibrium state in this work.

## 3.7 Constitutive laws

In order to define a diffusive mixture theory for the mushy region, Hills et al [4] postulate a constitutive model for the mushy region where the fluxes $\mathbf{i}, \mathbf{k}, \mathbf{q}$ and $\mathbf{f}$ are expressed as general functions of P, T and $\bar{C}$ where each expression is linear in $\mathbf{w}$ and the gradients of P, T and $\bar{C}$, viz.

$$\psi = \gamma_P^\psi \nabla \mathrm{P} + \gamma_T^\psi \nabla \mathrm{T} + \gamma_{\bar{C}}^\psi \nabla \bar{C} + \gamma_w^\psi \mathbf{w}\,, \tag{3.42}$$

for $\psi = \mathbf{i}, \mathbf{k}, \mathbf{q}$ and $\mathbf{f}$, and where the coefficients $\gamma$ are general functions of P, T and $\bar{C}$.

As stated by Hills and Roberts [21], $\phi(\boldsymbol{x})$ and $\bar{C}(\boldsymbol{x})$ can be non-uniform with respect to $\boldsymbol{x}$, at equilibrium. Thus a constitutive law that includes the term $\nabla \bar{C}$ would prevent an arbitrary variation in $\bar{C}(\boldsymbol{x})$ being a possible solution in the equilibrium or non(quasi)-equilibrium states. As a result, all the coefficients of $\nabla \bar{C}$ in the constitutive equations are set to zero , viz. $\gamma_{\bar{C}}^\psi = 0$. The constitutive equations for the mushy region, therefore, become linear functions of $\mathbf{w}$ and the gradients of P and T, and are expressed as:

$$\psi = \gamma_P^\psi \nabla \mathrm{P} + \gamma_T^\psi \nabla \mathrm{T} + \gamma_w^\psi \mathbf{w}\,, \tag{3.43}$$

for $\psi = \mathbf{i}, \mathbf{k}, \mathbf{q}$ and $\mathbf{f}$, and where the coefficients $\gamma$ are general functions of P and T.

This constitutive model holds for the mushy models based on local equilibrium and non-equilibrium assumptions, as defined in Chapter 2. For the local equilibrium case this is illustrated in the fact that $\bar{C}$ varies with respect to $C^L = C^L(P,T)$ and $C^S = C^S(P,T)$ for an arbitrary value of $\phi$. For the local non-equilibrium case, $\bar{C}$ varies with respect to $C^L = C^L(P,T)$ for an arbitrary value of $\phi$. Therefore, for both cases, a variation in $\bar{C}$ is dependent on variations in P and T for any arbitrary value of $\phi$, in the mushy region.

The constitutive model as it stands holds only for the mushy region. In the pure liquid region,

$\bar{C} = C^L \neq C^L(P,T)$ for both the equilibrium and non-equilibrium cases. In the pure solid region, $\bar{C} = C^S \neq C^S(P,T)$ for the local equilibrium case, and $\bar{C} = \bar{C}^S \neq \bar{C}^S(P,T)$, for the local non-equilibrium case. To define a constitutive model which holds for the whole domain it is necessary to include gradient terms of $C^S$ and $C^L$.

On a global scale the diffusion in the solid is far slower than that of the liquid. It can thus be assumed, even for the local equilibrium based models, that the gradient term in $C^S$ is neglected. Hence, a constitutive model which is defined for the whole region (ie. solid, liquid and mushy regions) is

$$\boldsymbol{\psi} = \gamma_P^{\psi}\nabla \mathrm{P} + \gamma_T^{\psi}\nabla \mathrm{T} + \gamma_{C^L}^{\psi}\nabla C^L + \gamma_w^{\psi}\mathbf{w}\,, \tag{3.44}$$

for $\boldsymbol{\psi} = \mathbf{i}, \mathbf{k}, \mathbf{q}$ and $\mathbf{f}$ where the coefficients $\gamma$ are general functions of P, T and $\bar{C}$.

Note that in the mushy region $C^L = C^L(P,T)$, and thus equation (3.44) reverts back to equation (3.43). For the pure solid region the fluxes $\mathbf{f} = 0$ and $\mathbf{i} = 0$ and the other fluxes $\mathbf{k}$ and $\mathbf{q}$ will be functions of gradients in P and T. For the liquid region the flux $\mathbf{f} = 0$ and the fluxes $\mathbf{i}, \mathbf{k}$ and $\mathbf{q}$ will become functions of gradients in P, T and $\bar{C}$ where $\bar{C} = C^L$.

By substituting in the constitutive equations(ie. equation (3.44)) into the entropy inequality (equation (3.40)) the entropy inequality will become a quadratic function in terms of $\mathbf{w}$, and gradients of P and T for the mushy region, gradients of P, T and $\bar{C}$ for the liquid region and gradients of P and T for the solid region. Thus the inequality can be expressed as

$$\mathrm{Q} = \boldsymbol{b}^T \boldsymbol{A}\, \boldsymbol{b} \geq 0\,, \tag{3.45}$$

where, $\boldsymbol{b} = [\mathbf{w}\,,\, \nabla \mathrm{P}\,,\, \nabla \mathrm{T}]^T$ for the mushy region, $\boldsymbol{b} = [\nabla \mathrm{P}\,,\, \nabla \mathrm{T}\,,\, \nabla \bar{C}]^T$ for the liquid region and $\boldsymbol{b} = [\nabla \mathrm{P}\,,\, \nabla \mathrm{T}]^T$ for the solid region. The matrix $\boldsymbol{A}$ is the matrix of constitutive coefficients. To maintain positive entropy growth the appropriate principal minors of the determinant of $\boldsymbol{A}$ should be non-negative. This places some restriction on the choice of coefficients for the constitutive model. For example, in the mushy region, the first non-negative principal minor is $-\gamma_w^f \geq 0$ where $\gamma_w^f = -\nu^L/\tilde{\gamma}$, which gives a measure of the small scale viscous interaction between the liquid and solid in the dendrite channels and which must be greater than or equal to zero. Note $\nu^L$ is the liquid viscosity and $\tilde{\gamma}$ is the square of a typical channel radius in the dendrite pores.

## 3.8 Evaluation of fluxes and expanded generalized conservation equations

The evaluation of the constitutive coefficients for the local equilibrium based mushy region are clearly explained in the paper by Hills et al [4]. For the local non-equilibrium based mushy region model the constitutive coefficients have a similar structure but differ in content to the

equilibrium constitutive coefficients. The constitutive coefficients for the non-equilibrium case differ from those of the equilibrium case, as the thermodynamic coefficients, on which they depend differ for the two cases, as presented in Chapter 2. For the non-equilibrium case, the equilibrium solid solute concentration used to describe the constitutive coefficients represents the solid interface solute concentration value, whereas for the equilibrium case this value is the uniform solid solute concentration.

The final forms of the entropy diffusion flux $\mathbf{k}$, heat diffusion flux $\mathbf{q}$, solute diffusion flux $\mathbf{i}$ and the interdendritic diffusion flux $\mathbf{f}$ are expressed as follows:

$$\mathbf{k} = (\bar{s}^L + \bar{\mu}^L k_T/T)\mathbf{i} - \mathcal{K}/T\nabla T - \mathbf{j}\,\mathrm{L}^L/T)\,, \tag{3.46}$$

$$\mathbf{q} = -\mathcal{K}/T\nabla T - \{\frac{L^L}{(C^L - \hat{C}^S)} + \bar{\mu}^L k_T\}\mathbf{i}'\,, \tag{3.47}$$

$$\mathbf{i} = -\rho\boldsymbol{D}\{\nabla C^L + (k_P/P)\nabla P + (k_T/T)\nabla T\} + (C^L - \hat{C}^S)\mathbf{j}\,, \tag{3.48}$$

and

$$\mathbf{f} = -P\nabla\phi - (\nu^L/\tilde{\gamma})\mathbf{w} + \mu\nabla\gamma_w^i + T\nabla\gamma_w^k - \nabla\gamma_w^q\,, \tag{3.49}$$

where $\bar{s}^L = \partial\mu^L/\partial T$ is the specific liquid entropy with $\mu^L$ being the liquid chemical potential, $\bar{\mu}^L = \partial\mu^L/\partial C^L$ is the specific liquid chemical potential, $\mathcal{K} = g^S\mathcal{K}^S + g^L\mathcal{K}^L$ is the thermal conductivity tensor of the phase mixture, $\mathbf{j} = -\phi(1-\phi)\mathbf{w}$ is the diffusive flux of particles in the interdendritic liquid, $\mathbf{w} = \mathbf{u}^L - \mathbf{u}^S$ is the relative phase velocity, $k_T$ is the Soret thermal diffusion ratio, $\mathrm{L}^L$ is the liquid latent heat, $\mathbf{i}'$ is the solute diffusion flux neglecting the diffusive flux of particles, $\hat{C}^S = C^S$ where $C^S$ is the average solid solute concentration for the local equilibrium case and $\hat{C}^S = C_*^S$ where $C_*^S$ is the solid interface solute concentration for the local non-equilibrium case, $\boldsymbol{D} = (1-\phi)\boldsymbol{D}^L$ is the material diffusion matrix of the phase mixture with solid diffusion being zero, $k_P$ is the barodiffusion ratio, $\nu^L$ is the liquid viscosity, $\tilde{\gamma} = \bar{\mathrm{K}}/(g^L)^2$ is the square of the channel radius in the interdendritic pores with, $\bar{\mathrm{K}}$ being the permeability tensor, $\mu = (\boldsymbol{\Phi}^S - \boldsymbol{\Phi}^L)/(\hat{C}^S - C^L)$ is the phase mixture chemical potential, $\gamma_w^i = \rho\phi(1-\phi)(C^L - \hat{C}^S)$ and $\gamma_w^k = (\bar{s} + (\bar{\mu}^L k_T)/T)\gamma_w^i$ with $\bar{s} = (S_*^S - S_*^L)/(C^L - \hat{C}^S)$. The contribution to $\mathbf{f}$ made by the coefficient $\gamma_w^q$ which represents the heat flux diffusion by $\mathbf{w}$ is cancelled out by the contribution to the partial pressure and will not be considered further.

Note that these flux vectors defined for the mushy region also hold for the pure solid and liquid regions.

The expressions for the entropy diffusion flux $\mathbf{k}$, heat diffusion flux $\mathbf{q}$, solute diffusion flux $\mathbf{i}$ and the interdendritic diffusion flux $\mathbf{f}$ are substituted into the conservation equations of energy, momentum, mass and solute, resulting from the expanded forms of these equations, which are expressed as follows:

### 3.8.1 Conservation of energy

The conservation of energy equation can be reduced to the entropy balance expression ,viz.

$$\rho T\frac{DS}{Dt} + T\nabla \bullet \mathbf{k} = \rho r + Q\,, \tag{3.50}$$

which holds for both the local equilibrium and the local non-equilibrium ('quasi-equilibrium') cases. Thus substituting in the constitutive equations for the diffusive fluxes and expanding the entropy rate in terms of P, T and $\bar{C}$, the conservation of energy expression is expressed as

$$\begin{aligned}
&\alpha_{t_0} T\frac{DP}{Dt} + \rho C_{p_0}\frac{DT}{Dt} - L^L\frac{D^S(\rho\phi)}{Dt} = \nabla \bullet (\mathcal{K}\nabla T + \bar{\mu}^L k_T \mathbf{i}) + \\
&\{\bar{\delta}\,\mathbf{i}' + \frac{1}{(C^L - \hat{C}^S)}(\alpha^L_{t_\bullet}/\rho^L_* - \alpha^S_{t_\bullet}/\rho^S_*)\,\mathbf{i}\} \bullet \nabla P + \\
&\{\frac{\bar{\mu}^L k_T}{T}(C^L - \hat{C}^S) - (C^L_{P_\bullet} - C^S_{P_\bullet})\}\,\nabla T \bullet \mathbf{j} + \\
&\frac{\nu^L (g^L)^2}{\bar{\mathbf{K}}}\,w^2 + (\boldsymbol{\sigma}^L + \bar{\mathrm{P}}^L\,\mathbf{I}) : \mathbf{D}^L + \rho r = 0\,,
\end{aligned} \tag{3.51}$$

where $\alpha_{t_0}$ is the lever rule thermal expansion coefficient given in equations (2.85) and (2.151), $C_{p_0}$ is the lever rule specific heat given in equations (2.86) and (2.152), $\bar{\delta}$ is the phase mixture volumetric expansion, given in equation (2.52) and the partial pressure $\bar{\mathrm{P}}^L$ is function of the total pressure and some interdendritic terms, viz. $\bar{\mathrm{P}}^L = (1-\phi)\,P + \mu\,\gamma^i_w + T\,\gamma^k_w - \gamma^q_w$.

### 3.8.2 Conservation of momentum

The conservation of momentum equation for the dendritic mushy region, where the solid is assumed perfectly rigid, can also be expanded in terms of the constitutive equations. Thus equation (3.34) becomes

$$\begin{aligned}
\rho(1-\phi)\frac{D^L\mathbf{u}^L}{Dt} &= -\frac{\nu^L(\mathrm{g}^L)^2}{\bar{\mathbf{K}}} + \mathrm{g}^L\dot{m}^L\mathbf{u}^L + \rho(1-\phi)\{\mathbf{F}^L - \frac{1}{\rho^L_*}\nabla P\} \\
&+ \rho\phi(1-\phi)(C^L - \hat{C}^S)\frac{\bar{\mu}^L k_T}{T}\nabla T \\
&+ \nabla \bullet [\frac{2}{3}\nu^L\, tr\,\mathbf{D}^L\,\mathbf{I} + 2\nu^L\,\mathbf{D}^L]\,.
\end{aligned} \tag{3.52}$$

In this case the liquid body force $\mathbf{F}^L$ vector is the gravitational field constant $\boldsymbol{b}_g$ and $\mathrm{g}^L\dot{m}^L$ is the rate of creation of the liquid phase.

### 3.8.3 Conservation of mass

Similarly the expanded form of the conservation of mass equation is

$$-\beta_0 \frac{DP}{Dt} + \alpha_{t_0} \frac{DT}{Dt} - \rho \delta^L \frac{D\phi}{Dt} = \nabla \bullet \{(1-\phi)\mathbf{w}\} + \delta^L \nabla \bullet \mathbf{i}\,, \tag{3.53}$$

where $\nabla \bullet \mathbf{u}^S = 0$, therefore $\nabla \bullet \mathbf{u} = \nabla \bullet \{(1-\phi)\mathbf{w}\}$. The terms $\beta_0$ and $\alpha_{t_0}$ are the lever rule expressions of the coefficients of isothermal compression given in equations (2.84) and (2.150), and thermal expansion given in equations (2.85 and 2.151), respectively. The term $\delta^L$ is the specific volume change of the liquid given in equation (2.51).

### 3.8.4 Conservation of solute

The expanded form of the equation for conservation of solute, given in equation (3.16), is

$$\rho \frac{D\bar{C}}{Dt} = \nabla \bullet \{\rho(1-\phi)\,\mathbf{D}^L [\nabla C^L + (k_P/P)\nabla P + (k_T/T)\nabla T] + (C^L + \hat{C}^S)\mathbf{j}\}\,. \tag{3.54}$$

## 3.9 Practical simplifying assumptions

The generalized forms of the conservation equations can be simplified using some practical assumptions. A list of these assumptions follows.

a ) The solidus and liquidus are assumed to be in a constant ratio, therefore, as expressed by equation (2.73); $C^S(P,T) = kC^L(P,T)$.

b ) It is assumed that the following thermodynamic coefficients are equal, as shown in equations (2.76 - 2.78), $\delta^L = \delta^S = \delta$, $L^S = L^L = L$ and $\bar{\mu}^L = k\bar{\mu}^S = \bar{\mu}$.

c ) The Oberbeck - Boussinesq approximation is used, where it assumes that the density is constant everywhere except in the buoyancy force where the density depends on the pressure, temperature and solute concentration fields (see Hills et al [4]).

d ) The externally applied pressure field is assumed to be of the order of the atmospheric pressure (as in most metallurgical processes) and is thus constant with negligible effect on the process.

e ) As a result of assumption (d) and the application of the Oberbeck - Boussinesq approximation, the effects of compressibility and thermal expansion in the pure and mixed phase regions will be very small, and are neglected (see Hills et al [4]).

f) The Soret and barodiffusion effects are neglected, as in most metallurgical process their effect is negligible, therefore $k_T = 0$ and $k_P = 0$.

### 3.9.1 Conservation of mass

Thus a simplified form of the equation for conservation of mass is

$$\nabla \bullet \{(1-\phi)\mathbf{w}\} = 0 \tag{3.55}$$

or

$$\nabla \bullet \mathbf{u} = 0\,, \tag{3.56}$$

where $\nabla \bullet \mathbf{u}^S = 0$ as the solid is assumed perfectly rigid.

### 3.9.2 Conservation of energy

Neglecting the inertial and viscous terms for both the liquid and mushy regions, and the sixth term on the right hand side of equation (3.51) (this term vanishes in the outer phase regions and is small in comparison to the advective part of the lever rule specific heat contribution), the conservation of energy expression is obtained as follows:

$$\rho C_{p_0} \frac{DT}{Dt} - \rho L \frac{D^S \phi}{Dt} = \nabla \bullet \boldsymbol{\mathcal{K}} \nabla T + \rho r\,, \tag{3.57}$$

where

$$C_{p_0} = \phi C_{p_\bullet}^S + (1-\phi) C_{p_\bullet}^L \tag{3.58}$$

and

$$\boldsymbol{\mathcal{K}} = \mathrm{g}^S \boldsymbol{\mathcal{K}}^S + \mathrm{g}^L \boldsymbol{\mathcal{K}}^L\,. \tag{3.59}$$

Equation (3.57) can be re-expressed in terms of the effective specific heat $C_p$ as

$$\rho C_p \frac{\partial T}{\partial t} + \rho L \mathbf{u}^S \bullet \nabla \phi + \rho C_{p_0} \mathbf{u} \bullet \nabla T = \nabla \bullet \boldsymbol{\mathcal{K}} \nabla T + \rho r\,, \tag{3.60}$$

where

$$C_p = C_{p_0} - L \partial \phi / \partial T \tag{3.61}$$

and

$$L = H^L - H^S\,, \tag{3.62}$$

with

$$H^S = \int_{Tref}^{T} C_p^S(\tau, \boldsymbol{x}, t)d\tau \tag{3.63}$$

and

$$H^L = \int_{Tref}^{T} C_p^L(\tau, \boldsymbol{x}, t)d\tau + \Delta H_{ref}^f . \tag{3.64}$$

Given the fact that $C_p = \partial H/\partial T$, where

$$H = \phi H^S + (1-\phi)H^L , \tag{3.65}$$

equation (3.57) is therefore re-expressed in terms of enthalpy H as

$$\rho\frac{\partial H}{\partial t} + \rho C_{p_0}\mathbf{u}\bullet\nabla T + \rho L\mathbf{u}^S\bullet\nabla\phi = \nabla\bullet\boldsymbol{\mathcal{K}}\nabla T + \rho r . \tag{3.66}$$

Note that in equation (3.66) that the enthalpy is not advected, as dendritic solidification is being considered. The latent heat is not advected by the liquid velocity as latent heat can only be liberated or absorbed on phase change and thus its advection can only be a function of the solid velocity. In the papers by Bennon and Incropera [1,33] and Voller et al [18,34] this point is neglected. In many models of dendritic systems the solid velocity is assumed zero (ie. $\mathbf{u}^S = 0$), Rappaz et al [20], resulting in equation (3.66) being reduced to

$$\rho\frac{\partial H}{\partial t} + \rho C_{p_0}\mathbf{u}\bullet\nabla T = \nabla\bullet\boldsymbol{\mathcal{K}}\nabla T + \rho r . \tag{3.67}$$

### 3.9.3 Conservation of solute

The simplified form the conservation of solute is thus

$$\rho\frac{\partial \bar{C}}{\partial t} + \rho\mathbf{u}\bullet\nabla\bar{C} = \rho\nabla\bullet\boldsymbol{D}\nabla C^L , \tag{3.68}$$

where $\boldsymbol{D} = (1-\phi)\boldsymbol{D}^L$.

### 3.9.4 Conservation of momentum

Finally the simplified expression for the conservation of momentum is

$$\begin{aligned}\frac{\partial}{\partial t}(\bar{\rho}^L \mathbf{u}^L) \;+\; \nabla \bullet (\bar{\rho}^L \mathbf{u}^L \mathbf{u}^L) \;&=\; -\frac{\nu^L (\mathrm{g}^L)^2}{\bar{\mathbf{K}}}\mathbf{w} + \bar{\rho}^L \boldsymbol{b}_g - \mathrm{g}^L \nabla P \\ +\; \nabla \bullet [\nu^L \nabla(\mathrm{g}^L \mathbf{u}^L) + \nu^L \nabla(\mathrm{g}^L \mathbf{u}^L)^T - \frac{2}{3}\nu^L \nabla \bullet (\mathrm{g}^L \mathbf{u}^L)\mathbf{I}] \,. \end{aligned} \tag{3.69}$$

In the interdendritic region the flow of liquid slows down as the dendrites become more closely spaced and the channels between them get smaller therefore $\mathbf{u}^L \longrightarrow 0$ and the inertial and higher order drag terms fall away, and the flow becomes steady. The liquid volume fractions become uniform and the forces of the liquid-liquid interactions become negligible. Thus equation (3.69) reduces to Darcy's law;

$$\mathbf{w} \;=\; \frac{\bar{\mathbf{K}}}{\nu^L \mathrm{g}^L}(\rho_*^L \boldsymbol{b}_g - \nabla P) \,, \tag{3.70}$$

where $\bar{\mathbf{K}}$ is the permeability tensor which may be isotropic or orthotropic.

The vector expression for the conservation of momentum, equation (3.69) can be re-expressed, after some manipulation, in terms of the mass averaged velocity of the continuum mixture $\mathbf{u}$ as follows

$$\begin{aligned}\frac{\partial}{\partial t}(\rho \mathbf{u}) + \nabla \bullet (\rho \mathbf{u}\mathbf{u}) \;&=\; \nabla \bullet (\nu^L \frac{\rho}{\rho_*^L}\nabla \mathbf{u}) - \nu^L \frac{\rho}{\rho_*^L}\mathbf{u}^S \nabla^2 \phi - 2\frac{\rho}{\rho_*^L}\nabla \mathbf{u}^S \bullet \nabla \phi \\ &-\; \nabla \bullet \{ \sum_{\alpha=S,L} \bar{\rho}^\alpha (\mathbf{u}^\alpha - \mathbf{u})(\mathbf{u}^\alpha - \mathbf{u})\} + \bar{\rho}^L \boldsymbol{b}_g \\ &-\; \mathrm{g}^L \nabla \bar{P} - \frac{\nu^L}{3}\frac{\nabla \bullet (\mathrm{g}^L \mathbf{u}^L)}{\mathrm{g}^L}\mathbf{I} \bullet \nabla \mathrm{g}^L + \mathrm{g}^L \frac{\nu^L}{\bar{\mathbf{K}}}\frac{\rho}{\rho_*^L}(\mathbf{u} - \mathbf{u}^S) \\ &+\; \frac{\partial}{\partial t}(\bar{\rho}^S \mathbf{u}^S) + \nabla \bullet (\bar{\rho}^S \mathbf{u}^S \mathbf{u}^S) \,. \end{aligned} \tag{3.71}$$

where

$$\bar{P} = P - \frac{\nu^L}{3}\frac{\nabla \bullet (\mathrm{g}^L \mathbf{u}^L)}{\mathrm{g}^L} \,, \tag{3.72}$$

$$\mathrm{g}^L \mathbf{u}^L = \frac{\rho}{\rho_*^L}(\mathbf{u} - \phi \mathbf{u}^S) \tag{3.73}$$

and

$$\mathrm{g}^L \mathbf{w} = \frac{\rho}{\rho_*^L}(\mathbf{u} - \mathbf{u}^S) \,. \tag{3.74}$$

In deriving equation (3.71) it is assumed that the solid is rigid, hence $\nabla^2 \mathbf{u}^S = 0$, that the liquid viscosity is locally invariant ($\nu^L \approx 0$) and that the viscous stresses arising from local density variations are negligible, therefore $\nabla(\rho/\rho_*^L) = 0$.

Prescott et al [31] developed an $x$ component expression for the momentum of the continuum mixture which is similar to the $x$ component form of equation (3.71). The main differences in the two formulations is that the pressure term P in equation (3.71) is the total applied pressure, not the intrinsic liquid pressure as in [31] and the fourth last term on the right hand side of equation (3.71) is not included in [31]. The reason for these differences is that the constitutive law for the phase interaction force $\mathbf{f}^L$, given in equation (3.49), is expressed in terms of the total pressure, where the total pressure contribution to the partial liquid pressure $\bar{\mathrm{p}}^L$ is $(1-\phi)P$. The description of phase interaction force $\mathbf{f}^L$ in [31] is expressed using the intrinsic mean liquid pressure $P_*^L$, where its contribution to the partial liquid pressure $\bar{\mathrm{p}}^L$ is $g^L P_*^L$. As a result, in [31] the equivalent expression to equation (3.72), is expressed in terms of $P_*^L$ and when the expression for the solid momentum is added to the general momentum equation, the fourth last term on the right hand side of equation (3.71) is cancelled out by the solid phase interaction force contribution. As it stands, the solid phase interaction force in the solid momentum contribution to equation (3.71), only canceled out the total pressure multiplied by the gradient in liquid volume fraction. Note that the approach used in dealing with the phase interaction forces in this work is similar to the approach used by Gansen and Poirier [32].

Collectively, the first three terms on the right hand side of equation (3.71) represent the viscous straining of the liquid. The second term on the right-hand side of equation (3.71) is written in terms of solid translation, and the third term is written in terms of solid rotation, where $\nabla \mathbf{u}^S = -\Omega \times \mathbf{I}$, Prescott et al [31]. The fourth term represents the inertial forces established as a consequence of variations in relative phase velocities. Since the solid mass fraction and liquid volume fraction gradients are zero in the single-phase regions, the second, third and seventh terms on the right hand side of equation (3.71) vanish outside the mushy region. In the pure liquid region, the first and sixth terms on the right hand side of equation (3.71), which represent pure liquid viscous and pressure variations, are the only remaining terms. In the pure solid region, all the terms on the right hand side of (3.71), except for the last two, vanish, as the liquid stress is not defined in this region. In the mushy region the permeabilities are considered to be so small ($O(10^{-11})m^2$, Poirier [35]) that the Darcian damping force (third last term on the right hand side of (3.71)) dominates over the advection and viscous terms. Therefore the second, third, fourth and sixth terms are neglected. From assumptions (c) and (d), at the beginning of this section, the total pressure field is equivalent to the mean intrinsic liquid pressure. Hence, the continuum momentum equation (3.71) reduces to

$$\begin{aligned}
\frac{\partial}{\partial t}(\rho \mathbf{u}) + \nabla \bullet (\rho \mathbf{u}\mathbf{u}) &= \nabla \bullet (\nu^L \frac{\rho}{\rho_*^L} \nabla \mathbf{u}) + \bar{\rho}^L \boldsymbol{b}_g \\
&- \mathrm{g}^L \nabla \bar{P} + \mathrm{g}^L \frac{\nu^L}{\bar{\mathbf{K}}} \frac{\rho}{\rho_*^L} (\mathbf{u} - \mathbf{u}^S) \\
&+ \frac{\partial}{\partial t}(\bar{\rho}^S \mathbf{u}^S) + \nabla \bullet (\bar{\rho}^S \mathbf{u}^S \mathbf{u}^S) \,. \qquad (3.75)
\end{aligned}$$

The $x$ component form of equation (3.75) is, therefore, the same as that presented in [31]. Note that this equation is limited to situations corresponding to a single continuous and non-deforming solid phase; for example a system of primary dendrites and eutectic lamellae.

## 3.10 Conclusions

In this chapter, a continuum formulation for analyzing macroscopic phase change behaviour has been developed. The microscopic descriptions of local equilibrium and local non-equilibrium phase change, have been integrated with the principles of classical mixture theory, to obtain a consistent set of equations governing the conservation of mass, momentum, energy and solute. These equations hold for the pure solid, pure liquid and mushy regions. This enables a fixed grid computational procedure to be employed, to model the global phase change problem in its entirety using a single set of conservation equations. The set of conservation equations are expressed generally and is coupled with constitutive equations which describe the solute, entropy, phase interaction and heat fluxes in the mixed and pure phase regions. Using a set of practical assumptions, the conservation equations are simplified into a form that describes most metallurgical problems.

Hills, Loper and Roberts [4] have developed a similar generalized continuum formulation based on local equilibrium criterion. In Chapter 2, an expression for the free energy of the system for the local non-equilibrium case was developed as a function of P,T and $\bar{C}$. This enabled a constitutive law to be developed, for the non-equilibrium case, in a similar fashion to that for the equilibrium case; as a function of P,T and $\bar{C}$. The constitutive law and conservation equations are expressed per unit mass and volume of the whole system.

The conservation of momentum equation is derived for the continuum as a whole, where the solid phase is assumed to be rigid and the liquid as Newtonian. The description of the conservation of momentum in this work is only relevant to systems which are dendritic or eutectic in nature. A full vector form of the momentum equation is developed in terms of the continuum mixture velocity $\mathbf{u}$. The $x$ component form of this equation is similar to that developed by Prescott et al [31], even though the starting bases are different.

The continuum formulation developed in this chapter eliminates the need to track phase interfaces and is well suited for accommodating continuous phenomena such as the absorption or liberation of latent heat over a finite temperature range, which is generally associated with multiconstituent systems. This formulation is generally considered unsuitable for addressing discrete phase change and tends to 'smear' the discrete phenomena. Such smearing is inherent in the continuum formulation and is a direct consequence of approximating discontinuous functions, such as enthalpy or viscosity, with continuous functions. The effect of smearing can be reduced by using fine computational meshes, but cannot be entirely eliminated. As solidification of multiconstituent systems are of primary importance here, the continuum formulation is clearly adequate.

# CHAPTER 4
# THE NUMERICAL MODEL

## 4.1 Introduction

Two basic numerical solution techniques are used to model the solidification/melting processes.

The first technique is the front tracking method where the solid and liquid regions are modelled separately with a moving interface condition between the two phases. This approach is only applicable for discrete phase change systems where the interface shape is not complex as in dendritic solidification. In this method the discrete phase front, which is an unknown function of space and time, needs to be tracked continuously so that the solid and liquid domains are tracked accurately and that compatibility between the conservation equations is maintained with the moving interface boundary condition. In order to do this a deforming mesh and/or coordinate mapping procedures have to be used, which complicates the application of the technique. These techniques are used in modelling semiconductor crystal growth, biomedical applications and solidification of pure substances; Yoo and Rubinsky [7], Kececioglu and Rubinsky [36], Lynch et al [5] and [6], and Bonnerot and Jamet [37].

The second technique is the fixed grid technique where a non-deforming numerical grid or mesh is used to model the problem spatially. In this case the phase interface is not tracked but derived afterwards, thus explicit consideration of the interface in the formulation is eliminated. This technique is suitable for non-discrete phase change problems where phase change takes place over a region. Thus the solidification of multiconstituent (ie. binary) systems or systems with impurities are best modelled using this technique. The phase change behavior of such systems, as described in Chapters 2 and 3, depends on many factors including the phase change environment, composition, and thermodynamic descriptions of the specific phase transformations. As a result, solidification occurs over an extended temperature range and solid formation often occurs as a permeable crystalline-like matrix which coexists with the liquid phase. For the binary or multiconstituent systems the conservation equations are thus composed in a continuum form where a single set of equations is defined for the whole domain, as described in Chapter 3. This lends itself to a simple implementation into the fixed grid numerical solution procedure. The solutions of the fixed grid method are very dependent on the mesh discretizion. In order to pick up the local effects in the mushy region a very fine mesh has to be used. This makes the solution process very slow and the process computationaly expensive. One way to get round this is to use adaptive mesh refinement techniques where the mesh is refined in the mushy region and is coarse in the pure solid and liquid regions. Lewis et al [38] and Huang and Lewis [39] applied this technique based on error estimates relating to heat transfer modelling of the solidification process.

There are many different numerical procedures or methods that can be employed to numerically

discretize the problem, namely the finite difference method, the finite volume method, the finite element method and the boundary element method. Each method has its own advantages and disadvantages. For example the finite difference and finite volume method are easier to implement and are computationaly less expensive than the finite element method but are not as robust as the finite element method when it comes to modelling complex geometries typically found in casting problems. The majority of continuum based numerical models on binary alloy solidification are based on finite difference techniques [34,19, 33]. Thevoz et al [40] and Rappaz [41] uses finite elements to develop a micro-macro model for equiaxed and dendritic solidification based on a global heat transfer model with microscopic models which consider the evolution of mass fraction. The finite element method has also been extensively used to model macro heat transfer based solidification (ie. Lewis and Roberts [42], Samonds [43], Comini [44], Morgan et al [45] and Morgan [46]). A full continuum based formulation as presented in Chapters 2 and 3 has not, to my knowledge, been implemented into a finite element code.

A fixed grid finite element method is thus used to model the binary alloy solidification/melting problem. Due to the complexity in implementing fluid convection into the finite element code, convection (bulk and interdendritic) is neglected. It is realized that the bulk, and in particular the interdendritic convection play an important role in the solidification process. Their exclusion in this finite element model is only considered as a first step in the process of modelling solidification. The aim of this work is to observe what effects the microscopic models of local equilibrium and local non-equilibrium have on the finite element modelling of the solidification process. Therefore only a simplified form of the global conservation equations coupled with the microscopic phase change models are considered. The simplified global conservation equations are therefore the conservation of energy (Fourier's law) and the conservation of solute (Fick's law) which are respectively expressed as

$$\rho C_p \frac{\partial T}{\partial t} = \nabla \cdot \boldsymbol{\mathcal{K}} \nabla T + Q_H \tag{4.1}$$

and

$$\rho \frac{\partial \bar{C}}{\partial t} = \nabla \cdot \rho \boldsymbol{D} \nabla C^L + Q_C \, . \tag{4.2}$$

It should be pointed out in equation (4.2) that the solute diffusion model assumes complete solute mixing within the liquid phase and undercooling is neglected. As a result, position of the dendrite tips are located at the equilibrium liquidus temperature.

In the phase change region the specific heat $C_p$ experiences a dirac-delta behaviour, see Figure 4.1, which leads to significant numerical difficulties when trying to solve the conservation of energy equation. To circumvent this difficulty, enthalpy is introduced into the conservation equation (4.1) to give

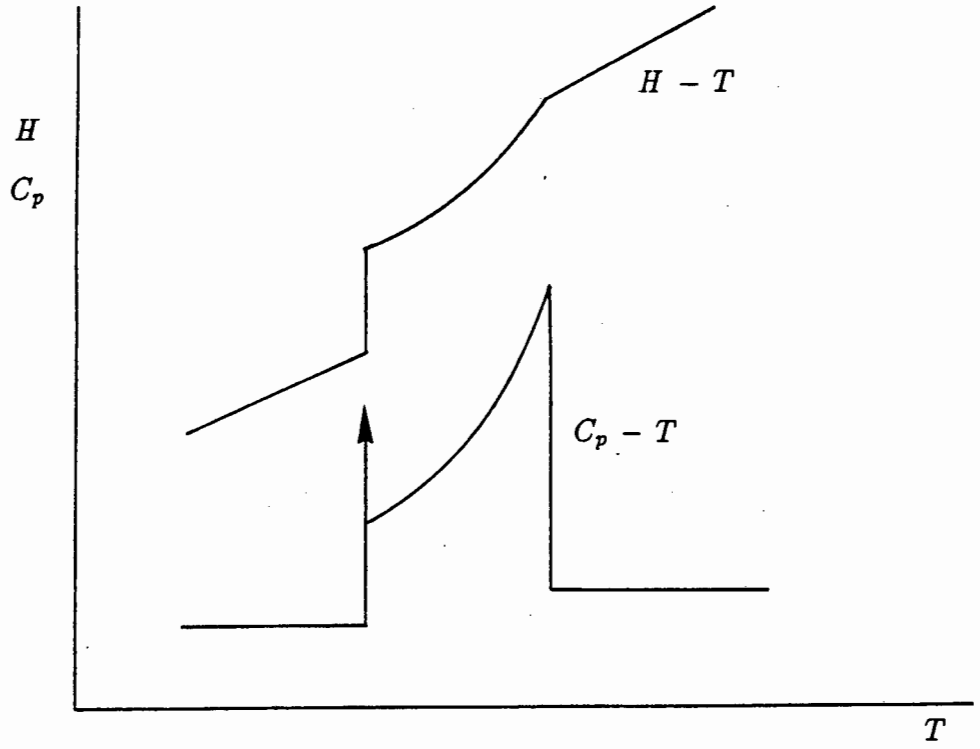


Figure 4.1: Enthalpy and specific heat versus temperature

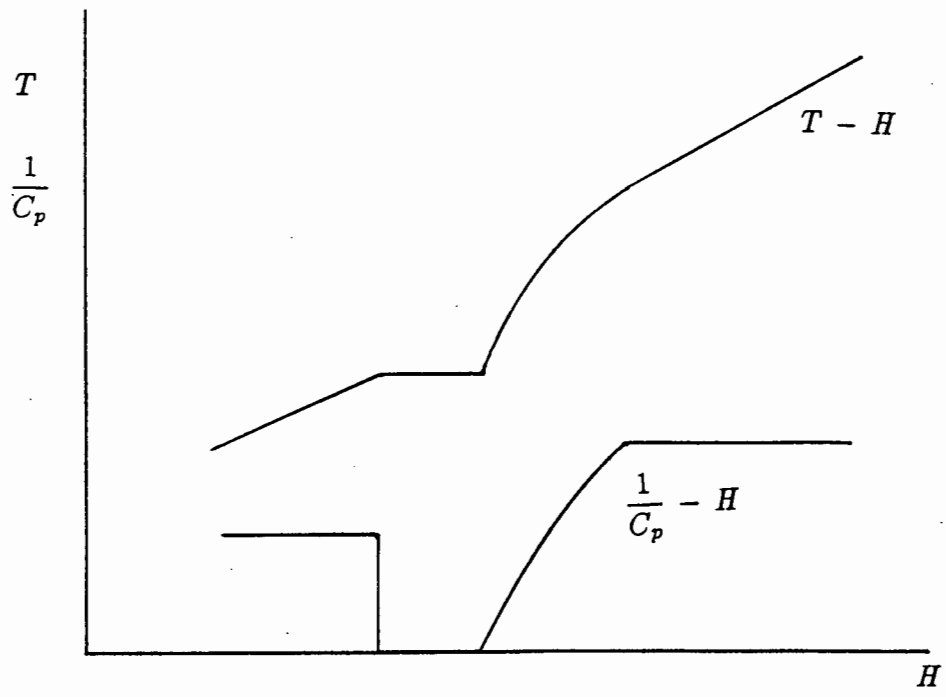


Figure 4.2: Temperature and inverse specific heat versus enthalpy

$$\rho\frac{\partial H}{\partial t} = \nabla \cdot \mathcal{K}\nabla T + Q_H. \tag{4.3}$$

By rewriting the rate term in (4.3), in terms of enthalpy, numerical difficulties are only circumvented when a mushy phase change (non-discrete phase change) takes place where the $T - H$ curve is a smooth function throughout the domain as shown in Figure 4.1. However, as illustrated in Figure 4.1, the $T - H$ curve exhibits a discontinuity at the eutectic point of an alloy or at the melting temperature of a pure substance. Therefore at the eutectic, enthalpy becomes multivalued, making the accurate solution of equation (4.3) very difficult and energy conservation cannot be ensured. If enthalpy is chosen as the field variable, rather than temperature, the function becomes single valued and this problem can be overcome with the energy being totally conserved. This is illustrated in Figure 4.2, it is clear that the $H - T$ curve experiences no discontinuity and also $\frac{\partial T}{\partial H}$, which is $\frac{1}{C_p}$, is zero in the eutectic region. Equation (4.3) expressed in terms of enthalpy is therefore

$$\rho\frac{\partial H}{\partial t} = \nabla \cdot \mathcal{K}\nabla T(H) + Q_H \tag{4.4}$$

$$= \nabla \cdot \frac{\mathcal{K}}{C_p}\nabla H + Q_H, \tag{4.5}$$

where

$$\mathcal{K} = \mathcal{K}(T(H(\boldsymbol{x},t)),\boldsymbol{x},t) \tag{4.6}$$

and

$$Q_H = Q_H(T(H(\boldsymbol{x},t)),\boldsymbol{x},t). \tag{4.7}$$

The advantage in using this enthalpy formulation is that it is characterized by a strictly decreasing or increasing enthalpy for solidification or melting respectively, where energy conservation is ensured. It must be noted that even when using the full enthalpy approach the discontinuity which is implicit in the formulation cannot be correctly modelled using the fixed grid finite element formulation. The standard finite elements cannot handle a discontinuity within the elements and the jump in enthalpy will be smeared over the element or elements depending on the solution scheme used. It is also clear that to model this jump condition reasonably a fine mesh would have to be used.

## 4.2 Finite element formulation

In this section, the solution of the global conservation equations of energy and solute, using a fixed grid finite element approach, is discussed.

First, the strong form of the initial boundary-value problem (IBVP) is defined. This leads to the weighted residual or weak form of the problem. Next, the Galerkin approximation is introduced which, along with an assumed spatial discretization, leads to the finite element matrix form of the problem. The finite element matrix equations are then temporally discretized. The solution of the resulting nonlinear matrix equations motivates the development of iterative algorithms. Finally, the linear problem generated by the iterative algorithms is discussed.

## 4.3 Strong form of the initial boundary-value problem

To define the strong form, we must first define the problem domain, material properties, boundary and initial conditions.

### 4.3.1 Problem domain

The problem is posed for a body occupying a spatial domain $\Omega$, a finite region of $\Re^{N_{sd}}$ where $\Re$ is the set of real numbers and $N_{sd}$ is the number of space dimensions. A general point in $\bar{\Omega}$ will be denoted as $\boldsymbol{x} = \{x_i\}$, $i = 1, 2, ..., N_{sd}$ where $\bar{\Omega}$ denotes a closed domain, i.e. the total domain including boundaries. The closed domain $\bar{\Omega}$ is divided up into different subregions as shown in Figure 4.1, with

$$\bar{\Omega} = \overline{\Omega^S \cup \Omega^L \cup \Omega^M}$$

where

$\Omega^S \subset \Re^{N_{sd}} \times \tau$ (solid region of the domain),

$\Omega^L \subset \Re^{N_{sd}} \times \tau$ (liquid region of the domain),

$\Omega^M = \overline{\Omega^S \cap \Omega^L}$ (phase change region of the domain which includes the mushy and eutectic regions)

and $\tau$ denotes time.

The three subdomains $\Omega^S, \Omega^L$ and $\Omega^M$ vary with time. When the width of $\Omega^M$ tends to zero a discrete phase change results between $\Omega^S$ and $\Omega^L$. This is described as

$$\Omega^S \cap \Omega^L = \emptyset, \tag{4.8}$$

where $\emptyset$ denotes the empty set.

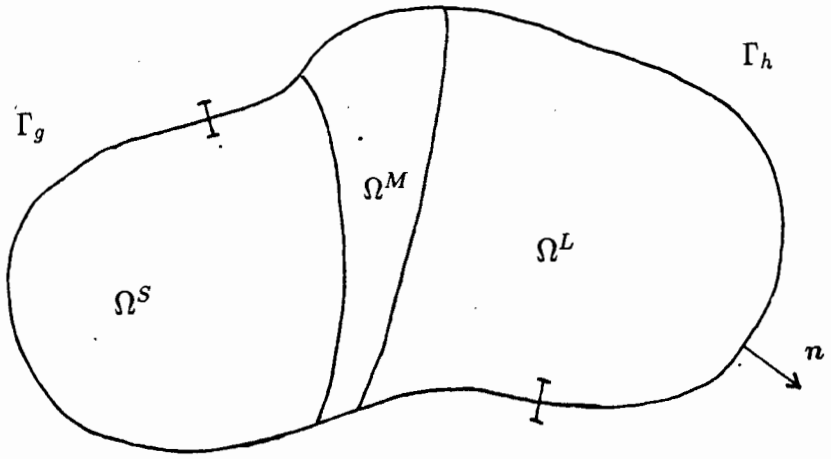


Figure 4.3: Problem domain

The boundary of $\Omega$, denoted $\Gamma$, is assumed to be piecewise smooth. At almost every point on $\Gamma$ there is a unique outward normal unit vector $\boldsymbol{n} = (n_i)$, $i = 1, 2, \ldots, N_{sd}$. In addition, $\Gamma$ can be subdivided into two disjoint sets, $\Gamma_g$ and $\Gamma_h$. Thus $\Gamma$ admits the following decomposition

$$\Gamma = \Gamma_g \cup \Gamma_h \tag{4.9}$$

and

$$\emptyset = \Gamma_g \cap \Gamma_h, \tag{4.10}$$

where

$$\Gamma_g = \overline{\Gamma_{g^L} \cup \Gamma_{g^M} \cup \Gamma_{g^S}} \tag{4.11}$$

and

$$\Gamma_h = \overline{\Gamma_{h^L} \cup \Gamma_{h^M} \cup \Gamma_{h^S}}. \tag{4.12}$$

The superposed bar represents set closure and $\emptyset$ denotes the empty set. The time interval under consideration is 0 to $\tau$, where $\tau$ is a given number.

### 4.3.2 Material Properties

The material properties vary with respect to the phase of the material. The material is considered to have a maximum of three phases (i.e. solid, liquid and mush) at any one time . The thermodynamic coefficients (i.e. effective specific heat $C_p$), the constitutive coefficients (i.e. conductivity $\mathcal{K}$, and diffusivity $\boldsymbol{D}$) and density $\rho$ of the phase mixture are expressed in terms of a lever rule with respect to the solid mass fraction $\phi$, with the exception of conductivity, which is expressed in terms of the phase volume fraction $g^{\alpha}$. These properties admit a nonlinear dependence on enthalpy H and average solute concentration $\bar{C}$.

A summary of the material properties defining the phase mixture follows.

a) The solid mass fraction is expressed as

$$\phi = \phi(T(H), \bar{C}, \boldsymbol{x}, t) = \begin{cases} 1 & \text{solid region} \\ 0 < \phi < 1 & \text{mushy region} \\ 0 & \text{liquid region} \end{cases}.$$

b) The enthalpy for the phase mixture is expressed as

$$H = \phi H^S + (1-\phi) H^L \,, \tag{4.13}$$

where

$$H^S = H^S(T(H), \boldsymbol{x}, t) = \int_{Tref}^{T(H)} C_p^S(\tau, \boldsymbol{x}, t) d\tau \tag{4.14}$$

and

$$H^L = H^L(T(H), \boldsymbol{x}, t) = \int_{Tref}^{T(H)} C_p^L(\tau, \boldsymbol{x}, t) d\tau + \Delta H_{ref}^f, \tag{4.15}$$

where $C_p^S = C_p^S(T(H), \boldsymbol{x}, t)$ is the specific heat of the solid, $C_p^L = C_p^L(T(H), \boldsymbol{x}, t)$ is the specific heat of the liquid and $\Delta H_{ref}^f$ is the heat of formation of the liquid alloy which is constant. Dependency on the solute concentration of $C_p^{\alpha}$ in both phases are ignored.

c) The average solute concentration of the phase mixture is expressed as

$$\bar{C} = \phi \bar{C}^S + (1-\phi) C^L, \tag{4.16}$$

where $\bar{C}^S$ is the average solute concentration of the solute in the solid and is expressed for the local non-equilibrium case by equation (2.106) and for the local equilibrium case as $\bar{C}^S = C^S$ where $C^S = C^S(T(H), \boldsymbol{x}, t)$ in the mushy region and $C^S = \bar{C}(\boldsymbol{x}, t)$ in the solid. The term $C^L$ is the average solute concentration of the solute in the liquid which is expressed for the equilibrium and non-equilibrium case in the mushy region as $C^L = C^L(T(H), \boldsymbol{x}, t)$ and in the liquid region as $C^L = \bar{C}(\boldsymbol{x}, t)$.

d) The phase mixture density $\rho$ is expressed as

$$\rho = \mathrm{g}^S \rho_*^S + \mathrm{g}^L \rho_*^L, \tag{4.17}$$

where $\mathrm{g}^S = (\rho/\rho_*^S)\phi$ is the solid volume fraction, $\mathrm{g}^L = (\rho/\rho_*^L)(1-\phi)$ is the liquid volume fraction, $\rho_*^S$ is the actual solid density and $\rho_*^L$ is the actual liquid density. Note that the Oberbeck-Boussinesq approximations are used where it is assumed that $\rho$ = constant (except in the bouyancy terms for the fluid flow case). To maintain phase mixture saturation, solid and liquid densities are assumed to be equal, therefore $\rho_*^S = \rho_*^L$ = constant. From these assumptions therefore, $\mathrm{g}^S = \phi$ and $\mathrm{g}^L = (1-\phi)$.

e) The conductivity of the phase mixture is expressed as

$$\mathcal{K} = \mathrm{g}^S \mathcal{K}^S(T(H), \bar{C}, \boldsymbol{x}, t) + \mathrm{g}^L \mathcal{K}^L(T(H), \bar{C}, \boldsymbol{x}, t), \tag{4.18}$$

where $\mathcal{K}^S$ is the conductivity of the solid and $\mathcal{K}^L$ is the conductivity of the liquid. Note that $\mathcal{K}^\alpha$ is allowed to be anisotropic although symmetry is assumed [47].

f) The diffusivity of the phase is expressed as

$$\boldsymbol{D} = \phi \boldsymbol{D}^S(T(H), \bar{C}, \boldsymbol{x}, t) + (1-\phi)\boldsymbol{D}^L(T(H), \bar{C}, \boldsymbol{x}, t), \tag{4.19}$$

where $\boldsymbol{D}^S$ is the diffusivity of the solid and $\boldsymbol{D}^L$ is the diffusivity of the liquid. It is assumed that the solid diffusion is zero, therefore $\boldsymbol{D}^S = \boldsymbol{0}$.

g) The effective specific heat of the phase mixture $C_p$ is expressed as

$$C_p = C_{p_0} - L\partial\phi/\partial T\ , \tag{4.20}$$

where $C_{p_0}$ is the lever rule specific heat of the phase mixture and is expressed as

$$C_{p_0} = \phi C_p^S(T(H), \boldsymbol{x}, t) + (1-\phi) C_p^L(T(H), \boldsymbol{x}, t) \tag{4.21}$$

and L is the latent heat (enthalpy of fusion), which is expressed as

$$L = \int_{Tref}^{T(H)} (C_p^L(\tau, \boldsymbol{x}, t) - C_p^S(\tau, \boldsymbol{x}, t)) d\tau + \Delta H_{ref}^f \,. \tag{4.22}$$

The internal heat generation $Q_H$ is expressed as $Q_H = Q_H(T(H), \boldsymbol{x}, t)$ and the solute source $Q_C$ is expressed as $Q_C = Q_C(\bar{C}, \boldsymbol{x}, t)$.

The domains and ranges of the functions defining the material properties are given as follows:

$\rho$ : $\Omega \longrightarrow \Re^+$ (mass density),

$C_p$ : $\Re^+ \times \Omega \times ]\,0, \tau\,[ \longrightarrow \Re^+$ (effective specific heat),

$\boldsymbol{\mathcal{K}}$ : $\Re^+ \times \Omega \times ]\,0, \tau\,[ \longrightarrow Sym^+$ (thermal conductivity),

$\boldsymbol{D}$ : $\Re^+ \times \Omega \times ]\,0, \tau\,[ \longrightarrow Sym^+$ (solute diffusivity),

$Q_H$ : $\Re^+ \times \Omega \times ]\,0, \tau\,[ \longrightarrow \Re^+$ (internal heat generation)

and

$Q_C$ : $\Re^+ \times \Omega \times ]\,0, \tau\,[ \longrightarrow \Re^+$ (internal solute source),

where $\Re^+$ denotes positive real numbers and $Sym^+$ is the set of all symmetric positive definite two-tensors.

### 4.3.3 Boundary and initial conditions

Different types of boundary conditions are defined on the subsets $\Gamma_g$ and $\Gamma_h$ of $\Gamma$. On $\Gamma_g$ a 'g-type' boundary condition [48] (ie. essential boundary condition) is applied. This type of boundary condition prescribes a given temperature $g_H$ and/or a given solute concentration $g_C$ which may depend on both position and time. Therefore,

$$g = g_H \quad : \quad \Gamma_g \quad \times \quad ]\,0, \tau\,[ \longrightarrow \Re^+ \text{ (prescribed temperature)} \tag{4.23}$$

and/or

$$g = g_C \quad : \quad \Gamma_g \quad \times \quad ]\,0, \tau\,[ \longrightarrow \Re^+ \text{ (prescribed solute concentration)} \,. \tag{4.24}$$

Subset $\Gamma_h$ contains those points on the boundary at which an 'h-type' boundary condition [48] (ie. 'natural' boundary condition) applies. This type of boundary condition can be described as a heat flux $h_H$ and/or solute flux $h_C$. The heat flux $h_H$ may depend on temperature, position and time, and the solute flux $h_C$ may depend on solute concentration, position and time. Therefore,

$$h = h_H \quad : \quad \Re^+ \quad \times \quad \Gamma_h \quad \times \quad ]\,0,\tau\,[ \longrightarrow \Re^{N_{sd}} \text{ (prescribed heat flux)} \tag{4.25}$$

and/or

$$g = g_C \quad : \quad \Re^+ \quad \times \quad \Gamma_h \quad \times \quad ]\,0,\tau\,[ \longrightarrow \Re^{N_{sd}} \text{ (prescribed solute flux) .} \tag{4.26}$$

The prescribed fluxes to be used in this work are described as:

a) the adiabatic or no-flux boundary condition

$$h_H = 0 \text{ and/or } h_C = 0\,, \tag{4.27}$$

b) the prescribed heat flux condition

$$h_H = h_{f_1}(\boldsymbol{x}, t), \tag{4.28}$$

where $h_{f_1}$ is a given function,

c) the prescribed solute flux condition

$$h_C = h_{f_2}(\boldsymbol{x}, t), \tag{4.29}$$

where $h_{f_2}$ is a given function,

d) the convection boundary condition

$$h_H = h_{conv}(\boldsymbol{x}, t)(T(H(\boldsymbol{x}, t)) - T_{conv}(\boldsymbol{x}, t)), \tag{4.30}$$

where $h_{conv}$ is a given function defining the convection coefficient and $T_{conv}$ is the equilibrium temperature at which no convection occurs, and/or

e) the radiation boundary condition

$$h_H = h_{rad}(T(H(\boldsymbol{x},t)))(T(H(\boldsymbol{x},t)) - T_{rad}(\boldsymbol{x},t)), \tag{4.31}$$

where $h_{rad}$ is a function defining the radiation coefficient expressed as

$$h_{rad} = \epsilon\sigma\left\{T(H(\boldsymbol{x},t))^2 + T_{rad}^2(\boldsymbol{x},t)\right\}\{T(H(\boldsymbol{x},t)) + T_{rad}(\boldsymbol{x},t)\}, \tag{4.32}$$

where $\epsilon$ is the emissivity, $\sigma$ is the Stefan Boltzman constant and $T_{rad}$ is the equilibrium temperature at which no radiation occurs.

The initial temperature distribution in the body is

$$T_0 : \Omega \longrightarrow \Re^+ \text{ (initial temperature)}, \tag{4.33}$$

therefore the initial enthalpy is defined as

$$H_0(\boldsymbol{x}) = \int_{Tref}^{T_0} C_p(\tau,\boldsymbol{x},t)d\tau, \tag{4.34}$$

where

$$H_0 : \Omega \longrightarrow \Re^+ \text{ (initial enthalpy)}. \tag{4.35}$$

The initial solute concentration distribution in the body is

$$C_0 : \Omega \longrightarrow \Re^+ \text{ (initial solute concentration)}. \tag{4.36}$$

For physical reasons, $T_0$ and $C_0$ need not be continuous.

### 4.3.4 The Strong Form

A summary of the assumptions which are used to describe the basis of the strong form of the IBVP follows.

a) The effects of compressibility and thermal expansion of the liquid and solid are negligible see Chapter 3 § (3.9) and are neglected.

b) The Soret and Dufour effects are also negligible within the time frame of the solidification process and are neglected.

c) The Oberbeck-Boussinesq approximation is adopted where $\rho$ = constant, and $\rho_*^S = \rho_*^L$ to ensure phase mixture saturation. (Note for fluid flow this would not hold for the bouyancy terms.)

d) The effects of convection are neglected.

e) Diffusion coefficient in the solid is assumed negligible relative to that in the liquid, therefore $\boldsymbol{D}^S = 0$.

f) Isotropic properties in the liquid are assumed.

g) Effects of small disturbances in the fields (e.g. dispersion fluxes, supercooling of the liquid, etc.) are neglected.

h) Thermodynamic equilibrium at the solid-liquid interface is assumed.

i) The solidus and liquidus of the equilibrium phase diagram are assumed linear.

Based on these assumptions the IBVP describing the solidification/melting process is defined. Therefore the strong form (S) of the IBVP can thus be stated as follows.

Given $\rho$, $C_P$, $\boldsymbol{\kappa}$, $\boldsymbol{D}$, $g_H$, $g_C$, $h_H$, $h_C$, $T_0$ and $\bar{C}_0$, as in § 4.3.2 – 4.3.3,

find

$$H \quad : \ \bar{\Omega} \times [0,\tau] \longrightarrow R^+, \text{ expressed in § 4.3.2,}$$

and

$$\bar{C} \quad : \ \bar{\Omega} \times [0,\tau] \longrightarrow R^+, \text{ expressed in § 4.3.2,}$$

such that the following coupled equations hold:

$$\rho \frac{\partial H}{\partial t} = \nabla \cdot \frac{\boldsymbol{\kappa}}{C_p} \nabla H + Q_H \text{ on } \Omega \times ]0,\tau[ \tag{4.37}$$

and

$$\rho \frac{\partial \bar{C}}{\partial t} = \nabla \cdot \rho \boldsymbol{D} \nabla C^L + Q_C \text{ on } \Omega \times ]0,\tau[ \, . \tag{4.38}$$

The essential boundary conditions are

$$H = g_H \text{ on } \Gamma_g \times ]0,\tau[ \tag{4.39}$$

and

$$\bar{C} = g_C \text{ on } \Gamma_g \times ]0,\tau[ . \tag{4.40}$$

The natural boundary conditions are

$$\boldsymbol{n} \bullet (\frac{\kappa}{C_p} \nabla H) = h_H = h_{f_1} + h_{conv} + h_{rad} \text{ on } \Gamma_H \times ]0,\tau[ \tag{4.41}$$

and

$$\boldsymbol{n} \bullet (\rho \boldsymbol{D} \nabla C^L) = h_C = h_{f_2} \text{ on } \Gamma_C \times ]0,\tau[ . \tag{4.42}$$

The initial conditions are

$$H(\boldsymbol{x},0) = h_0(\boldsymbol{x}) \; \forall \; \boldsymbol{x} \in \Omega \tag{4.43}$$

and

$$\bar{C}(\boldsymbol{x},0) = \bar{C}_0(\boldsymbol{x}) \; \forall \; \boldsymbol{x} \in \Omega . \tag{4.44}$$

It must be noted that the enthalpy essential boundary condition is expressed, with respect to temperature, as

$$g_H = \int_{Tref}^{T(H)} C_p(\tau, \boldsymbol{x}, t) d\tau \text{ on } \Gamma_g \times ] \, 0, \tau \, [ . \tag{4.45}$$

## 4.4 Weighted residual form of the initial boundary-value problem

The 'weighted residual' or 'weak' form of **(S)** is generated by a suitable choice of solution and variational spaces and the application of the divergence theorem, Mitchell [49] and Strang [50].

### 4.4.1 Solution and Variational Spaces

In order to develop a weak formulation for the IBVP, a total solution and a variational space are defined. Let $H$ and $w_1$ denote the enthalpy fields and $\bar{C}$ and $w_2$ denote the solute concentration fields. The solution space $\mathcal{S}$ is defined as $\mathcal{S} = \mathcal{S}_{\mathcal{H}} \cup \mathcal{S}_{\mathcal{C}}$ where

$$\begin{aligned} \mathcal{S}_H \;=\; \{H \mid H &= g_H \text{ on } \Gamma_g \text{ and where} \\ H &= H^L \text{ in } \Omega^L \\ H &= \phi H^S + (1-\phi) H^L \text{ in } \Omega_M \\ H &= H^S \text{ in } \Omega^S\} \end{aligned}$$

and where

$$\begin{aligned} \mathcal{S}_C \;=\; \{\bar{C} \mid \bar{C} &= g_C \text{ on } \Gamma_g \text{ and where} \\ \bar{C} &= C^L \text{ in } \Omega^L \\ \bar{C} &= \phi \bar{C}^S + (1-\phi) C^L \text{ in } \Omega_M \\ \bar{C} &= \bar{C}^S \text{ in } \Omega^S\}. \end{aligned}$$

The variational space $\mathcal{V}$ is defined as $\mathcal{V} = \mathcal{V}_H \cup \mathcal{V}_C$ where

$$\mathcal{V}_H = \{w_1 \mid w_1 = 0 \text{ on } \Gamma_g\} \tag{4.46}$$

and

$$\mathcal{V}_C = \{w_2 \mid w_2 = 0 \text{ on } \Gamma_g\}. \tag{4.47}$$

Note that $\mathcal{S}$ is time dependent due to its use of the $g$-type condition, while $\mathcal{V}$ is time independent.

### 4.4.2 The Weak Form

The weak form of the problem **(W)** is obtained by multiplying (4.37) and (4.43) by $w_1 \in \mathcal{V}_H$ and (4.38) and (4.44) by $w_2 \in \mathcal{V}_C$, integrating over $\Omega$, applying the divergence theorem, and making use of the boundary conditions (4.39) – (4.42) to simplify the result. This yields weak form for the IBVP as follows.

Given $\rho, C_p$, $\boldsymbol{\kappa}$, $\boldsymbol{D}$, $g_H$, $g_C$, $h_H$, $h_C$, $H_0$ and $\bar{C}_0$, as in § 4.3.2 – 4.3.3,

find

$$H : [\,0,\tau\,] \longrightarrow \mathcal{S}_H \tag{4.48}$$

and

$$\bar{C} : [\,0,\tau\,] \longrightarrow \mathcal{S}_C\,, \tag{4.49}$$

such that for every $w_H \in \mathcal{V}_H$ and $w_C \in \mathcal{V}_C$

$$\mathcal{M}_H(\dot{H}, w_H) + \mathcal{K}_H(H, w_H) = \mathcal{F}_H(Q_H, w_H) + \mathcal{H}_H(h_H, w_H) \text{ on } ]\,0, \tau\,[\,, \tag{4.50}$$

$$\mathcal{M}_C(\dot{\bar{C}}, w_C) + \mathcal{K}_C(C^L, w_C) = \mathcal{F}_C(Q_C, w_C) + \mathcal{H}_C(h_C, w_C) \text{ on } ]\,0, \tau\,[\,, \tag{4.51}$$

$$(H(\boldsymbol{x}, 0) - H_0, w_H) = 0 \text{ on } \Omega, \tag{4.52}$$

and

$$(\bar{C}(\boldsymbol{x}, 0) - \bar{C}_0, w_C) = 0 \text{ on } \Omega. \tag{4.53}$$

The operators $\mathcal{M}_H$, $\mathcal{K}_H$, $\mathcal{F}_H$, $\mathcal{H}_H$, $\mathcal{M}_C$, $\mathcal{K}_C$, $\mathcal{F}_C$, $\mathcal{H}_C$ and $(.,.)$ are defined respectively as:

$$\mathcal{M}_H(\dot{H}, w_H) = \int_\Omega \dot{H}(\boldsymbol{x}, t)\, w_H(\boldsymbol{x})\, d\Omega\,, \tag{4.54}$$

$$\mathcal{K}_H(H, w_H) = \int_\Omega \nabla H(\boldsymbol{x}, t) \bullet \frac{\mathcal{K}(T(H(\boldsymbol{x}, t)), \bar{C}(\boldsymbol{x}, t), \boldsymbol{x}, t)}{C_p(T(H(\boldsymbol{x}, t)), \bar{C}(\boldsymbol{x}, t), \boldsymbol{x}, t)} \nabla w_H(\boldsymbol{x})\, d\Omega\,, \tag{4.55}$$

$$\mathcal{F}_H(H, w_H) = \int_\Omega Q_H(T(H(\boldsymbol{x}, t)), \boldsymbol{x}, t)\, w_H(\boldsymbol{x})\, d\Omega\,, \tag{4.56}$$

$$\mathcal{H}_H(h_H, w_H) = \int_{\Gamma_h} h_H(T(H(\boldsymbol{x}, t)), \boldsymbol{x}, t)\, w_H(\boldsymbol{x})\, d\Gamma\,, \tag{4.57}$$

$$\mathcal{M}_C(\dot{\bar{C}}, w_c) = \int_\Omega \dot{\bar{C}}(\boldsymbol{x}, t)\, \rho(\boldsymbol{x})\, w_C(\boldsymbol{x})\, d\Omega\,, \tag{4.58}$$

$$\mathcal{K}_C(C^L, w_C) = \int_\Omega \nabla C^L \bullet \rho(\boldsymbol{x}) \boldsymbol{D}(T(H(\boldsymbol{x}, t)), \bar{C}(\boldsymbol{x}, t), \boldsymbol{x}, t) \nabla w_C(\boldsymbol{x})\, d\Omega\,, \tag{4.59}$$

$$\mathcal{F}_C(Q_C, w_C) = \int_\Omega Q_C(\bar{C}(\boldsymbol{x}, t), \boldsymbol{x}, t)\, w_C(\boldsymbol{x})\, d\Omega\,, \tag{4.60}$$

$$\mathcal{H}_C(h_C, w_C) = \int_{\Gamma_C} h_C(\bar{C}(\boldsymbol{x}, t), \boldsymbol{x}, t)\, w_C(\boldsymbol{x})\, d\Gamma\,, \tag{4.61}$$

$$(H, w_H) = \int_\Omega H(\boldsymbol{x}, t)\, w_H(\boldsymbol{x})\, d\Omega \tag{4.62}$$

and

$$(\bar{C}, w_C) = \int_\Omega \bar{C}(\boldsymbol{x}, t)\, w_C(\boldsymbol{x})\, d\Omega. \tag{4.63}$$

Note that:

a) given suitable smoothness conditions a solution of **(S)** is a solution **(W)**,

(S) $\Longleftrightarrow$ (W),

b) $\mathcal{M}_H(\dot{H}, w_H)$, $\mathcal{K}_H(H, w_H)$, $\mathcal{M}_C(\dot{\bar{C}}, w_C)$, $\mathcal{K}_C(C^L, w_C)$, $(\bar{C}, w_C)$ and $(H, w_H)$ are symmetric bilinear forms.

## 4.5 Galerkin approximation of the initial boundary-value problem

The Garlerkin form is derived from the weak form by approximating the variational and solution spaces with finite-dimensional subspaces.

### 4.5.1 Galerkin spaces of approximation

The Garlerkin approximation uses a finite number of linear independent functions to span a subspace $\mathcal{V}^h$ and $\mathcal{S}^h$ where $\mathcal{V}^h \subset \mathcal{V}$ and $\mathcal{S}^h \subset \mathcal{S}$.

We represent $\mathcal{V}^h$ as

$$\mathcal{V}^h = \mathcal{V}_H^h \cup \mathcal{V}_C^h , \tag{4.64}$$

where

$$\mathcal{V}_H^h = \left\{ w_H^h \mid w_H^h = \sum_{A=1} N_A(\boldsymbol{x}) d_A,\ w_H^h = 0 \text{ on } \Gamma_g \right\} \tag{4.65}$$

and

$$\mathcal{V}_C^h = \left\{ w_C^h \mid w_C^h = \sum_{A=1} N_A(\boldsymbol{x}) \hat{d}_A,\ w_C^h = 0 \text{ on } \Gamma_g \right\}, \tag{4.66}$$

where $N_A$, $A = 1, 2 \cdots n$, are linearly independent functions in $\mathcal{V}$ and $d_A$ and $\hat{d}_A$ are constants.

Similarly, the approximation to the trial solution space $\mathcal{S}^h$ is defined as $\mathcal{S}^h = \mathcal{S}_H^h \cup \mathcal{S}_C^h$, where

$$\mathcal{S}_H^h = \left\{ H^h \mid H^h = v_H^h + g_H^h,\ v_H^h \in \mathcal{V}_H^h,\ g_H^h \in \mathcal{S}_H^h \right\} \tag{4.67}$$

and

$$\mathcal{S}_C^h = \left\{ \bar{C}^h \mid \bar{C}^h = v_C^h + g_C^h,\ v_C^h \in \mathcal{V}_C^h,\ g_C^h \in \mathcal{S}_C^h \right\}. \tag{4.68}$$

### 4.5.2 The Galerkin Form

The Galerkin approximation **(G)** of the IBVP may be stated as follows.

Given $\rho, C_p$, $\boldsymbol{\mathcal{K}}$, $\boldsymbol{D}$, $g_H$, $g_C$, $h_H$, $h_C$, $H_0$ and $\bar{C}_0$, as in § 4.3.2 – 4.3.3,

find

$$H^h = v_H^h + g_H^h \ : \ [\,0,\tau\,] \longrightarrow \mathcal{S}_H^h$$

and

$$\bar{C}^h = v_C^h + g_C^h \ : \ [\,0,\tau\,] \longrightarrow \mathcal{S}_C^h \ ,$$

such that for every $w_H^h \in \mathcal{S}_H^h$ and $w_C^h \in \mathcal{S}_C^h$

$$\begin{aligned} &\mathcal{M}_H(\dot{v}_H^h, w_H^h) + \mathcal{K}_H(v_H^h, w_H^h) = \mathcal{F}_H(Q_H, w_H^h) + \\ &\mathcal{H}_H(h_H^h, w_H^h) - \mathcal{M}_H(\dot{g}_H^h, w_H^h) - \mathcal{K}_H(g_H^h, w_H^h) \ \text{ on } \ ]\,0,\tau\,[, \end{aligned} \tag{4.69}$$

$$\begin{aligned} &\mathcal{M}_C(\dot{v}_C, w_C^h) + \mathcal{K}_C(v_C^h, w_C^h) = \mathcal{F}_H(Q_C, w_C^h) + \\ &\mathcal{H}_H(h_C^h, w_C^h) - \mathcal{M}_C(\dot{g}_C^h, w_C^h) - \mathcal{K}_C(g_C^h, w_C^h) \text{ on } ]\,0,\tau\,[, \end{aligned} \tag{4.70}$$

$$(v_H^h(\boldsymbol{x},0), w_H^h) = (H_0 - g_H^h(\boldsymbol{x},0)) \text{ on } \Omega \tag{4.71}$$

and

$$(v_C^h(\boldsymbol{x},0), w_C^h) = (\bar{C}_0 - g_C^h(\boldsymbol{x},0)) \text{ on } \Omega. \tag{4.72}$$

## 4.6 Finite element matrix approximation of the initial boundary-value problem

The finite element matrix equations are derived from the Galerkin form by defining the approximation of the variational and solution spaces based on a given spatial discretization.

### 4.6.1 Spatial Discretization

To obtain the finite element matrix form of the IBVP, the domain $\Omega$ must be discretized into disjoint element subdomains $\Omega^e$, $e = 1, 2, \cdots, N_{el}$, where $N_{el}$ is the number of elements. Thus

$$\bigcup_{e=1}^{N_{el}} \bar{\Omega}^e = \bar{\Omega} \tag{4.73}$$

and

$$\bigcap_{e=1}^{N_{el}} \Omega^e = \emptyset. \tag{4.74}$$

$\Gamma^e$ is the boundary of an element subdomain $\Omega^e$.

Each element subdomain is defined by an ordered set of nodal points. These element nodal points belong to the set $\eta$ of nodal points contained in the domain $\Omega$.

The set of nodal points is defined as $\eta = \{1, 2, \cdots N_{np}\}$ where $N_{np}$ is the total number of nodal points. Let those nodes at which $H^h = g_H$ and $\bar{C}^h = g_C$ are prescribed, be contained in the set $\eta_{g^H}$ and $\eta_{g^C}$ respectively where

$$\eta_{g^H} \cup \eta_{g^C} = \eta_g. \tag{4.75}$$

The complement of $\eta_{g^H}$ or $\eta_{g^C}$ in $\eta$, denoted $\eta - \eta_{g^H}$ and $\eta - \eta_{g^C}$, are the set of nodes at which $H^h$ and $\bar{C}^h$ are to be determined. The number of nodes in $\eta - \eta_{g^H}$ is $N_{eq}^H$ and the number of nodes $\eta - \eta_{g^C}$ is $N_{eq}^C$, where $N_{eq}^H$ is the number of equations needed to solve the energy conservation and $N_{eq}^C$ is the number of equations needed to solve the solute conservation.

### 4.6.2 Approximation Spaces

A finite element basis for $\mathcal{S}^h$ and $\mathcal{V}^h$ is defined by using a finite number of linear independent functions $N_a(\boldsymbol{x})$ which span $\mathcal{S}^h$ and $\mathcal{V}^h$,

$$\text{where } N_a(\boldsymbol{x}) = \begin{cases} 1 & \boldsymbol{x} = \boldsymbol{x}_a \\ 0 & \boldsymbol{x} = \boldsymbol{x}_b, b \neq a \\ 0 & \boldsymbol{x} \text{ is non-local .} \end{cases}$$

Local is taken to mean elements connected to the node under consideration. Thus we can write

$$v_H^h(\boldsymbol{x},t) = \sum_{A\epsilon\eta - \eta_{gH}} N_a(\boldsymbol{x})h_a(t) : [\,0,t\,] \longrightarrow \mathcal{V}_H^h, \tag{4.76}$$

$$v_C^h(\boldsymbol{x},t) = \sum_{A\epsilon\eta - \eta_{gC}} N_a(\boldsymbol{x})c_a(t) : [\,0,\tau] \longrightarrow \mathcal{V}_C^h \tag{4.77}$$

and

$$g_H^h(\boldsymbol{x},t) = \sum_{A\epsilon\eta_{gH}} N_a(\boldsymbol{x})g_{H_a}(t) : [\,0,\tau] \longrightarrow \mathcal{S}_H^h, \tag{4.78}$$

$$g_C^h(\boldsymbol{x},t) = \sum_{A\epsilon\eta_{gC}} N_a(\boldsymbol{x})g_{C_a}(t) : [\,0,\tau] \longrightarrow \mathcal{S}_C^h. \tag{4.79}$$

From (4.76), we see that a function in $\mathcal{V}_H^h$ may be represented in terms of a time-varying vector $\boldsymbol{h}$ of $N_{EQ}^H$ components that are coefficients associated with shape functions. Similarly a function in $\mathcal{V}_C^h$ may be represented in terms of a time-varying vector $\boldsymbol{c}$ of $N_{EQ}^C$ components that are coefficients associated with shape functions. Note that the time-dependent coefficients $g_{H_a}$ and $g_{C_a}$ are chosen so that $g_H^h$ is a 'good' approximation of $g_H$ and $g_C^h$ is a 'good' approximation of $g_C$.

### 4.6.3 The Finite Element Matrix Form

The finite element matrix form **(M)** of the IBVP is:

Given $\rho$, $C_p$, $\boldsymbol{\mathcal{K}}$, $\boldsymbol{D}$, $g_H$, $g_C$, $h_H$, $h_C$, $H_0$ and $\bar{C}_0$, as in § 4.3.2 – 4.3.3,

find

$$\boldsymbol{h} \;:\; [\,0,\tau\,] \longrightarrow \Re^{N_{eq}^H}$$

and

$$\boldsymbol{c} \;:\; [\,0,\tau\,] \longrightarrow \Re^{N_{eq}^C}$$

such that

$$M\,\dot{\boldsymbol{h}} + \boldsymbol{K}_H(\boldsymbol{h},\boldsymbol{c},t)\boldsymbol{h} = \boldsymbol{F}_H(\boldsymbol{h},t), \tag{4.80}$$

$$M\,\dot{\boldsymbol{c}} + \boldsymbol{N}_C(\boldsymbol{h},\boldsymbol{c},t) = \boldsymbol{F}_C(\boldsymbol{c},t), \tag{4.81}$$

$$\boldsymbol{h}(0) = \boldsymbol{h}^0 \tag{4.82}$$

and

$$\boldsymbol{c}(0) = \boldsymbol{c}^0, \tag{4.83}$$

where $\boldsymbol{h}(t)$ and $\boldsymbol{c}(t)$ are respectively vectors of nodal enthalpy and solute concentration at time $t$, and $\boldsymbol{h}^0$ and $\boldsymbol{c}^0$ are a 'good' approximation to the exact initial enthalpy $H_0$ and $\bar{C}_0$ respectively.

**4.6.3.1** The mass matrix $M$ which is constant for a fixed mesh is described as

$$M = \mathop{\mathsf{A}}_{e=1}^{Nel} m^e, \tag{4.84}$$

with the element mass matrix $m^e$ given as

$$m^e = m^e_{ab} = \int_{\Omega^e} \rho(\boldsymbol{x}) N_a(\boldsymbol{x}) N_b(\boldsymbol{x}) d\Omega. \tag{4.85}$$

**4.6.3.2** The enthalpy conductivity matrix $\boldsymbol{K}_H$ is described as

$$\boldsymbol{K}_H(\boldsymbol{h},\boldsymbol{c},t) = \mathop{\mathsf{A}}_{e=1}^{Nel} \boldsymbol{k}^e_H(\boldsymbol{h}^e,\boldsymbol{c}^e,t), \tag{4.86}$$

with the element matrix $\boldsymbol{k}^e_H$ given as

$$\boldsymbol{k}^e_H(\boldsymbol{h}^e,\boldsymbol{c}^e,t) = \{k^e_H(\boldsymbol{h}^e,\boldsymbol{c}^e,t)\}_{ab} \tag{4.87}$$

$$= \int_{\Omega^e} B_a(\boldsymbol{x}) \frac{\mathcal{K}(T(H^h),\bar{C}^h,\boldsymbol{x},t)}{C_p(T(H^h),\bar{C}^h,\boldsymbol{x},t)} \boldsymbol{B}_b(\boldsymbol{x})\, d\Omega. \tag{4.88}$$

**4.6.3.3** The internal heat flux and $h_H$ - type boundary condition vector $\boldsymbol{F}_H$ is described as

$$\boldsymbol{F}_H(\boldsymbol{h},t) = \mathop{\mathsf{A}}_{e=1}^{Nel} \boldsymbol{f}_H^e(\boldsymbol{h}^e,t), \tag{4.89}$$

with the element vector $\boldsymbol{f}_H^e$ given as

$$\begin{aligned} \boldsymbol{f}_H^e(\boldsymbol{h}^e,t) &= \{f_H^e(\boldsymbol{h}^e,t)\}_a & (4.90)\\ &= \int_{\Omega^e} N_a(\boldsymbol{x}) Q_H(T(H^h),\boldsymbol{x},t)d\Omega \\ &+ \int_{\Gamma^e\cap\Gamma_H} N_a(\boldsymbol{x}) h_H(T(H^h),\boldsymbol{x},t)d\Gamma. & (4.91)\end{aligned}$$

**4.6.3.4** The solute diffusive flux vector $\boldsymbol{N}_C$ is described as

$$\boldsymbol{N}_C(\boldsymbol{c},\boldsymbol{h},t) = \mathop{\mathsf{A}}_{e=1}^{Nel} \boldsymbol{n}_C^e(\boldsymbol{c}^e,\boldsymbol{h}^e,t), \tag{4.92}$$

with the element solute diffusive flux vector $\boldsymbol{n}_C^e$ given as

$$\begin{aligned} \boldsymbol{n}_C^e(\boldsymbol{c}^e,\boldsymbol{h}^e,t) &= \{n_C^e(\boldsymbol{c}^e,\boldsymbol{h}^e,t)\}_a & (4.93)\\ &= \int_{\Omega^e} \boldsymbol{B}_a^T(\boldsymbol{x})\rho(\boldsymbol{x})\boldsymbol{D}(T(H^h),\bar{C}^h,\boldsymbol{x},t)\boldsymbol{\nabla}C^L d\Omega. & (4.94)\end{aligned}$$

If $\Omega^e$ is totally liquid (i.e. $\phi = 0$) at each integration point in the element, then

$$\begin{aligned} \{n_C^e(\boldsymbol{c}^e,\boldsymbol{h}^e,t)\}_a &= \int_{\Omega^e} \boldsymbol{B}_a^T(\boldsymbol{x})\rho(\boldsymbol{x})\boldsymbol{D}(T(H^h),\bar{C}^h,\boldsymbol{x},t)\boldsymbol{B}_b^T(\boldsymbol{x})d\Omega\, c_b^e & (4.95)\\ &= \{K_{CL}^e\}_{ab}\, c_b^e. & (4.96)\end{aligned}$$

If $\Omega^e$ is totally mushy (i.e. $0 < \phi < 1$) at each integration point in the element, then

$$\begin{aligned} \{n_C^e(\boldsymbol{c}^e,\boldsymbol{h}^e,t)\}_a &= \int_{\Omega^e} \boldsymbol{B}_a^T(\boldsymbol{x}) \frac{\rho(\boldsymbol{x})\boldsymbol{D}(T(H^h),\bar{C}^h,\boldsymbol{x},t)}{m^L C_p(T(H^h),\bar{C}^h,\boldsymbol{x},t)}\, \boldsymbol{B}_b(\boldsymbol{x})d\Omega\, h_b^e & (4.97)\\ &= \{K_{CM}^e\}_{ab}\, h_b^e. & (4.98)\end{aligned}$$

If $\Omega^e$ is totally solid (i.e. $\phi = 1$) at each integration point in the element or, if the element was partially solid and partially eutectic, then

$$\{n^e_{C_a}(\boldsymbol{c}^e, \boldsymbol{h}^e, t)\}_a = 0. \tag{4.99}$$

If $\Omega^e$ is partially liquid and mushy or partially liquid, mushy and eutectic (i.e. $\phi = 0$ at some of the element integration points and $0 < \phi < 1$ at the remainder), or if $\Omega^e$ is partially liquid, mushy, eutectic and solid (i.e. $\phi = 0$ at some integration points, $\phi = 1$ at other integration points and $0 < \phi < 1$ at the remainder), then

$$\boldsymbol{n}^e_C(\boldsymbol{c}^e, \boldsymbol{h}^e, t) = \hat{\boldsymbol{K}}^e_{CL}\boldsymbol{c}^e + \hat{\boldsymbol{K}}^e_{CM}\boldsymbol{h}^e, \tag{4.100}$$

where $\hat{\boldsymbol{K}}^e_{CL}$ is a reduced form of $\boldsymbol{K}^e_{CL}$ which consists of contributions from those integration points that are liquid in the element. Similarly $\hat{\boldsymbol{K}}^e_{CM}$ is a reduced form of $\boldsymbol{K}^e_{CM}$ which consists of contributions from those integration points that are mushy.

If the element is partial mushy and eutectic or mushy, eutectic and solid then

$$\{\boldsymbol{n}^e_C(\boldsymbol{c}^e, \boldsymbol{h}^e, t)\}_a = \hat{\boldsymbol{K}}^e_{CM}\boldsymbol{h}^e. \tag{4.101}$$

In summary, for solidification/melting $\boldsymbol{n}^e_C = \boldsymbol{n}^e_C(\boldsymbol{c}^e, \boldsymbol{h}^e, t)$ can be described for the following cases as follows:

a ) for a totally liquid element, $\boldsymbol{n}^e_C = \boldsymbol{K}^e_{CL}\boldsymbol{c}^e$ ,

b ) for a totally mushy element, $\boldsymbol{n}^e_C = \boldsymbol{K}^e_{CM}\boldsymbol{h}^e$ ,

c ) for a totally solid or partially solid and eutectic element, $\boldsymbol{n}^e_C = \boldsymbol{0}$ ,

d ) for a partially liquid and mushy element, $\boldsymbol{n}^e_C = \hat{\boldsymbol{K}}_{CL}\boldsymbol{c}^e + \hat{\boldsymbol{K}}_{CM}\boldsymbol{h}^e$ ,

e ) for a partially liquid and mushy element or a partially liquid, mushy and eutectic element, $\boldsymbol{n}^e_C = \hat{\boldsymbol{K}}_{CL}\boldsymbol{c}^e + \hat{\boldsymbol{K}}_{CM}\boldsymbol{h}^e$, and

f ) for a partially mushy and eutectic or mushy solid and eutectic element, $\boldsymbol{n}^e_C = \hat{\boldsymbol{K}}_{CM}\boldsymbol{h}^e$ .

**4.6.3.5** The internal solute source and $h_C$-type boundary condition vector $\boldsymbol{F}_C$ is described as

$$\boldsymbol{F}_C(\boldsymbol{c}, t) = \mathop{\mathsf{A}}_{e=1}^{Nel} \boldsymbol{f}^e_C(\boldsymbol{c}^e, t), \tag{4.102}$$

with the element vector $\boldsymbol{f}_C^e$ given as

$$\begin{aligned} \boldsymbol{f}_C^e(\boldsymbol{c}^e,t) &= \{f_C^e(\boldsymbol{c}^e,t)\}_a \qquad (4.103)\\ &= \int_{\Omega^e} Q_C(\bar{C}^h,\boldsymbol{x},t)N_a(\boldsymbol{x})d\Omega \\ &+ \int_{\Gamma^e\cap\Gamma_h} h_C(C^L,\boldsymbol{x},t)N_a(\boldsymbol{x})\,d\Gamma. \qquad (4.104)\end{aligned}$$

Note that in most solidification/melting cases being looked at in this work $h_C(C^L,\boldsymbol{x},t) = 0$ and $Q_C(\bar{C}^h,\boldsymbol{x},t) = 0$. The solute source will come from the initial condition value.

## 4.7 Temporal Algorithm

The semi-discrete matrix form (M) of the coupled nonlinear ordinary differential equations has now to be discretized in terms of time enabling an algorithm for the generation of the approximate solution of the differential equations to be formulated.

### 4.7.1 Temporal Discretization

The real enthalpy $\boldsymbol{h}(t_n)$ and the real solute concentration $\boldsymbol{c}(t_n)$ are approximated by discrete values $\boldsymbol{h}_n$ and $\boldsymbol{c}_n$, thus

$$\boldsymbol{h}_n \approx \boldsymbol{h}(t_n) \qquad (4.105)$$

and

$$\boldsymbol{c}_n \approx \boldsymbol{c}(t_n). \qquad (4.106)$$

Similarly for the rate terms of $\boldsymbol{h}(t_n)$ and $\boldsymbol{c}(t_n)$ we get

$$\dot{\boldsymbol{c}}_n \approx \dot{\boldsymbol{c}}\,(t_n) \qquad (4.107)$$

and

$$\dot{\boldsymbol{h}}_n \approx \dot{\boldsymbol{h}}\,(t_n). \qquad (4.108)$$

The discrete solution times are given by

$$t_n = n\Delta t\,, \qquad (4.109)$$

where $\Delta t$ can be a constant or varying time step depending on the degree of nonlinearity of the problem.

### 4.7.2 Generalized Trapezoidal rule

The time-integration method chosen is the generalized trapezoidal rule (**T**). Applying it to the matrix form of the problem (**M**) leads to the following time-integration scheme:

Given $\boldsymbol{M}, \boldsymbol{K}_H, \boldsymbol{F}_H, \boldsymbol{N}_C$ and $\boldsymbol{F}_C$, as in equations (4.84) - (4.104),

find

$$\boldsymbol{h}_n \ , \ n \in \{0, 1 \cdots N_{steps}\}$$

and

$$\boldsymbol{c}_n \ , \ n \in \{0, 1 \cdots N_{steps}\},$$

such that

$$\boldsymbol{M}\, \dot{\boldsymbol{h}}_{n+1} + \boldsymbol{K}_H(\boldsymbol{h}_{n+1}, \boldsymbol{c}_{n+1}, t_{n+1})\boldsymbol{h}_{n+1} = \boldsymbol{F}_H(\boldsymbol{h}_{n+1}, t_{n+1}), \tag{4.110}$$

$$\boldsymbol{M}\, \dot{\boldsymbol{c}}_{n+1} + \boldsymbol{N}_C(\boldsymbol{h}_{n+1}, \boldsymbol{c}_{n+1}, t_{n+1}) = \boldsymbol{F}_C(\boldsymbol{c}_{n+1}, t_{n+1}), \tag{4.111}$$

$$\boldsymbol{h}_o = \boldsymbol{h}^\circ, \tag{4.112}$$

$$\boldsymbol{c}_o = \boldsymbol{c}^\circ, \tag{4.113}$$

$$\boldsymbol{h}_{n+1} = \boldsymbol{h}_n + \Delta t \left\{ (1-\alpha)\, \dot{\boldsymbol{h}}_n + \alpha\, \dot{\boldsymbol{h}}_{n+1} \right\} \tag{4.114}$$

and

$$\boldsymbol{c}_{n+1} = \boldsymbol{c}_n + \Delta t \left\{ (1-\alpha)\, \dot{\boldsymbol{c}}_n + \alpha\, \dot{\boldsymbol{c}}_{n+1} \right\}, \tag{4.115}$$

where $\alpha = [0, 1]$.

In this algorithm $\alpha$ is chosen so that the solution will be unconditionally stable, as in most solidification problems the solution is sought over very long time periods compared to the stability limit for the explicit form of the operator (i.e. when $\alpha = 0$), Abaqus [16]. Of these algorithms, the central difference method (i.e. $\alpha = \frac{1}{2}$) has the highest accuracy. However, this method tends to produce oscillations in the early time solution. These oscillations are not present in the backward difference method (i.e. $\alpha = 1$). Thus the backward difference method is recommended.

The rate terms of enthalpy $\dot{h}_{n+1}$ and solute concentration $\dot{c}_{n+1}$ in (4.114) and (4.115) respectively are discretized using the backward difference method, thus

$$\dot{h}_{n+1} = \frac{h_{n+1} - h_n}{\Delta t} \tag{4.116}$$

and

$$\dot{c}_{n+1} = \frac{c_{n+1} - c_n}{\Delta t}. \tag{4.117}$$

The two conservation equations in (**M**) can thus be expressed using the backward difference method as

$$M(\frac{h_{n+1} - h_N}{\Delta t}) + K_H(h_{n+1}, c_{n+1}, t_{n+1})h_{n+1} = F_{n+1}(h_{n+1}, t_{n+1}) \tag{4.118}$$

and

$$M(\frac{c_{n+1} - c_n}{\Delta t}) + N_C(h_{n+1}, c_{n+1}, t_{n+1}) = F_C(c_{n+1}, t_{n+1}). \tag{4.119}$$

## 4.8 Nonlinear Solution Scheme

In the preceding section we reduced the solution of a set of nonlinear ordinary differential equations to the solution of a nonlinear algebraic equation for each time step. The iterative scheme proposed for solving the nonlinear algebraic problem is a variant of Newton-Raphson iteration, which makes use of the continuity of the temporal discretization; it is termed a *predictor- corrector* method. The first phase of the algorithm uses the previously- computed results for the enthalpy and average solute concentration and their velocity components at step $n$ to *predict* what the enthalpy and average solute concentration will be at step $n + 1$. The second phase then does successive *corrections* until convergence is achieved. The corrections require the use of the *linearized* operator to compute solution increments. A 'consistent' linearization of the nonlinear operators, Hughes [51], results in a non-symmetric linear equation system which ensures quadratic convergence.

### 4.8.1 Newton-Raphson Iteration Scheme

Obtain values $h_{n+1}$ and $c_{n+1}$ such that the residual $r(h_{n+1}, r_{n+1}) = 0$ where

$$\boldsymbol{r}(\boldsymbol{h}_{n+1}, \boldsymbol{c}_{n+1}) = \begin{bmatrix} \boldsymbol{r}_H(\boldsymbol{h}_{n+1}, \boldsymbol{c}_{n+1}) \\ \boldsymbol{r}_C(\boldsymbol{h}_{n+1}, \boldsymbol{c}_{n+1}) \end{bmatrix} = \begin{bmatrix} \boldsymbol{0} \\ \boldsymbol{0} \end{bmatrix} = \boldsymbol{0}, \tag{4.120}$$

where

$$\begin{aligned} \boldsymbol{r}_H(\boldsymbol{h}_{n+1}, \boldsymbol{c}_{n+1}) &= \boldsymbol{M}(\frac{\boldsymbol{h}_{n+1} - \boldsymbol{h}_n}{\Delta t}) + \boldsymbol{K}_H(\boldsymbol{h}_{n+1}, \boldsymbol{c}_{n+1}, t_{n+1})\boldsymbol{h}_{n+1} & (4.121) \\ &- \boldsymbol{F}_H(\boldsymbol{h}_{n+1}, t_{n+1}) & (4.122) \end{aligned}$$

and

$$\begin{aligned} \boldsymbol{r}_C(\boldsymbol{h}_{n+1}, \boldsymbol{c}_{n+1}) &= \boldsymbol{M}(\frac{\boldsymbol{c}_{n+1} - \boldsymbol{c}_n}{\Delta t}) + \boldsymbol{N}_C(\boldsymbol{h}_{n+1}, \boldsymbol{c}_{n+1}, t_{n+1}) & (4.123) \\ &- \boldsymbol{F}_C(\boldsymbol{c}_{n+1}, t_{n+1}). & (4.124) \end{aligned}$$

Using a Taylor series expansion about the exact solutions $\boldsymbol{c}_{n+1}$ and $\boldsymbol{h}_{n+1}$, we may approximate the residual $\boldsymbol{r}$ at the values $\boldsymbol{h}^i_{n+1}$ and $\boldsymbol{c}^i_{n+1}$ by

$$\begin{aligned} \boldsymbol{r}(\boldsymbol{c}_{n+1}, \boldsymbol{h}_{n+1}) &= \boldsymbol{r}(\boldsymbol{c}^i_{n+1}, \boldsymbol{h}^i_{n+1}) + \left[\frac{\partial \boldsymbol{r}(\boldsymbol{c}, \boldsymbol{h})}{\partial \boldsymbol{h}}\right]_{\substack{h = h^i_{n+1} \\ c = c^i_{n+1}}} (\boldsymbol{h}_{n+1} - \boldsymbol{h}^i_{n+1}) \\ &+ \left[\frac{\partial \boldsymbol{r}(\boldsymbol{c}, \boldsymbol{h})}{\partial \boldsymbol{c}}\right]_{\substack{h = h^i_{n+1} \\ c = c^i_{n+1}}} (\boldsymbol{c}_{n+1} - \boldsymbol{c}^i_{n+1}) + \cdots \end{aligned} \tag{4.125}$$

and the Jacobian tangent operators are defined as

$$\boldsymbol{D}_h \boldsymbol{r}(\boldsymbol{c}_{n+1}, \boldsymbol{h}_{n+1}) = \left[\frac{\partial \boldsymbol{r}(\boldsymbol{c}, \boldsymbol{h})}{\partial \boldsymbol{h}}\right]_{\substack{h = h^i_{n+1} \\ c = c^i_{n+1}}} = \begin{bmatrix} \frac{\partial \boldsymbol{r}_H}{\partial \boldsymbol{h}} \\ \frac{\partial \boldsymbol{r}_C}{\partial \boldsymbol{h}} \end{bmatrix}_{\substack{h = h^i_{n+1} \\ c = c^i_{n+1}}} \tag{4.126}$$

and

$$\boldsymbol{D}_c \boldsymbol{r}(\boldsymbol{c}_{n+1}, \boldsymbol{h}_{n+1}) = \left[\frac{\partial \boldsymbol{r}(\boldsymbol{c}, \boldsymbol{h})}{\partial \boldsymbol{c}}\right]_{\substack{h = h^i_{n+1} \\ c = c^i_{n+1}}} = \begin{bmatrix} \frac{\partial \boldsymbol{r}_H}{\partial \boldsymbol{c}} \\ \frac{\partial \boldsymbol{r}_C}{\partial \boldsymbol{c}} \end{bmatrix}_{\substack{h = h^i_{n+1} \\ c = c^i_{n+1}}} . \tag{4.127}$$

Ignoring higher order terms in the Taylor expansion, we may write

$$[\boldsymbol{D}_h \boldsymbol{r}(\boldsymbol{c}_{n+1}, \boldsymbol{h}_{n+1})\ \boldsymbol{D}_c \boldsymbol{r}(\boldsymbol{r}_{n+1}, \boldsymbol{h}_{n+1})] \begin{bmatrix} \Delta \boldsymbol{h}^i_{n+1} \\ \Delta \boldsymbol{c}^i_{n+1} \end{bmatrix} = -\boldsymbol{r}(\boldsymbol{c}^i_{n+1}, \boldsymbol{h}^i_{n+1}), \tag{4.128}$$

which can be rewritten as

$$\begin{bmatrix} \frac{\partial \boldsymbol{r}_H}{\partial \boldsymbol{h}} & \frac{\partial \boldsymbol{r}_H}{\partial \boldsymbol{c}} \\ \frac{\partial \boldsymbol{r}_C}{\partial \boldsymbol{h}} & \frac{\partial \boldsymbol{r}_C}{\partial \boldsymbol{c}} \end{bmatrix}_{\substack{h = h^i_{n+1} \\ c = c^i_{n+1}}} \begin{bmatrix} \Delta \boldsymbol{h}^i_{n+1} \\ \Delta \boldsymbol{c}^i_{n+1} \end{bmatrix} = \begin{bmatrix} -\boldsymbol{r}_H(\boldsymbol{c}^i_{n+1}, \boldsymbol{h}^i_{n+1}) \\ -\boldsymbol{r}_C(\boldsymbol{c}^i_{n+1}, \boldsymbol{h}^i_{n+1}) \end{bmatrix}. \tag{4.129}$$

The solution of this equation allows a better approximation to the exact solution, thus

$$\boldsymbol{c}^{i+1}_{n+1} = \boldsymbol{c}^i_{n+1} + \Delta \boldsymbol{c}^i_{n+1} \tag{4.130}$$

and

$$\boldsymbol{h}^{i+1}_{n+1} = \boldsymbol{h}^i_{n+1} + \Delta \boldsymbol{h}^i_{n+1}. \tag{4.131}$$

### 4.8.2 Evaluation of the Jacobian Operator

Examining the terms in the Jacobian in more detail, we obtain the following:

$$\begin{aligned} \boldsymbol{D}_h \boldsymbol{r}_H(\boldsymbol{h}_{n+1}, \boldsymbol{c}_{n+1}) &= \boldsymbol{D}_h \left\{ \boldsymbol{M} \frac{\boldsymbol{h}_{n+1} - \boldsymbol{h}_n}{\Delta t} \right\} + \boldsymbol{D}_h \{ \boldsymbol{K}_H(\boldsymbol{h}_{n+1} \boldsymbol{c}_{n+1}) \boldsymbol{h}_{n+1} \} \\ &- \boldsymbol{D}_h \boldsymbol{F}_H(\boldsymbol{h}_{n+1}), \end{aligned} \tag{4.132}$$

$$\begin{aligned} \boldsymbol{D}_c \boldsymbol{r}_H(\boldsymbol{h}_{n+1}, \boldsymbol{c}_{n+1}) &= \boldsymbol{D}_c \left\{ \boldsymbol{M} \frac{\boldsymbol{h}_{n+1} - \boldsymbol{h}_n}{\Delta t} \right\} + \boldsymbol{D}_c \{ \boldsymbol{K}_H(\boldsymbol{h}_{n+1} \boldsymbol{c}_{n+1}) \boldsymbol{h}_{n+1} \} \\ &- \boldsymbol{D}_c \boldsymbol{F}_H(\boldsymbol{h}_{n+1}), \end{aligned} \tag{4.133}$$

$$\begin{aligned} \boldsymbol{D}_h \boldsymbol{r}_C(\boldsymbol{h}_{n+1}, \boldsymbol{c}_{n+1}) &= \boldsymbol{D}_h \left\{ \boldsymbol{M} \frac{\boldsymbol{c}_{n+1} - \boldsymbol{c}_n}{\Delta t} \right\} + \boldsymbol{D}_h \{ \boldsymbol{N}_C(\boldsymbol{h}_{n+1} \boldsymbol{c}_{n+1}) \} \\ &- \boldsymbol{D}_h \boldsymbol{F}_C(\boldsymbol{c}_{n+1}) \end{aligned} \tag{4.134}$$

and

$$\begin{aligned} \boldsymbol{D_c r_C}(\boldsymbol{h}_{n+1}, \boldsymbol{c}_{n+1}) &= \boldsymbol{D_c}\left\{\boldsymbol{M}\frac{\boldsymbol{c}_{n+1}-\boldsymbol{c}_n}{\Delta t}\right\} + \boldsymbol{D_c}\{\boldsymbol{N_C}(\boldsymbol{h}_{n+1}\boldsymbol{c}_{n+1})\} \\ &- \boldsymbol{D_c F_C}(\boldsymbol{c}_{n+1}). \end{aligned} \tag{4.135}$$

A description of the different contributions to each of the four Jacobian terms follows.

**4.8.2.1** In this section the contributions to $\boldsymbol{D_h r_H}(\boldsymbol{h}_{n+1}, \boldsymbol{c}_{n+1})$ are described.

a) The enthalpy rate contribution is

$$\boldsymbol{D_h}\left\{\boldsymbol{M}\frac{\boldsymbol{h}_{n+1}-\boldsymbol{h}_n}{\Delta t}\right\} = \mathop{\mathsf{A}}_{e=1}^{Nel} \boldsymbol{D}^e_{h^e}\left\{\boldsymbol{m}^e\frac{\boldsymbol{h}^e_{n+1}-\boldsymbol{h}^e_n}{\Delta t}\right\}, \tag{4.136}$$

with its element contributions,

$$\boldsymbol{D}^e_{h^e}\left\{\boldsymbol{m}^e\frac{\boldsymbol{h}^e_{n+1}-\boldsymbol{h}^e_n}{\Delta t}\right\} = \left\{\frac{1}{\Delta t}m^e_{ab}\delta_{bc}\right\}_{\substack{h^e = h^{e^i}_{n+1} \\ c^e = c^{e^i}_{n+1}}} \tag{4.137}$$

$$= \{\mathcal{M}^e_{HH}\}_{ac} \tag{4.138}$$

and components,

$$\frac{1}{\Delta t}m^e_{ac} = \int_{\Omega^e} \rho(\boldsymbol{x}) N_a(\boldsymbol{x}) N_c(\boldsymbol{x})\, d\Omega. \tag{4.139}$$

b) The enthalpy conduction contribution is

$$\boldsymbol{D_h}\{\boldsymbol{K_H}(\boldsymbol{h}_{n+1}, \boldsymbol{c}_{n+1})\boldsymbol{h}_{n+1}\} = \mathop{\mathsf{A}}_{e=1}^{Nel} \boldsymbol{D}^e_{h^e}\left\{\boldsymbol{K}^e_H(\boldsymbol{h}^e_{n+1}, \boldsymbol{c}^e_{n+1})\boldsymbol{h}^e_{n+1}\right\}, \tag{4.140}$$

with its element contributions,

$$\begin{aligned} \boldsymbol{D}^e_{h^e}\left\{\boldsymbol{K}^e_H(\boldsymbol{h}^e_{n+1}, \boldsymbol{c}^e_{n+1})\boldsymbol{h}^e_{n+1}\right\} &= \left\{\frac{\partial\{K^e_H(\boldsymbol{h}^e, \boldsymbol{c}^e)\}_{ab}}{\partial h^e_c}h^e_b\right. \\ &+ \left.\{K^e_H(\boldsymbol{h}^e, \boldsymbol{c}^e)\}_{ab}\,\delta^e_{bc}\right\}_{\substack{h^e = h^{e^i}_{n+1} \\ c^e = c^{e^i}_{n+1}}} \end{aligned} \tag{4.141}$$

$$= \{\mathcal{K}^e_{HH}\}_{ac} \tag{4.142}$$

and components,

$$\frac{\partial \{K_H^e(\boldsymbol{h}^e, \boldsymbol{c}^e)\}_{ab}}{\partial h_c^e} h_b^e = \int_{\Omega^e} \boldsymbol{B}_a^T(\boldsymbol{x}) \frac{\partial}{\partial H^h}\left(\frac{\boldsymbol{\mathcal{K}}}{C_p}\right) N_c(\boldsymbol{x}) \boldsymbol{B}_b(\boldsymbol{x})\, d\Omega\, h_b$$
$$= \{\mathcal{K}\}_{ac}^{NSYM} \tag{4.143}$$

and

$$\left\{K_H(\boldsymbol{h}_{n+1}^e, \boldsymbol{c}_{n+1}^e\right\}_{ac} = \int_{\Omega^e} \boldsymbol{B}_a^T(\boldsymbol{x}) \left(\frac{\boldsymbol{\mathcal{K}}}{C_p}\right) \boldsymbol{B}_c(\boldsymbol{x})\, d\Omega\,, \tag{4.144}$$
$$= \{\mathcal{K}_{HH}^e\}_{ac}^{SYM}\,, \tag{4.145}$$

where:

$$\frac{\partial}{\partial H^h}\left(\frac{\boldsymbol{\mathcal{K}}}{C_p}\right) = \frac{1}{(C_p)^2}\left(\frac{\partial \boldsymbol{\mathcal{K}}}{\partial T} - \frac{\boldsymbol{\mathcal{K}}}{C_p}\frac{\partial C_p}{\partial T}\right), \tag{4.146}$$

$$\frac{\partial \boldsymbol{\mathcal{K}}}{\partial T} = \phi\, \frac{\partial \boldsymbol{\mathcal{K}}^S}{\partial T} + (1-\phi)\, \frac{\partial \boldsymbol{\mathcal{K}}^L}{\partial T} + (\boldsymbol{\mathcal{K}}^S - \boldsymbol{\mathcal{K}}^L)\frac{\partial \phi}{\partial T} \tag{4.147}$$

and

$$\frac{\partial C_p}{\partial T} = \phi\, \frac{\partial C_p^S}{\partial T} + (1-\phi)\, \frac{\partial C_p^L}{\partial T} + \left\{\int_0^T (C_p^S - C_p^L) dT - L\right\} \frac{\partial^2 \phi}{\partial T^2}$$
$$+ \left\{2(C_p^S - C_p^L)\right\} \frac{\partial \phi}{\partial T}. \tag{4.148}$$

c) The internal heat flux and $h_H$-type boundary condition vector contribution is

$$\boldsymbol{D}_h \boldsymbol{F}_H(\boldsymbol{h}_{n+1}) = \mathop{\mathsf{A}}_{e=1}^{Nel} \boldsymbol{D}_{h^e}^e \boldsymbol{f}_H(\boldsymbol{h}_{n+1}^e), \tag{4.149}$$

with its element contributions,

$$\boldsymbol{D}_{h^e}^e \boldsymbol{f}_H^e(\boldsymbol{h}_{n+1}^e) = \left\{\frac{\partial \{f_H(\boldsymbol{h}^e)\}_a}{\partial h_c}\right\}_{\substack{h^e = h_{n+1}^{e^i} \\ c^e = c_{n+1}^{e^i}}} \tag{4.150}$$

and components,

$$\frac{\partial \{f_H\}_a}{\partial h_c} = \int_\Omega N_a(\boldsymbol{x}) \frac{1}{C_p} \frac{\partial Q_H}{\partial T^h} N_c(\boldsymbol{x}) \, d\Omega + \int_{\Gamma^e n \Gamma^h} N_a(\boldsymbol{x}) \frac{1}{C_p} \frac{\partial q_H}{\partial T^h} N_c(\boldsymbol{x}) \, d\Gamma \quad (4.151)$$

$$= \{\mathcal{F}^e_{HH}\}_{ac}. \quad (4.152)$$

The internal heat flux contribution in many cases is zero, as the dependence of $Q_H(T(H^h), \boldsymbol{x}, t)$ is relatively weak. If $h_H(T(H^h), \boldsymbol{x}, t)$ is a convection boundary condition then

$$\frac{\partial h_H}{\partial T} = h_{conv}(\boldsymbol{x}, t). \quad (4.153)$$

If $h_H(T(H^h), \boldsymbol{x}, t)$ is a radiation boundary condition then

$$\frac{\partial h_H}{\partial T} = 4\sigma e (T(H^h))^3. \quad (4.154)$$

Using expressions (4.153) and (4.154), equation (4.151) becomes

$$\frac{\partial \{f_H\}_a}{\partial h_c} = \int_{\Omega^e} N_a(\boldsymbol{x}) \frac{1}{C_p} \frac{\partial Q_H}{\partial T} N_c(\boldsymbol{x}) \, d\Omega + \int_{\Gamma^e n \Gamma^h} N_a(\boldsymbol{x}) \frac{h_{conv}}{C_p} N_c(\boldsymbol{x}) \, d\Omega + 4\sigma e \int_{\Gamma^e n \Gamma^h} N_a(\boldsymbol{x}) \frac{(T(H^h))^3}{C_p} N_c(\boldsymbol{x}) \, d\Omega \quad (4.155)$$

$$= \left\{\mathcal{F}^e_{Q_H}\right\}^{SYM}_{ac} + \{\mathcal{F}^e_{conv}\}^{SYM}_{ac} + \{\mathcal{F}^e_{rad}\}^{SYM}_{ac}. \quad (4.156)$$

**4.8.2.2** In this section the contributions to $\boldsymbol{D}_c \boldsymbol{r}_h(\boldsymbol{h}_{n+1}, \boldsymbol{c}_{n+1})$ are described.

a) The enthalpy rate contribution is

$$\boldsymbol{D}_c \left\{ \boldsymbol{M} \frac{\boldsymbol{h}_{n+1} - \boldsymbol{h}_n}{\boldsymbol{\Delta t}} \right\} = \boldsymbol{0}. \quad (4.157)$$

b) The enthalpy conduction contribution is

$$\boldsymbol{D}_c\{\boldsymbol{K}_H(\boldsymbol{h}_{n+1},\boldsymbol{c}_{n+1})\boldsymbol{h}_{n+1}\} = \mathop{\mathsf{A}}_{e=1}^{Nel} \boldsymbol{D}^e_{c^e}\left\{\boldsymbol{K}^e_H(\boldsymbol{h}^e_{n+1},\boldsymbol{c}^e_{n+1})\boldsymbol{h}^e_{n+1}\right\}, \tag{4.158}$$

with is element contributions,

$$\boldsymbol{D}^e_{c^e}\left\{\boldsymbol{K}^e_H(\boldsymbol{h}^e_{n+1},\boldsymbol{c}^e_{n+1})\boldsymbol{h}^e_{n+1}\right\} = \left\{\frac{\partial\{K^e_H(\boldsymbol{h}^e,\boldsymbol{c}^e)\}_{ab}}{\partial c^e_c}\, h^e_b\right\}_{\substack{h^e = h^{e^i}_{n+1} \\ c^e = c^{e^i}_{n+1}}} \tag{4.159}$$

$$= \{K^e_{HC}\}_{ac} \tag{4.160}$$

and components,

$$\frac{\partial\{K^e_H(\boldsymbol{h}^e,\boldsymbol{c}^e)\}_{ab}}{\partial c^e_c}\, h^e_b = \int_{\Omega^e} \boldsymbol{B}^T_a(\boldsymbol{x})\frac{\partial}{\partial C^h}\left(\frac{\boldsymbol{\kappa}}{C_p}\right) N_c(\boldsymbol{x})\boldsymbol{B}_b(\boldsymbol{x})\, d\Omega\, h_b\,, \tag{4.161}$$

where:

$$\frac{\partial}{\partial \bar{C}^h}\left(\frac{\boldsymbol{\kappa}}{C_p}\right) = \frac{\boldsymbol{\kappa}}{(C_p)}\left(\frac{\partial \boldsymbol{\kappa}}{\partial \bar{C}^h} - \frac{\boldsymbol{\kappa}}{C_p}\frac{\partial C_p}{\partial \bar{C}^h}\right), \tag{4.162}$$

$$\frac{\partial \boldsymbol{\kappa}}{\partial \bar{C}^h} = \phi\,\frac{\partial \boldsymbol{\kappa}^S}{\partial \bar{C}^h} + (1-\phi)\,\frac{\partial \boldsymbol{\kappa}^L}{\partial \bar{C}^h} + (\boldsymbol{\kappa}^S - \boldsymbol{\kappa}^L)\frac{\partial \phi}{\partial \bar{C}^h} \tag{4.163}$$

and

$$\frac{\partial C_p}{\partial \bar{C}^h} = (C^S_p - C^L_p)\frac{\partial \phi}{\partial \bar{C}^h} + \left\{\int_0^{T(H)} (C^S_p - C^L_p)dT - L\right\}\frac{\partial^2 \phi}{\partial T \partial \bar{C}^h}\,. \tag{4.164}$$

c) The internal heat flux and $h_H$ - type boundary condition vector contribution is

$$\boldsymbol{D}_c\boldsymbol{F}_H(\boldsymbol{h}_{n+1}) = \boldsymbol{0}. \tag{4.165}$$

**4.8.2.3** In this section the contributions to $\boldsymbol{D}_h\boldsymbol{r}_C(\boldsymbol{h}_{n+1},\boldsymbol{c}_{n+1})$ are described.

a) The solute rate contribution is

$$\boldsymbol{D}_h\left\{\boldsymbol{M}\frac{\boldsymbol{c}_{n+1} - \boldsymbol{c}_n}{\Delta t}\right\} = \boldsymbol{0}\,. \tag{4.166}$$

b) The solute diffusive flux contribution is

$$\boldsymbol{D}_h \boldsymbol{N}_C(\boldsymbol{h}_{n+1}, \boldsymbol{c}_{n+1}) = \mathop{\mathsf{A}}_{e=1}^{Nel} \boldsymbol{n}_C^e(\boldsymbol{h}_{n+1}^e, \boldsymbol{c}_{n+1}^e), \tag{4.167}$$

with its element contributions,

$$\boldsymbol{D}_{h^e}^e \boldsymbol{n}_C^e(\boldsymbol{h}_{n+1}, \boldsymbol{c}_{n+1}^e) = \left\{ \frac{\partial \{n_C^e(\boldsymbol{h}^e, \boldsymbol{c}^e)\}_a}{\partial h_c^e} \right\}_{\substack{h^e = h_{n+1}^{e^i} \\ c^e = c_{n+1}^{e^i}}} \tag{4.168}$$

and components,

$$\frac{\partial \{n_C^e\}_a}{\partial h_c^e} = \int_{\Omega^e} \boldsymbol{B}_a^T(\boldsymbol{x}) \rho(\boldsymbol{x}) \frac{\partial}{\partial H^h} (\boldsymbol{D} \boldsymbol{\nabla} C^L) N_c(\boldsymbol{x}) \, d\Omega. \tag{4.169}$$

If the element is totally liquid then

$$\frac{\partial \{n_C^e\}_a}{\partial h_c^e} = \frac{\partial \{K_{CL}^e\}_{ab}}{\partial h_c^e} c_b^e \tag{4.170}$$

$$= \int_{\Omega^e} \boldsymbol{B}_a^T(\boldsymbol{x}) \rho(\boldsymbol{x}) \frac{\partial \boldsymbol{D}^L}{\partial H^h} N_c(\boldsymbol{x}) \boldsymbol{B}_b(\boldsymbol{x}) \, d\Omega \, c_b^e \tag{4.171}$$

$$= \{K_{CHL}^e\}_{ac}^{NSYM}, \tag{4.172}$$

where

$$\frac{\partial \boldsymbol{D}^L}{\partial H^L} = \frac{1}{C_p} \frac{\partial \boldsymbol{D}^L}{\partial T}. \tag{4.173}$$

If the element is totally solid or partially solid and eutectic then

$$\frac{\partial \{n_C^e\}_a}{\partial h_c^e} = 0. \tag{4.174}$$

If the element is totally mushy then

$$\frac{\partial \{n_C^e\}_a}{\partial h_c^e} = \frac{\partial}{\partial h_c^e}\{\{K_{CM}^e\}_{ab} h_b^e\} \tag{4.175}$$

$$= \frac{\partial \{K_{CM}^e\}_{ab}}{\partial h_c^e} h_b^e + \{K_{CM}^e\}_{ab}\,\delta_{bc} \tag{4.176}$$

$$= \{\mathcal{K}_{CHM}\}_{ac}^{NSYM} + \{\mathcal{K}_{CHM}\}_{ac}^{SYM} = \{\mathcal{K}_{CHM}\}_{ac} \text{ (non-symmetric)}, \tag{4.177}$$

where

$$\{K_{CM}^e\}_{ac} = \int_{\Omega^e} \boldsymbol{B}_a^T(\boldsymbol{x}) \frac{\rho(\boldsymbol{x})}{C_p m^L} \boldsymbol{D} \boldsymbol{B}_c(\boldsymbol{x})\, d\Omega \tag{4.178}$$

and

$$\frac{\partial \{K_{CM}^e\}_{ab}}{\partial h_c^e} h_b^e = \int_{\Omega^e} \boldsymbol{B}_a^T(\boldsymbol{x}) \rho(\boldsymbol{x}) \frac{\partial}{\partial H^h}\left(\frac{\boldsymbol{D}}{C_p m^L}\right) N_c(\boldsymbol{x}) \boldsymbol{B}_b(\boldsymbol{x})\, d\Omega\, h_b\,, \tag{4.179}$$

where

$$\frac{\partial}{\partial H^h}\left(\frac{\boldsymbol{D}}{C_p m^L}\right) = \frac{1}{m^L C_p^2}\left(\frac{\partial \boldsymbol{D}}{\partial T} - \frac{\boldsymbol{D}}{C_p}\frac{\partial C_p}{\partial T}\right) \tag{4.180}$$

and where

$$\frac{\partial \boldsymbol{D}}{\partial T} = (1-\phi)\frac{\partial \boldsymbol{D}^L}{\partial T} - \boldsymbol{D}^L \frac{\partial \phi}{\partial T}\,. \tag{4.181}$$

In summary:

a ) if the element is totally liquid, $\boldsymbol{D}_{h^e}^e \boldsymbol{n}_C^e = \boldsymbol{\mathcal{K}}^e{}_{CHL}$ (non-symmetric),

b ) if the element is totally solid or partially solid and eutectic, $\boldsymbol{D}_{h^e}^e \boldsymbol{n}_C^e = 0$,

c ) if the element is totally mushy, $\boldsymbol{D}_{h^e}^e \boldsymbol{n}_C^e = \boldsymbol{\mathcal{K}}^e{}_{CHM} = [\boldsymbol{\mathcal{K}}_{CHM}^{NSYM} + \boldsymbol{\mathcal{K}}_{CHM}^{SYM}]^e$ (non-symmetric),

d ) if the element is partially mushy and liquid or partially mushy, liquid, and eutectic (or eutectic and solid), $\boldsymbol{D}_{h^e}^e \boldsymbol{n}_C^e = \hat{\boldsymbol{\mathcal{K}}}_{CHM}^e + \hat{\boldsymbol{\mathcal{K}}}_{CHL}^e$ (non-symmetric), and

e ) if the element is partially mushy, solid and eutectic or mushy and eutectic, $\boldsymbol{D}^e_{h^e}\boldsymbol{n}^e_C = \hat{\boldsymbol{\mathcal{K}}}^e_{CHM}$ (non-symmetric).

Note as in § 4.6.3.4 $\hat{\boldsymbol{\mathcal{K}}}^e_{CHM}$ and $\hat{\boldsymbol{\mathcal{K}}}^e_{CHL}$ are reduced forms of $\boldsymbol{\mathcal{K}}^e_{CHM}$ and $\boldsymbol{\mathcal{K}}^e_{CHL}$, where $\hat{\boldsymbol{\mathcal{K}}}^e_{CHM}$ and $\hat{\boldsymbol{\mathcal{K}}}^e_{CHL}$ result from contributions from those integration points in the element that are mushy and liquid respectively.

c) The internal solute source and $h_C$-type boundary condition vector contribution is

$$\boldsymbol{D}_h\boldsymbol{F}_C(\boldsymbol{c}_{n+1}) = \boldsymbol{0}. \tag{4.182}$$

**4.8.2.4** In this section the contributions to $\boldsymbol{D}_c\boldsymbol{r}_C(\boldsymbol{h}_{n+1}, \boldsymbol{c}_{n+1})$ are described.

a) The solute rate contribution is

$$\boldsymbol{D}_c\left\{\boldsymbol{M}\frac{\boldsymbol{c}_{n+1}-\boldsymbol{c}_n}{\boldsymbol{\Delta t}}\right\} = \mathop{\mathsf{A}}_{e=1}^{Nel} \boldsymbol{D}^e_{c^e}\left\{\boldsymbol{m}^e\frac{\boldsymbol{c}^e_{n+1}-\boldsymbol{c}^e_n}{\boldsymbol{\Delta t}}\right\}, \tag{4.183}$$

with its element contributions,

$$\boldsymbol{D}^e_{c^e}\left\{\boldsymbol{m}^e\frac{\boldsymbol{c}^e_{n+1}-\boldsymbol{c}^e_n}{\boldsymbol{\Delta t}}\right\} = \left\{\frac{1}{\Delta t}m^e_{ab}\delta_{bc}\right\}_{\substack{h^e = h^{e^i}_{n+1} \\ c^e = c^{e^i}_{n+1}}} \tag{4.184}$$

$$= \{\mathcal{M}^e_{CC}\}_{ac} \tag{4.185}$$

and components,

$$\frac{1}{\Delta t}m^e_{ac} = \int_{\Omega^e}\rho(\boldsymbol{x})N_a(\boldsymbol{x})N_c(\boldsymbol{x})\,d\Omega. \tag{4.186}$$

b) The solute diffusive flux contribution is

$$\boldsymbol{D}_c\{\boldsymbol{N}_C(\boldsymbol{h}_{n+1}, \boldsymbol{c}_{n+1})\} = \mathop{\mathsf{A}}_{e=1}^{Nel} \boldsymbol{D}^e_{c^e}\boldsymbol{n}^e_C(\boldsymbol{h}^e_{n+1}, \boldsymbol{c}^e_{n+1}), \tag{4.187}$$

with its element contributions,

$$\boldsymbol{D}^e_{c^e} \boldsymbol{n}^e_C(\boldsymbol{h}^e_{n+1}, \boldsymbol{c}^e_{n+1}) = \left\{ \frac{\partial \{n^e_C(\boldsymbol{h}^e, \boldsymbol{c}^e)\}_a}{\partial c^e_c} \right\}_{\substack{h^e = h^{e^i}_{n+1} \\ c^e = c^{e^i}_{n+1}}} \tag{4.188}$$

and components,

$$\frac{\partial \{n^e_C\}_a}{\partial c^e_c} = \int_{\Omega^e} \boldsymbol{B}^T_a(\boldsymbol{x}) \frac{\partial}{\partial \bar{C}^h} (\boldsymbol{D} \boldsymbol{\nabla} C^L) N_c(\boldsymbol{x}) \, d\Omega. \tag{4.189}$$

If the element is totally liquid then

$$\frac{\partial \{n^e_C\}_a}{\partial c^e_c} = \frac{\partial \{K^e_{CL}\}_{ab}}{\partial c^e_c} c^e_b + \{K^e_{CL}\}_{ab} \delta_{bc} \tag{4.190}$$

$$= \{\mathcal{K}^e_{CCL}\}^{NSYM}_{ac} + \{\mathcal{K}^e_{CCL}\}^{SYM}_{ac} = \{\mathcal{K}^e_{CCL}\}_{ac} \text{ (non-symmetric)}, \tag{4.191}$$

where

$$\frac{\partial \{K^e_{CL}\}_{ab}}{\partial c^e_c} c^e_b = \int_{\Omega^e} \boldsymbol{B}^T_a(\boldsymbol{x}) \frac{\partial \boldsymbol{D}^L}{\partial \bar{C}^h} N_c(\boldsymbol{x}) \boldsymbol{B}_b(\boldsymbol{x}) \, d\Omega \; c^e_b \tag{4.192}$$

and

$$\{K^e_{CL}\}_{ac} = \int_{\Omega^e} \boldsymbol{B}^T_a(\boldsymbol{x}) \boldsymbol{D}^L \boldsymbol{B}_c(\boldsymbol{x}) \, d\Omega. \tag{4.193}$$

If the element is totally mushy then

$$\frac{\partial \{n^e_C\}_a}{\partial c^e_c} = \frac{\partial \{K^e_{CM}\}_{ab}}{\partial c^e_c} h^e_b \tag{4.194}$$

$$= \int_{\Omega^e} \boldsymbol{B}^T_a(\boldsymbol{x}) \frac{\partial}{\partial \bar{C}^h} \left\{ \frac{\boldsymbol{D}}{m^L C_p} \right\} N_c(\boldsymbol{x}) \boldsymbol{B}_b(\boldsymbol{x}) \, d\Omega \; h^e_b$$

$$= \{\mathcal{K}^e_{CCM}\}^{SYM}_{ac}, \tag{4.195}$$

where

$$\frac{\partial}{\partial \bar{C}^h}\left\{\frac{\boldsymbol{D}}{m^L C_p}\right\} = \frac{1}{m^L C_p}[-\boldsymbol{D}^L \frac{\partial \phi}{\partial \bar{C}^h} - \frac{\boldsymbol{D}^L}{C_p}\frac{\partial C_p}{\partial \bar{C}^h}] \tag{4.196}$$

and where

$$\frac{\partial C_p}{\partial \bar{C}^h} = (C_p^S - C_p^L)\frac{\partial \phi}{\partial \bar{C}^h} + [\int_0^{T(H)} (C_p^S - C_p^L)dT - L]\frac{\partial^2 \phi}{\partial T \partial \bar{C}^h}. \tag{4.197}$$

If the element is totally solid or partially solid and eutectic then

$$\frac{\partial \{n_C^e\}_a}{\partial c_c^e} = 0. \tag{4.198}$$

Note that in the mushy region $\boldsymbol{D}^L = \boldsymbol{D}^L(T, \boldsymbol{x}, t)$ thus $\partial \boldsymbol{D}^L / \partial \bar{C}^h = \boldsymbol{0}$.

In summary:

a ) if the element is totally liquid, $\boldsymbol{D}_{c^e}^e \boldsymbol{n}_C^e = \boldsymbol{\mathcal{K}}^e{}_{CCL}$ (non-symmetric),

b ) if the element is totally mushy, $\boldsymbol{D}_{c^e}^e \boldsymbol{n}_C^e = \boldsymbol{\mathcal{K}}^e{}_{CCM}$ (non-symmetric),

c ) if the element is totally solid or partially solid and eutectic, $\boldsymbol{D}_{c^e}^e \boldsymbol{n}_C^e = \boldsymbol{0}$ ,

d ) if the element is partially mushy and liquid or partially mushy, liquid and eutectic (or eutectic and solid), $\boldsymbol{D}_{c^e}^e \boldsymbol{n}_C^e = \hat{\boldsymbol{\mathcal{K}}}^e{}_{CCM} + \hat{\boldsymbol{\mathcal{K}}}^e{}_{CCL}$ (non-symmetric), and

e ) if the element is partially mushy and eutectic or mushy, solid and eutectic, $\boldsymbol{D}_{c^e}^e \boldsymbol{n}_C^e = \hat{\boldsymbol{\mathcal{K}}}^e{}_{CCM}$ (non-symmetric).

Note as in Sections 4.6.3.4 and 4.8.2.3 $\hat{\boldsymbol{\mathcal{K}}}^e{}_{CCM}$ and $\hat{\boldsymbol{\mathcal{K}}}^e{}_{CCL}$ are reduced forms of $\boldsymbol{\mathcal{K}}_{CCM}^e$ and $\boldsymbol{\mathcal{K}}_{CCL}^e$, where $\hat{\boldsymbol{\mathcal{K}}}^e{}_{CCM}$ and $\hat{\boldsymbol{\mathcal{K}}}^e{}_{CCL}$ result from contributions from those integration points in the element that are mushy and liquid respectively.

c) The internal solute source and the $h_c$-type boundary condition contribution is

$$\boldsymbol{D}_c \boldsymbol{F}_C(\boldsymbol{c}_{n+1}) = \mathop{\mathsf{A}}_{e=1}^{Nel} \boldsymbol{D}_{c^e}^e \boldsymbol{f}_C^e(\boldsymbol{c}_{n+1}^e), \tag{4.199}$$

with its element contributions,

$$\boldsymbol{D}_{c^e}\boldsymbol{f}_C^e(\boldsymbol{c}_{n+1}^e) = \left\{\frac{\partial\{f_C(\boldsymbol{c}^e)\}_a}{\partial c_c^e}\right\}_{\substack{h^e = h_{n+1}^{e^i} \\ c^e = c_{n+1}^{e^i}}} \tag{4.200}$$

(4.201)

and components,

$$\frac{\partial\{f_C^e\}_a}{\partial c_c^e} = \int_{\Omega^e} N_a(\boldsymbol{x})\frac{\partial Q_c}{\partial \bar{C}^h}N_c(\boldsymbol{x})\,d\Omega + \int_{\Gamma^e{}_n\Gamma^h} N_a(\boldsymbol{x})\frac{\partial q_c}{\partial \bar{C}^h}N_c(\boldsymbol{x})\,d\Omega \tag{4.202}$$

$$= \{\mathcal{F}_{CC}\}_{ac}. \tag{4.203}$$

**4.8.2.5** In this section a summary of the element contributions to the Jacobian-operator matrix for each phase region is given.

a) The solid element contribution to the Jacobian operator is :

$$\boldsymbol{D}_{h^e}\boldsymbol{r}_H^e = \boldsymbol{\mathcal{M}}_{HH}^e + \boldsymbol{\mathcal{K}}_{HH}^e + \boldsymbol{\mathcal{F}}_{HH}^e\,, \tag{4.204}$$

$$\boldsymbol{D}_{c^e}\boldsymbol{r}_H^e = \boldsymbol{\mathcal{K}}_{HC}^e\,, \tag{4.205}$$

$$\boldsymbol{D}_{h^e}\boldsymbol{r}_C^e = \boldsymbol{0} \tag{4.206}$$

and

$$\boldsymbol{D}_{c^e}\boldsymbol{r}_C^e = \boldsymbol{\mathcal{M}}_{CC}^e + \boldsymbol{\mathcal{F}}_{CC}^e. \tag{4.207}$$

If the conductivity $\boldsymbol{\mathcal{K}}^S$ is independent of $\bar{C}^h$ then $\boldsymbol{\mathcal{K}}_{HC}^e = \boldsymbol{0}$, therefore the set of equations (4.129) will be uncoupled.

b) The liquid element contribution to the Jacobian operator is :

$$\boldsymbol{D}_{h^e}\boldsymbol{r}_H^e = \boldsymbol{\mathcal{M}}_{HH}^e + \boldsymbol{\mathcal{K}}_{HH}^e + \boldsymbol{\mathcal{F}}_{HH}^e\,, \tag{4.208}$$

$$\boldsymbol{D}_{c^e}\boldsymbol{r}_H^e = \boldsymbol{\mathcal{K}}_{HC}^e\,, \tag{4.209}$$

$$\boldsymbol{D}_{h^e}\boldsymbol{r}_C^e = \boldsymbol{\mathcal{K}}_{CHL}^e \tag{4.210}$$

and

$$\boldsymbol{D}_{c^e}\boldsymbol{r}_C^e = \boldsymbol{\mathcal{M}}_{CC}^e + \boldsymbol{\mathcal{K}}_{CHL}^e + \boldsymbol{\mathcal{F}}_{CC}^e\,. \tag{4.211}$$

If the conductivity $\mathcal{K}^L$ is independent of $\bar{C}^h$ and if the diffusivity $\boldsymbol{D}^L$ is independent of $T$ then $\mathcal{K}^e_{CHL} = \mathbf{0}$ and $\mathcal{K}^e_{HC} = \mathbf{0}$, therefore the set of equations (4.129) will be uncoupled.

c) The mushy element contribution to the Jacobian operator is :

$$\boldsymbol{D}_{h^e} \boldsymbol{r}^e_H = \mathcal{M}^e_{HH} + \mathcal{K}^e_{HH} + \mathcal{F}^e_{HH} , \tag{4.212}$$

$$\boldsymbol{D}_{c^e} \boldsymbol{r}^e_H = \mathcal{K}^e_{HC} , \tag{4.213}$$

$$\boldsymbol{D}_{h^e} \boldsymbol{r}^e_C = \mathcal{K}^e_{CHM} \tag{4.214}$$

and

$$\boldsymbol{D}_{c^e} \boldsymbol{r}^e_C = \mathcal{M}^e_{CC} + \mathcal{K}^e_{CHM} + \mathcal{F}^e_{CC}. \tag{4.215}$$

One can see that the set of equations (4.129) in this region are fully coupled.

d) Note that if a whole element goes eutectic then the contribution to the Jacobian operator would be :

$$\boldsymbol{D}_{h^e} \boldsymbol{r}^e_H = \mathcal{M}^e_{HH} , \tag{4.216}$$

$$\boldsymbol{D}_{c^e} \boldsymbol{r}^e_H = \mathbf{0} , \tag{4.217}$$

$$\boldsymbol{D}_{h^e} \boldsymbol{r}^e_C = \mathbf{0} \tag{4.218}$$

and

$$\boldsymbol{D}_{c^e} \boldsymbol{r}^e_C = \mathcal{M}^e_{CC} + \mathcal{F}^e_{CC}. \tag{4.219}$$

## 4.9 Predictor-Corrector Algorithm

For a given $\boldsymbol{h}_n$ and $\boldsymbol{c}_n$ the predictor-corrector iterative algorithm to compute the solution for step n + 1 is defined in the following steps.

1. Compute the predicted values : i = 0 ,

$$\boldsymbol{h}^i_{n+1} = \tilde{\boldsymbol{h}}_{n+1} = \boldsymbol{h}_n + \Delta t(1-\alpha)\, \dot{\boldsymbol{h}}_n, \tag{4.220}$$

$$\boldsymbol{c}^i_{n+1} = \tilde{\boldsymbol{c}}_{n+1} = \boldsymbol{c}_n + \Delta t(1-\alpha)\, \dot{\boldsymbol{c}}_n, \tag{4.221}$$

$$\dot{\boldsymbol{h}}^i_{n+1} = \dot{\tilde{\boldsymbol{h}}}^i_{n+1} = 0 \tag{4.222}$$

and

$$\dot{c}^i_{n+1} = \dot{\tilde{c}}^i_{n+1} = 0. \tag{4.223}$$

2. Calculate the residual vector,

$$r(h^i_{n+1}, c^i_{n+1}) = \begin{bmatrix} r_H(h^i_{n+1}, c^i_{n+1}) \\ r_C(h^i_{n+1}, c^i_{n+1}) \end{bmatrix} . \tag{4.224}$$

3. Calculate the Jacobian operator,

$$\left[ D_h r(h^i_{n+1}, c^i_{n+1})\, D_c r(h^i_{n+1}, c^i_{n+1}) \right] = \left[ \begin{matrix} \frac{\partial r_H}{\partial h} & \frac{\partial r_H}{\partial c} \\ \frac{\partial r_C}{\partial h} & \frac{\partial r_C}{\partial c} \end{matrix} \right]_{\substack{h = h^i_{n+1} \\ c = c^i_{n+1}}} . \tag{4.225}$$

4. Solve for the increments in enthalpy and solute concentration,

$$\left[ \begin{matrix} \frac{\partial r_H}{\partial h} & \frac{\partial r_H}{\partial c} \\ \frac{\partial r_C}{\partial h} & \frac{\partial r_C}{\partial c} \end{matrix} \right]_{\substack{h = h^i_{n+1} \\ c = c^i_{n+1}}} \begin{bmatrix} \Delta h^i_{n+1} \\ \Delta c^i_{n+1} \end{bmatrix} = \begin{bmatrix} -r_H(h^i_{n+1}, c^i_{n+1}) \\ -r_C(h^i_{n+1}, c^i_{n+1}) \end{bmatrix} . \tag{4.226}$$

5. Update the predicted solute concentrations, enthalpies and their rates:

$$c^{i+1}_{n+1} = c^i_{n+1} + \Delta c^i_{n+1}, \tag{4.227}$$

$$h^{i+1}_{n+1} = h^i_{n+1} + \Delta h^i_{n+1}, \tag{4.228}$$

$$\dot{h}^{i+1}_{n+1} = \frac{1}{\Delta t}(h^{i+1}_{n+1} - \tilde{h}_{n+1}) \tag{4.229}$$

and

$$\dot{c}^{i+1}_{n+1} = \frac{1}{\Delta t}(c^{i+1}_{n+1} - \tilde{c}_{n+1}). \tag{4.230}$$

6. Calculate the updated residual vector,

$$r(h^i_{n+1}, c^i_{n+1}) = \begin{bmatrix} r_H(h^i_{n+1}, c^i_{n+1}) \\ r_C(h_{n+1}, c_{n+1}) \end{bmatrix} . \tag{4.231}$$

7. Resolve equation (4.226).

8. Check for convergence,

$$\begin{bmatrix} max||\Delta h^i_{b^{n+1}}|| \\ max||\Delta c^i_{b^{n+1}}|| \end{bmatrix} \leq PTOL\,. \tag{4.232}$$

- If equation (4.232) is not satisfied repeat steps 3 – 8 for i = i + 1.
- If equation (4.232) is satisfied advance the solution n = n + 1.

Note:

(a) To carry out the convergence check (step 8) the magnitudes of solute concentration components $c_b$ have to be scaled so that the changes in the magnitude of the enthalpy components $h_b$ and solute concentration components $c_b$ are of the same order.

(b) In the initialization step, t = 0, the rate terms are obtained from equations (4.122) and (4.123) as follows:

$$\dot{\boldsymbol{h}}_0 = \boldsymbol{M}^{-1}(\boldsymbol{F}_H(\boldsymbol{h}_0,0) - \boldsymbol{K}_H(\boldsymbol{h}_0,\boldsymbol{c}_0,0)\boldsymbol{h}_0 \tag{4.233}$$

and

$$\dot{\boldsymbol{c}}_0 = \boldsymbol{M}^{-1}(\boldsymbol{F}_C(\boldsymbol{c}_0,0) - \boldsymbol{N}_C(\boldsymbol{h}_0,\boldsymbol{c}_0,0)). \tag{4.234}$$

(c) For the initialization of a time step an explicit operator ($\alpha = 0$) is chosen for the predictor (step 1). The fully implicit scheme ($\alpha = 1$) is used for the rest of the solution procedure.

## 4.10 Numerical evaluation of the finite element equations

To solve the equations which make up the residual vector and Jacobian matrix numerically, a numerical integration scheme must be introduced. The continuous integrals representing the residual and Jacobian, defined over the element, are approximated by sampling the integrand at different optimum points $\bar{\xi}(\boldsymbol{x})$ in the element, weighting their values and summing over the element to obtain an effective approximation to the element integral. Depending on the integration scheme used the residual and Jacobian will be evaluated at different sampling points in the element. For example, with the Newton Cotes integration scheme the sampling points are at the nodes of the element whereas with the Gaussian quadrature integration scheme the sampling points are positioned inside the element. The Newton Cotes integration scheme diagonalizes the mass matrix contribution to the Jacobian. This is equivalent to using a lumped mass method, where the masses are lumped at the nodes. In contrast the Gaussian quadrature scheme would cause the mass matrix contribution to the Jacobian to be fully consistent. It has been found that when the mass matrix contribution to the Jacobian is fully consistent, oscillations appear in the solution. When this matrix is diagonal (or lumped), oscillations do not occur. The Newton

Cotes integration scheme is consequently used to integrate the equations. It must be noted that a combination of the two schemes can also be used (ie. Newton Cotes for the mass terms and Gaussian quadrature for the conductivity and diffusivity terms), Abaqus [16] . For simplicity Newton Cotes is used throughout the computations in this work.

As the enthalpy solution is not smooth at the phase front, and at the eutectic, the use of low ordered linear elements are recommended since better behaviour from higher-order elements cannot be expected in this case.

Therefore a two dimensional, four noded, isoparametric, quadrilateral element is chosen where the nodal field variables are enthalpy and average solute concentration, and where the terms for the residual and Jacobian are evaluated at the nodes using a Newton Cotes integration scheme.

## 4.11 Solution of state variables

In order to evaluate the residual and the Jacobian operator at the specific sampling point $\bar{\xi}(x)$, the mass fraction $\phi(\bar{\xi})$ and the temperature $T(\bar{\xi})$ have to be calculated from the given enthalpy and average solute concentration fields. These unknown variables, $T(\bar{\xi}))$ and $\phi(\bar{\xi})$ at $\bar{\xi}(x)$, are termed the state variables of the problem. Therefore to calculate the state variables, the enthalpy and average solute concentration have to be established, at $\bar{\xi}(x)$, from their nodal values, for time $n+1$ and for the $i$th global iteration, as follows:

$$H^i_{n+1}(\bar{\xi}) = \sum_{i=1}^{nnode} N_i(\bar{\xi})\,(h_i)^i_{n+1} \tag{4.235}$$

and

$$\bar{C}^i_{n+1}(\bar{\xi}) = \sum_{i=1}^{nnode} N_i(\bar{\xi})\,(c_i)^i_{n+1}\,. \tag{4.236}$$

The temperature and solid mass fraction, at the integration point $\bar{\xi}(x)$, are calculated using the temperature (T) - enthalpy (H) relationship (shown in Figure 4.1) coupled the with the lever rule expression for the average solute concentration. For simplicity it is assumed that the slope of the (T - H) curve (ie. the specific heat $C_p$) is constant in the pure solid and liquid regions. The evaluation of the temperature can thus be directly obtained from the given enthalpy in these regions. In the mushy region this is not the case as the slope of the (T - H) curve is unknown. Therefore the temperature and mass fraction have to be obtained using a predictor-corrector method. A Newton Raphson method is chosen for this purpose where for time step $n+1$, global iteration $i$ and local iteration $k$ the residual is defined as

$${}^k r^i_{n+1} = H^i_{n+1} - {}^k\tilde{H}^i_{n+1} \tag{4.237}$$

and the Jacobian operator is defined as

$$ {}^{k}\left[\frac{\partial r}{\partial T}\right]^{i}_{n+1} = -{}^{k}C^{i}_{p_{n+1}} = {}^{k}\left[-C_{p_0} + L\,\frac{\partial \phi}{\partial T}\right]^{i}_{n+1} . \tag{4.238} $$

The term ${}^{k}\tilde{H}^{i}_{n+1}$ is the locally calculated predictor enthalpy defined as

$$ {}^{k}\tilde{H}^{i}_{n+1} = {}^{k}\left[C_{p_0}\,T + \Delta H^{f}_{ref}(1-\phi)\right]^{i}_{n+1} . \tag{4.239} $$

When going from the pure liquid to the mushy region or when going from the mushy region to the eutectic region or visa versa, the (T - H) curve experiences a kink or sharp change in slope. At these points, the Newton-Raphson method will not converge, so the secant method is then used to obtain convergence. To enhance the convergence process in these regions the *reguli falsi* technique (see Minkowycz et al [52] for explanation) is used to insure that the different predictors and their roots, comprising the secant term, bracket the exact solution. Therefore the secant term will only be used in place of the Jacobian when the following condition is satisfied

$$ (H^{i}_{n+1} - {}^{k}\tilde{H}^{i}_{n+1})(H^{i}_{n+1} - {}^{(k-p)}\tilde{H}^{i}_{n+1}) < 0 , \tag{4.240} $$

for $p = 1, 2..., k-1$ .

The secant approximation for the Jacobian is expressed as

$$ {}^{k}\left[\frac{\partial r}{\partial T}\right]^{i}_{n+1} \approx -\frac{{}^{k}\tilde{H}^{i}_{n+1} - {}^{(k-p)}\tilde{H}^{i}_{n+1}}{{}^{k}T^{i}_{n+1} - {}^{(k-p)}\,T^{i}_{n+1}} , \tag{4.241} $$

where

$$ {}^{k}T^{i}_{n+1} = T({}^{k}\tilde{H}^{i}_{n+1}) . \tag{4.242} $$

To evaluate the mass fraction, the lever rule expression for $\bar{C}$ is used for both the local equilibrium and local non-equilibrium cases together with the calculated predicted temperature obtained from the (T - H) relationship. The evaluation of the mass fraction for the local equilibrium assumption is straight forward. The expression for the mass fraction is obtained from the given average solute concentration $\bar{C}^{i}_{n+1}$ and the calculated predicted temperature $T({}^{k}\tilde{H}^{i}_{n+1})$ for time step $n+1$, global iteration $i$ and local iteration $k$ as

$$ {}^{k}\phi^{i}_{n+1} = \frac{\bar{C}^{i}_{n+1} - C^{L}({}^{k}T^{i}_{n+1})}{C^{S}({}^{k}T^{i}_{n+1}) - C^{L}({}^{k}T^{i}_{n+1})} . \tag{4.243} $$

The evaluation of the mass fraction for the local non-equilibrium assumption is not as straight forward as in the local equilibrium case. In the lever expression for $\bar{C}$, for the local non-equilibrium case, $\bar{C}_S$ is written as a integral of the solute concentration with respect to mass fraction, which is an unknown. This is therefore expressed as

$$ \bar{C}^{i}_{n+1} = (1 - {}^{k}\phi^{i}_{n+1})C^{L}({}^{k}T^{i}_{n+1}) + \bar{C}_{n} - (1-\phi_{n})C^{L}(T_{n}) + \int_{\phi_n}^{{}^{k}\phi^{i}_{n+1}} C^{S}_{*}(f^{S})\, df^{S} . \tag{4.244} $$

The integral term in equation (4.244) can be solved using different numerical integration schemes. The trapezoidal scheme is used in this case where the solute profile is assumed linear from $\phi_n$ to $\phi_{n+1}$. Voller et al [18] use the equivalent of the Euler backward scheme to perform this integration. For this problem the difference between $\phi_n$ and $\phi_{n+1}$ is small and therefore the difference between each of these schemes is small. Therefore

$$ \int_{\phi_n}^{{}^{k}\phi^{i}_{n+1}} C^{S}_{*}(f^{S})\, df^{S} \approx \frac{1}{2}({}^{k}\phi^{i}_{n+1} - \phi_{n})(C^{S}_{*}({}^{k}\phi^{i}_{n+1}) + C^{S}_{*}(\phi_{n})) . \tag{4.245} $$

The expression for the evaluation of the solid mass fraction for the non-equilibrium case is therefore expressed at time $n+1$ for the $i$th global and $k$th local iteration as

$$ {}^{k}\phi^{i}_{n+1} = \frac{\bar{C}^{i}_{n+1} - \bar{C}_{n} - C^{L}({}^{k}T^{i}_{n+1}) + (1-\phi_{n})C^{L}(T_{n}) + 1/2\phi_{n}(C^{S}_{*}(\phi_{n}) + C^{S}_{*}({}^{k}\phi^{i}_{n+1}))}{1/2(C^{S}_{*}(\phi_{n}) + C^{S}_{*}({}^{k}\phi^{i}_{n+1})) - C^{L}({}^{k}T^{i}_{n+1})} . \tag{4.246} $$

### 4.11.1 Predictor-corrector algorithm

For a given $H^{i}_{n+1}(\bar{\xi})$ and $\bar{C}^{i}_{n+1}(\bar{\xi})$ the predictor-corrector algorithm used to compute the state variables at the integration point $\bar{\xi}$, at time step $n+1$ and at the global iteration $k$ is defined in the following steps.

1. Compute the predicted values, set $k = 0$ and calculate:

$$ T_{\text{LIQ}} = T_{m} + ml\,\bar{C}^{i}_{n+1} , $$
$$ H_{\text{LIQ}} = C^{L}_{p}(T_{\text{LIQ}} - T_{ref}) + \Delta H^{f}_{ref} $$

and

$$H^S_{\text{EUT}} = C^S_p(T_{\text{EUT}} - T_{ref}) .$$

**1.1** Check if initially liquid: $H^i_{n+1} \geq H_{\text{LIQ}}$, if yes, then

$$^k\phi^i_{n+1} = 0$$

and

$$^kT^i_{n+1} = 1/C^L_p(H^i_{n+1} - \Delta H^f_{ref}) + T_{ref} .$$

**1.2** Check if initially solid: $H^i_{n+1} \leq H^S_{\text{EUT}}$, if yes, then

$$^k\phi^i_{n+1} = 1$$

and

$$^kT^i_{n+1} = 1/C^S_p H^i_{n+1} + T_{ref} .$$

**1.3** Check if initially mushy: $H^S_{\text{EUT}} < H^i_{n+1} < H_{\text{LIQ}}$, if yes, then

$$^k\phi^i_{n+1} = \phi^{i-1}_{n+1} , \quad \text{if } i > 1$$

and

$$^kT^i_{n+1} = T^{i-1}_{n+1} , \quad \text{if } i > 1 ,$$

or

$$^k\phi^i_{n+1} = \phi_n , \quad \text{if } i = 1$$

and

$$^kT^i_{n+1} = T_n , \quad \text{if } i = 1 .$$

**1.4** Calculate initial predictor enthalpy and specific heat.

If in a pure solid or pure liquid region then,

$$^k\tilde{H}^i_{n+1} = H^i_{n+1} ,$$
$$^kC^i_{p_{n+1}} = C^S_p \quad \text{(if solid)}$$

and

$$^kC^i_{p_{n+1}} = C^L_p \quad \text{(if liquid)} .$$

If in the mushy region then calculate:

$$^k\tilde{H}^{S^i}_{n+1} = C^S_p(^kT^i_{n+1} - T_{ref}) ,$$
$$^k\tilde{H}^{L^i}_{n+1} = C^L_p(^kT^i_{n+1} - T_{ref}) + \Delta H^f_{ref}$$

and

$$^kL^i_{n+1} = {}^k\tilde{H}^{L^i}_{n+1} - {}^k\tilde{H}^{L^i}_{n+1} .$$

Thus,

$$^k\tilde{H}^i_{n+1} = {}^k\phi^i_{n+1}\,{}^k\tilde{H}^{S^i}_{n+1} + (1 - {}^k\phi^i_{n+1})\,{}^k\tilde{H}^{L^i}_{n+1}$$

and

$$ {}^{k}C^{i}_{p_{n+1}} = {}^{k}\phi^{i}_{n+1} C^{S}_{p} + (1 - {}^{k}\phi^{i}_{n+1}) C^{L}_{p} - {}^{k}L^{i}_{n+1} \, {}^{k}(\partial\phi/\partial T)^{i}_{n+1} \, , $$

where

$$ {}^{k}(\partial\phi/\partial T)^{i}_{n+1} \approx ({}^{k}\phi^{i}_{n+1} - \phi_{n})/({}^{k}T^{i}_{n+1} - T_{n}) \, . $$

If in the eutectic region, ie. if $H^{i}_{n+1} > H^{S}_{\text{EUT}}$ and ${}^{k}T^{i}_{n+1} = T_{\text{EUT}}$, then calculate:

$$ {}^{k+1}\phi^{i}_{n+1} = 1 - \frac{(H^{i}_{n+1} - H^{S}_{\text{EUT}})}{{}^{k+1}L^{i}_{n+1}} \, , \tag{4.247} $$

where

$$ {}^{k}\tilde{H}^{i}_{n+1} = {}^{k}\phi^{i}_{n+1} \, {}^{k}\tilde{H}^{S^{i}}_{n+1} + (1 - {}^{k}\phi^{i}_{n+1}) \, {}^{k}\tilde{H}^{L^{i}}_{n+1} $$

and

$$ {}^{k}C^{i}_{p_{n+1}} = \text{some arbitrary large value} \, , $$

then proceed to step 8 and set k = k+1.

**2.** Calculate the residual,

$$ {}^{k}r^{i}_{n+1} = H^{i}_{n+1} - {}^{k}\tilde{H}^{i}_{n+1} \, . \tag{4.248} $$

**3.** Calculate the Jacobian operator,

$$ {}^{k}\left(\frac{\partial r}{\partial T}\right)^{i}_{n+1} = -{}^{k}C^{i}_{p_{n+1}} \, . \tag{4.249} $$

**4.** Check whether to use the secant operator instead of the Jacobian if in a transition from liquid to mush or from mush to eutectic to solid.

Therefore, check: $(H^{i}_{n+1} - {}^{k}\tilde{H}^{i}_{n+1})(H^{i}_{n+1} - {}^{(k-p)}\tilde{H}^{i}_{n+1}) < 0$ for $p = 1, 2, \ldots\ldots, k-1$.

If no for all $p$, then proceed with the Jacobian.
If yes for any $p$, then use the secant approximation to the Jacobian as follows:

$$ {}^{k}\left(\frac{\partial r}{\partial T}\right)^{i}_{n+1} \approx - \frac{{}^{k}\tilde{H}^{i}_{n+1} - {}^{(k-p)}\tilde{H}^{i}_{n+1}}{{}^{k}T^{i}_{n+1} - {}^{(k-p)}T^{i}_{n+1}} \, . \tag{4.250} $$

**5.** Solve:

$$ {}^{k}\left(\frac{\partial r}{\partial T}\right)^{i}_{n+1} \Delta {}^{k}T^{i}_{n+1} = {}^{k}r^{i}_{n+1} \, . \tag{4.251} $$

**6.** Update:

$$^{k+1}T^i_{n+1} = {}^kT^i_{n+1} + \Delta^kT^i_{n+1} \,. \tag{4.252}$$

**6.1** Calculate: $^{k+1}\tilde{H}^{S^i}_{n+1}$, $^{k+1}\tilde{H}^{L^i}_{n+1}$ and $^{k+1}L^i_{n+1}$ .

**6.2** Check if in liquid region : $^{k+1}T^i_{n+1} \geq T_{\text{LIQ}}$ , if yes, then $^{k+1}\phi^i_{n+1} = 0$ .

**6.3** Check if in solid region : $^{k+1}T^i_{n+1} \leq T_{\text{EUT}}$ , if yes, then $^{k+1}\phi^i_{n+1} = 1$ .

**6.4** Check if in eutectic region : $^{k+1}T^i_{n+1} = T_{\text{EUT}}$, if yes, then

$$^{k+1}\phi^i_{n+1} = 1 - \frac{(H^i_{n+1} - H^S_{\text{EUT}})}{^{k+1}L^i_{n+1}} \,. \tag{4.253}$$

**6.5** Check if in the mushy region: $^{k+1}T^i_{n+1} > T_{\text{EUT}}$ and $H^S_{\text{EUT}} < {}^k\tilde{H}^i_{n+1} < H_{\text{LIQ}}$ ,

if yes, then for the local equilibrium case,

$$^{k+1}\phi^i_{n+1} = \frac{\bar{C}^i_{n+1} - C^L(^{k+1}T^i_{n+1})}{C^S(^{k+1}T^i_{n+1}) - C^L(^{k+1}T^i_{n+1})} \,, \tag{4.254}$$

and for the local non-equilibrium case,

$$^k\phi^i_{n+1} = \frac{\bar{C}^i_{n+1} - \bar{C}_n - C^L(^{k+1}T^i_{n+1}) + (1-\phi_n)C^L(T_n) + 1/2\phi_n(C^S_*(\phi_n) + C^S_*(^{k+1}\phi^i_{n+1}))}{1/2(C^S_*(\phi_n) + C^S_*(^{k+1}\phi^i_{n+1})) - C^L(^{k+1}T^i_{n+1})} \,. \tag{4.255}$$

Note that when initially going from the liquid to the mush under the non-equilibrium assumption, equation (4.254) is used as a starting basis.

For the solidification case $C^S_*(^{k+1}\phi^i_{n+1}) = k\,C^L(^{k+1}T^i_{n+1})$ and $C^S_*(\phi_n) = k\,C^L(T_n)$.

**6.6** Calculate $^{k+1}\tilde{H}^i_{n+1}$ and $^{k+1}C^i_{p_{n+1}}$ .

**7.** Calculate the residual:

$$ {}^{k+1}r^{i}_{n+1} = H^{i}_{n+1} - {}^{k+1}\tilde{H}^{i}_{n+1} \, . \tag{4.256} $$

**8.** Check for convergence:

$$ ||{}^{k+1}r^{i}_{n+1}|| \leq HTOL \, , \tag{4.257} $$

where $HTOL$ is some tolerance value.

If no, repeat steps $(3 - 8)$.

If yes, calculate :

a) the conductivity, ${}^{k+1}\boldsymbol{\mathcal{K}}^{i}_{n+1} = {}^{k+1}\phi^{i}_{n+1}\boldsymbol{\mathcal{K}}^{S} + (1 + {}^{k+1}\phi^{i}_{n+1})\boldsymbol{\mathcal{K}}^{L}$ ,

b) the diffusivity, ${}^{k+1}\boldsymbol{D}^{i}_{n+1} = (1 + {}^{k+1}\phi^{i}_{n+1})\boldsymbol{D}^{L}$ and

c) the following derivatives: ${}^{k+1}\{\partial C_p/\partial T, \partial C_p/\partial \bar{C}, \partial \boldsymbol{\mathcal{K}}/\partial T, \partial \boldsymbol{\mathcal{K}}/\partial \bar{C}, \partial \boldsymbol{D}/\partial T, \partial \boldsymbol{D}/\partial \bar{C}\}^{i}_{n+1}$.

These derivatives involve derivatives of $\phi$ with respect to T and $\bar{C}$ as well as second order derivatives of $\phi$ with respect to T and $\bar{C}$. In all cases the Euler backward difference scheme is used. Due to lack of available data it is assumed that the conductivity and diffusivity in the pure phase regions are constant. Note in the eutectic region the derivatives of $\phi$ with respect to T are all assumed to have some arbitrary large value. This results in a discontinuity in the enthalpy which causes difficulties for the Newton-Raphson solution process. To help the solution process, the values of the derivatives of $\phi$ with respect to T are reduced to some finite value so as to introduce a slope into the enthalpy curve at the eutectic, thus making the solution smoother and easier to obtain. It is realized that this is not a true reflection of the physics of the problem but is necessary to enable the Newton-Raphson solution scheme to cope with the discontinuity in enthalpy at the eutectic.

## 4.12 Conclusions

In this chapter a fixed grid finite element formulation for binary alloy solidification is presented. Fluid convection is neglected, resulting in the discretization of equations for diffusion dominated heat and solute transfer. The heat transfer is described in terms of enthalpy. The resulting field variables in the problem are thus enthalpy and average solute concentration. The evolution of solid mass fraction and temperature are treated as the state variables which are evaluated from the element enthalpy and average solute concentration fields at the integration points. The resulting finite element matrix equations are discretized temporally using a generalized

trapezoidal rule where $\alpha = 1$ is used, resulting in an Euler backward temporal approximation. A Newton-Raphson iterative solution scheme is employed to solve the resulting set global coupled non-linear equations. At each integration point a Newton-Raphson solution scheme together with a secant method is used to solve for temperature and solid mass fraction from the values of enthalpy and average solute concentration at that point. A two dimensional, four noded, isoparametric element is chosen, as better behaviour from higher order isoparametric elements cannot be expected for this class of problem. Newton Cotes numerical integration is used where the integration points are positioned at the nodes resulting in a diagonal mass matrix contribution to the Jacobian operator which will alleviate any oscillations that may occur in the neighbourhood of the phase interface.

# CHAPTER 5
# NUMERICAL RESULTS AND DISCUSSION

## 5.1 Introduction

The finite element formulation described in Chapter 4 was implemented as a user element in a commercial finite element package, ABAQUS, version 4.9 [16]. The global solution procedure together with an automatic time stepping scheme in ABAQUS [16], was used to solve the problems. The convergence checks in ABAQUS [16] were carried out using the maximum change in the field variable and this also controlled the choice of time step to be used in the time stepping algorithm. As explained in Chapter 4 the Newton Raphson algorithm is used to solve these equations. It is clear in the results that this algorithm is useful for problems with smoothly varying solutions but is not efficient where there are sharp changes in the solution such as in discontinuities.

In this Chapter 2 solidification examples are investigated, one with an initial liquid solute concentration close to the eutectic and the other with a small or dilute initial liquid solute concentration, see Figure 5.1. The main objectives with modelling these two examples are, firstly to see whether consistent results can be obtained that are comparable with that in the literature, and secondly to see the effects of using the local non-equilibrium assumption as opposed to using the local equilibrium assumption. For each example mesh refinement studies are conducted to check for convergence and to obtain an optimal mesh to model the problem. Using the optimal mesh the two examples are analyzed using the local equilibrium and local non-equilibrium assumptions. These results are compared and discussed.

## 5.2 Problem Description

The problem under consideration is the solidification of a rectangular cavity as shown in Figure 5.2. The material ($NH_4Cl - H_20$) is initially all liquid at a temperature $T_0$ which is greater than the liquidus temperature corresponding to the initial uniform average solute concentration $\bar{C}_0$, see Figure 5.1 . At time $t = 0$, the temperature of the left wall is lowered to value $T_b$ which is less than the eutectic temperature $T_e$. All other walls of the cavity are insulated. Due to cooling, the material near the left wall begins to freeze, so that the cavity consists of a solid phase near the left wall, liquid near the right wall, and a two phase mushy region in between. Simplified $NH_4Cl - H_20$ thermophysical data, listed in table (5.1), together with an assumed linear phase diagram, see Figure 5.1, is used. This problem is similar to that considered by Bennon and Incropera [33].

The first solidification example has an initial temperature $T_0$ of 310.96K, an initial average solute

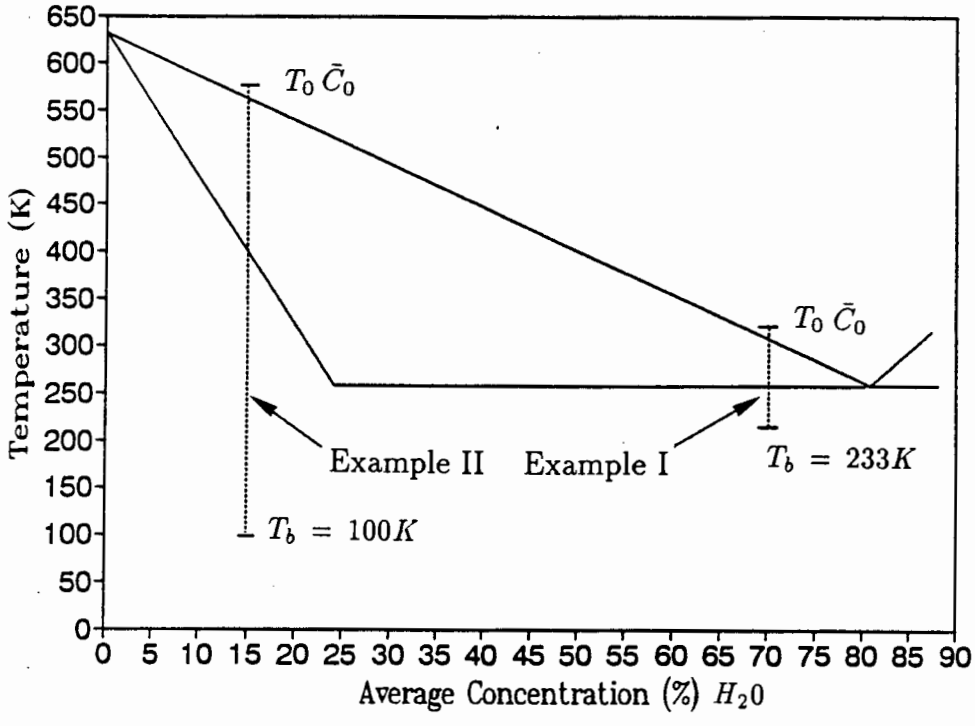


Figure 5.1: Phase diagram of a $NH_4Cl - H_20$ showing the initial and boundary values of T and $\bar{C}$ for the two examples.

concentration $\bar{C}_0$ of $H_20$ of 70% and a chill wall temperature $T_b$ of 223.15K. The second example has an initial temperature $T_0$ of 570K, an initial average solute concentration $\bar{C}_0$ of $H_20$ of 15% and a chill wall temperature $T_b$ of 100K as shown in Figure 5.1.

| Property Data | Value |
|---|---|
| Specific Heat ($J\,kg^{-1}K^{-1}$) | 3000.0 (S & L) |
| Thermal Conductivity ($W\,m^{-1}K^{-1}$) | 0.4 (S & L) |
| Density ($kg\,m^{-3}$) | 1078.0 (S & L) |
| Diffusion Coefficient ($m^2s^{-1}$) | $4.8 \times 10^{-9}$ (l) |
| Latent heat of fusion ($J\,kg^{-1}$) | $3.138 \times 10^5$ |
| Eutectic Temperature (K) | 257.75 |
| Eutectic Solute Concentration (%) | 80.3 |
| $NH_4Cl$ melting point (K) | 633.59 |
| Equilibrium partition ratio | 0.3 |

Table 5.1: Thermophysical data for examples

Due to the nature of the problem there will be no vertical gradients in temperature and solute concentration in these examples. Therefore the whole domain need not be analyzed. Instead, a single strip of elements extending through the width of the domain will be adequate to obtain

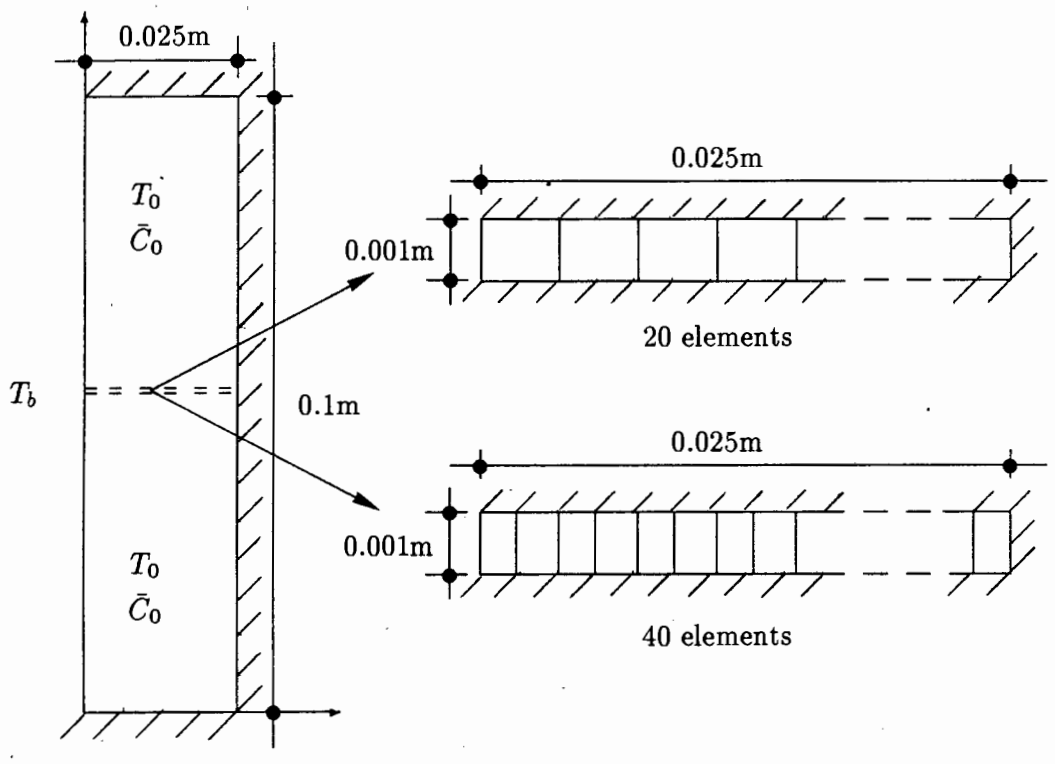


Figure 5.2: Domain of the problem with the representative finite element meshes used to model the problem.

results for the whole domain, as shown in Figure 5.2. The boundary conditions the two sides of the mesh in contact with the solidifying liquid are treated as being insulated as there will be no flow of heat or solute across these boundaries.

## 5.3 Results : Example I

As can be seen from the phase diagram most of the phase change is expected to take place at the eutectic. This will result in a discontinuity in enthalpy and solid mass fraction. Using the fixed grid finite element approach the discontinuity cannot be modelled correctly and will be smeared over an element if the discontinuity lies between the nodes. As the Newton Raphson solution algorithm is used to solve this problem severe numerical difficulties are encountered. If the discontinuity is encountered at a node or in an element the scheme has difficulty in converging with the time steps becoming smaller until convergence can no longer be achieved. To enable the Newton Raphson method to cope with the sudden large changes in enthalpy in those affected elements, a slope is introduced into the discontinuity in enthalpy, at the eutectic, see Figure

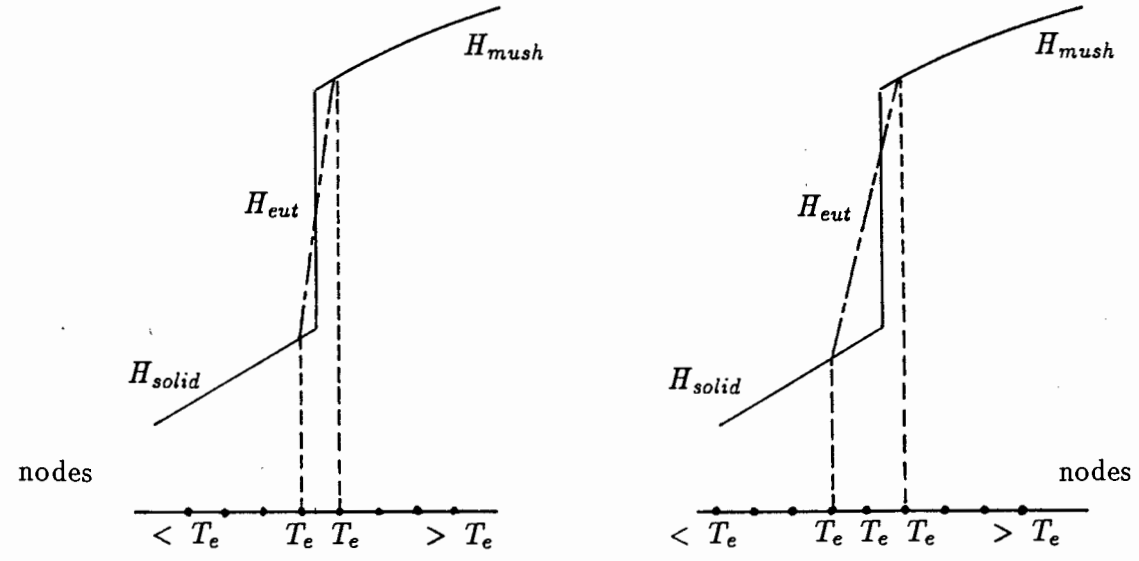


Smearing effect of a linear isoparametric element on the discontinuity

Effect of replacing the discontinuity with an induced slope.

Figure 5.3: Approximation of the enthalpy discontinuity at the eutectic

5.3. This will result in a false plateau in temperature distribution at the eutectic as depicted in Figure 5.7. The shallower the slope of the enthalpy the easier the convergence but the larger the eutectic plateau in temperature. Therefore different slopes of the enthalpy curve, at the eutectic, were experimented with in order to comprise between convergence rate of the Newton Raphson method and the narrowness of the eutectic plateau in temperature. A ratio of 1 : 5 of the mushy to the eutectic slope of the enthalpy curve was eventually chosen. It is realized that this is not an accurate approximation but a reasonable compromise for convergence. Using this approximation it seen in Figure 5.7 that at times t = 60s and t = 120s the plateau region is confined to one element but as time increases to t = 240s it spreads out to three elements. It is important to note that even though the discontinuity is not accurately modelled resulting in an incorrect temperature plateau, energy is conserved throughout the solidification process. It is suggested that by applying a secant approximation to the tangent operator for those elements that are experiencing eutectic phase change, a steeper jump in enthalpy could be accommodated with a greater rate of convergence and a better approximation of eutectic phase change.

A mesh study was carried out on this problem. Plots of the mass fraction and enthalpy for 20 element and 40 element meshes at t = 60s, t = 120s and t = 240s are shown in Figures 5.4 and 5.5, respectively. The difference in the results between the 20 element and the 40 element model are very small. Therefore the 40 element mesh is considered an adequately refined mesh to model the problem.

The second study involved using the 40 element mesh to compare the solidification models based on local equilibrium and local non-equilibrium assumptions. Figure 5.6 shows plots of the solid mass fraction at times t = 60s, 120s and 240s for both the local equilibrium and non-equilibrium cases. From Figure 5.6 it is clear that for this problem the results of the two models are the same.

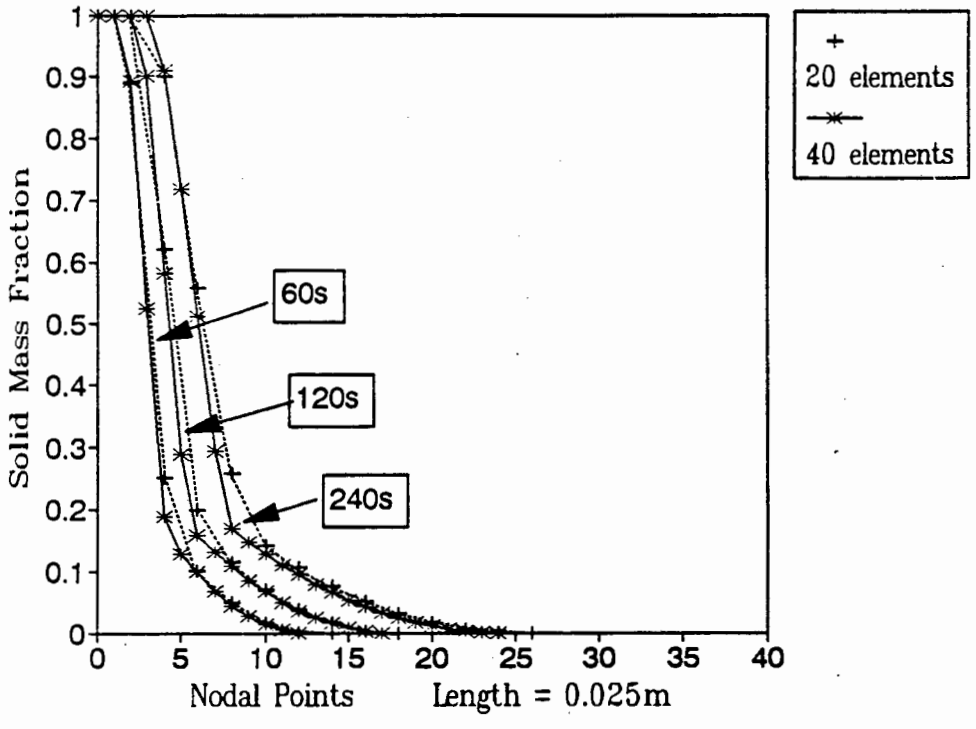


Figure 5.4: Mesh study of the variation in solid mass fraction at t = 60s, t = 120s and t = 240s.

Figures 5.7, 5.8 and 5.9 illustrate the variations in temperature, liquid solute concentration and average solute concentration at times t = 60s, t = 120s and t = 240s, respectively. It seen that during the early stages of solidification (ie. t = 60s), the mushy region propagates rapidly with the temperature gradients (Figure 5.7) being confined to the solid and mushy regions, while the bulk fluid remains nearly isothermal. Figure 5.8 shows that gradients in the liquid solute concentration are confined to the mushy region, with the largest being the eutectic water solute concentration appearing near the solidus front. Figure 5.9 shows that the change in average solute concentration is confined to the mushy region with the maximum value close to the eutectic and values in the bulk fluid remaining at their initial values. Solidification behaviour for times t = 120s and t = 240s is qualitatively similar to that described for t = 60s. While the initial bulk fluid superheat is gradually dissipated, energy diffusion in the bulk fluid prohibits the establishment of significant gradients in the region. Similarly, the liquid and average solute concentration gradients are confined primarily to the mushy region, and the bulk fluid remains very nearly at the initial solute concentrations.

Even though some of the thermophysical data is different to that of Bennon and Incropera [33] the trends in evolution in solid mass fraction, temperature ( with the exception of the eutectic plateau ) and the liquid solute concentration are the same for this example.

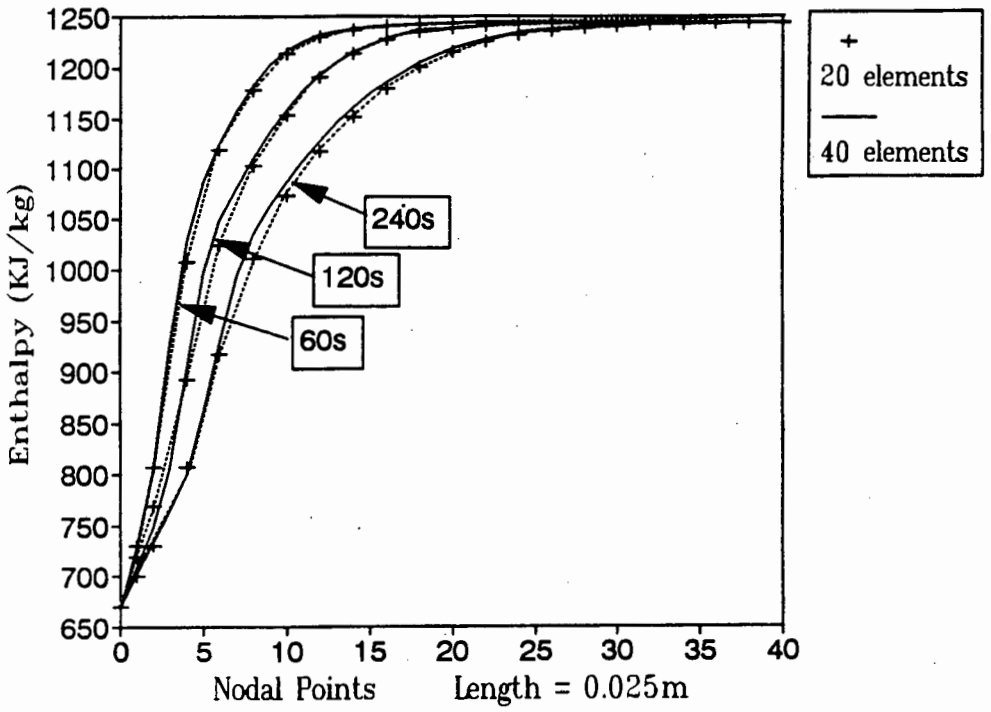


Figure 5.5: Mesh study of the variation in enthalpy at t = 60s, t = 120s and t = 240s.

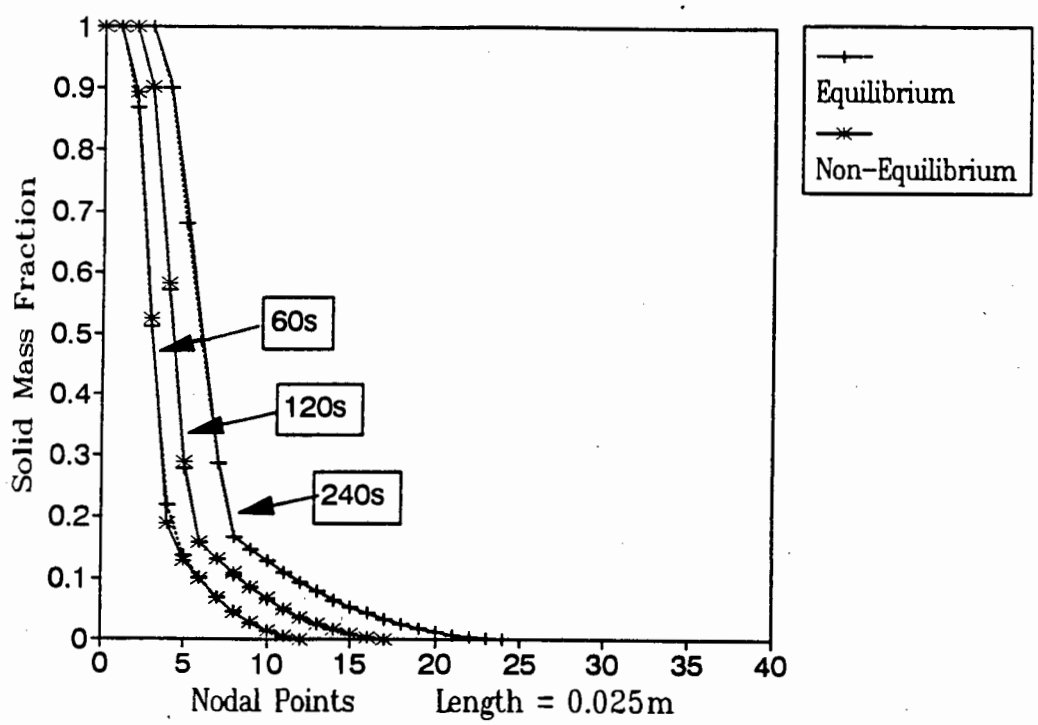


Figure 5.6: Variation of solid mass fraction at t = 60s, t = 120s and t = 240s for the local equilibrium and local non-equilibrium cases.

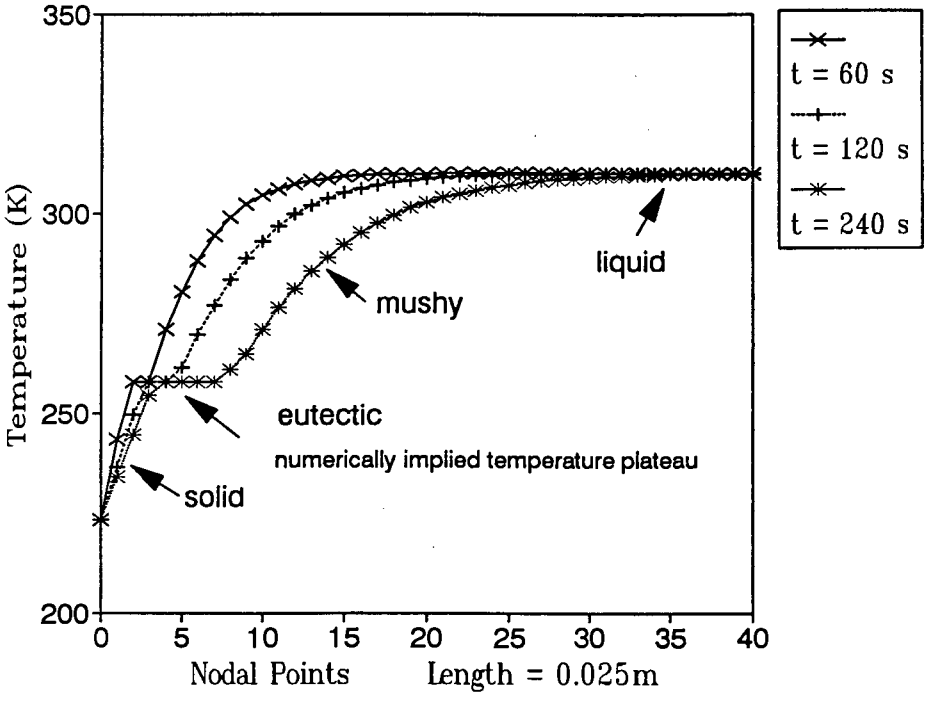


Figure 5.7: Variation in temperature at t = 60s, t = 120s and t = 240s. (See the discussion in the first paragraph in Section 5.3 with respect to the eutectic temperature plateau.)

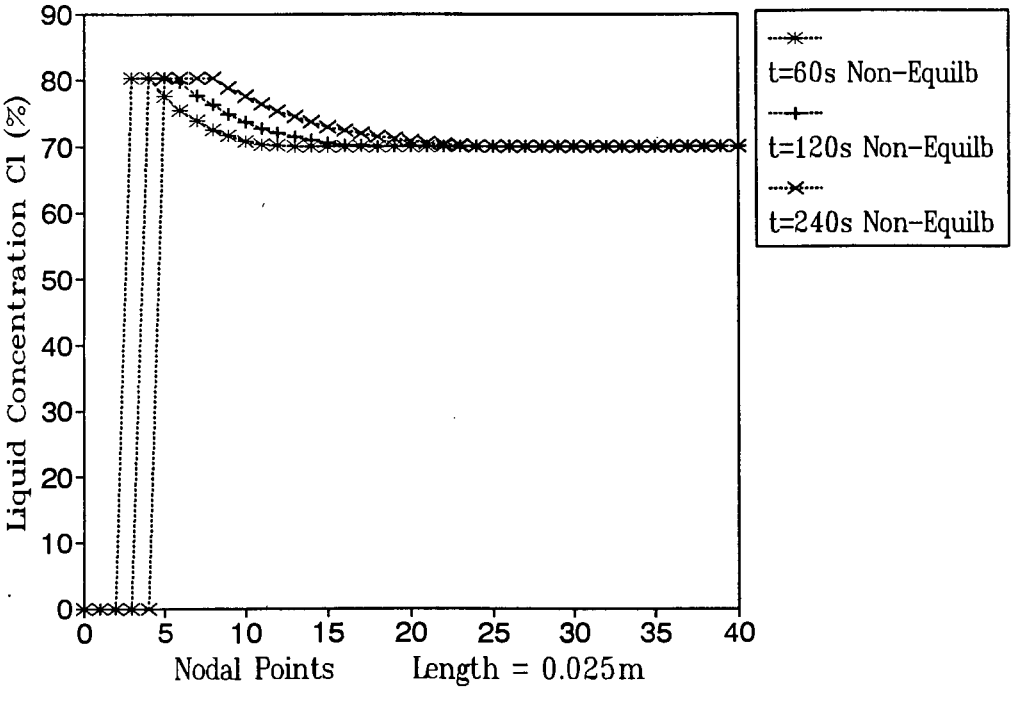


Figure 5.8: Variation in liquid solute concentration at t= 60s, t = 120s and t = 240s.

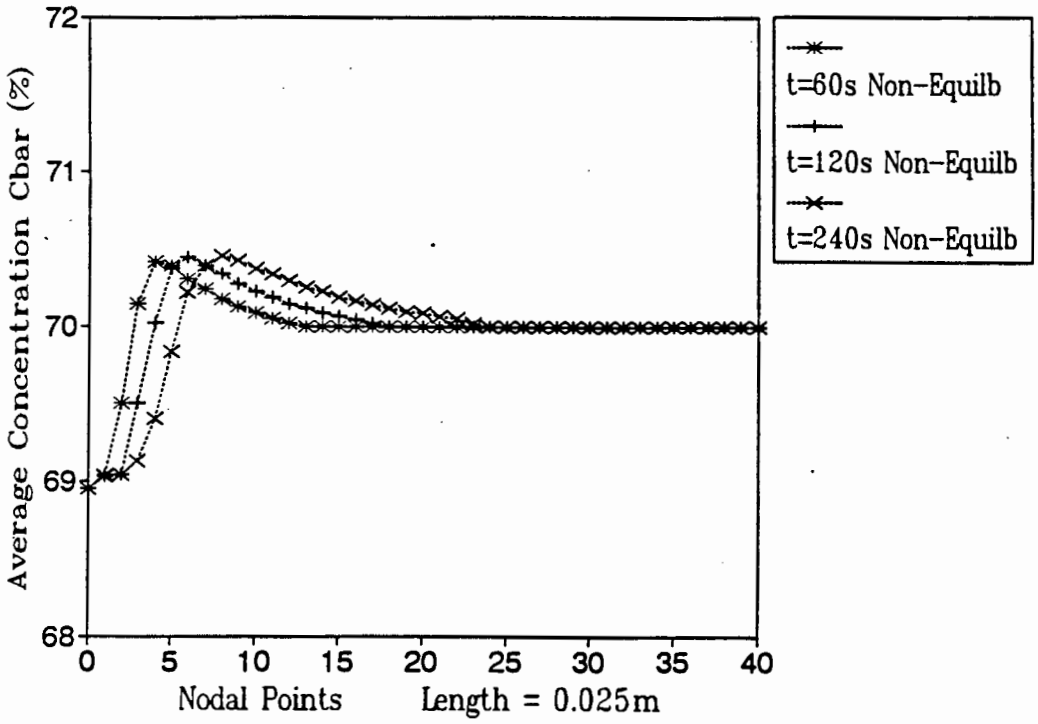


Figure 5.9: Variation in average solute concentration at t= 60s, t = 120s and t = 240s.

## 5.4 Results : Example II

In this example solidification takes place in a dilute solution of $H_20$ in $NH_4Cl$. The initial liquid solute concentration of $H_20$ is less than its maximum at the eutectic. Most of the solidification should therefore be of a dendritic nature. It is expected that for the model based on the local equilibrium assumption solid phase should form at temperatures above the eutectic, whereas for the model based on the local non-equilibrium assumption it is expected that the solid phase should form at lower temperatures close to the eutectic due the excess solute being rejected by the solid into the liquid which would delay the onset of solidification.

A mesh study was carried out on this problem using the local non-equilibrium assumption. Plots of the mass fraction and enthalpy for 20 element and 40 element meshes at t = 60s, t = 120s and t = 240s are shown in Figures 5.10 and 5.11 respectively. The difference in the results between the 20 element and the 40 element model are very small. Therefore the 40 element mesh is considered an adequately refined mesh to model the problem.

The second study involved using the 40 element mesh to compare the solidification models based on local equilibrium and local non-equilibrium assumptions. Figure 5.12 shows plots of the solid mass fraction at times t = 60s, 120s and 240s for both the local equilibrium and non-equilibrium cases. From Figure 5.12 it is clear that for this example the results of the two cases are different. For the non-equilibrium based model it is seen that approximately a 10% jump in the solid mass fraction occurs at the eutectic with the rest of the solid being formed as dendritic crystals in the mushy region. For the local equilibrium case the variation in solid mass fraction is smooth

resulting from complete dendritic solidification (ie. no eutectic solidification). In Figure 5.12 at times t = 60s, t = 120s and t = 240s the size of the mushy region is smaller for the equilibrium based model than for the non-equilibrium based model with a lager amount of solid being formed with the equilibrium based model. The extension of the mushy region into the liquid is the same for both cases.

Figures 5.13 to 5.16 illustrate the variations in temperature, enthalpy, liquid solute concentration and average solute concentration at times t = 60s, t = 120s and t = 240s, respectively. In Figures 5.13 the values of the temperature for the equilibrium based model are the same as those for the non-equilibrium based model. Maximum temperature gradients were found in the solid and mushy regions with no change in gradient going from mush to solid, while in the bulk fluid both values remains equally nearly isothermal. No plateau is experienced at the eutectic in the temperature variation plots of the non-equilibrium based model, Figure 5.13. The reason for this is that 10% of the solid, finally formed at the eutectic, results in a small jump in enthalpy which is spread over the element and is not shown up in the temperature plot. Figure 5.14 shows that gradients in the liquid solute concentration are confined to the mushy region, with the largest being the near the solidus front. The variations in liquid solute concentration are larger for the non-equilibrium based model than for the equilibrium based model. For the non-equilibrium based model the maximum values are close to the eutectic composition with the variations in solute concentration spreading out into the bulk fluid to the limit of the mushy region. For both the equilbrium and non-equilibrium cases the variations in liquid solute concentration occur only in the mushy region. Figure 5.15 shows that the change in average solute concentration for the equilibrium based model and Figure 5.16 shows the change in average solute concentration for the non-equilibrium based model. In both models variations in the average solute concentration is confined to the mushy region with the maximum value at the solidus front and values in the bulk fluid remaining at their initial values. The values especially in the solid region are lower for the non-equilibrium based model than for the equilibrium based model. This shows greater segregation occurring with the non-equilibrium based model than with the equilibrium based model.

## 5.5 Conclusions

For eutectic or discrete phase change problems accuracy is compromised using the Newton Raphson solution algorithm as a slope has to be introduced into the enthalpy discontinuity making the solution smooth enough for convergence. From the results obtained in Example I it is clear that a more efficient solution algorithm is needed to solve the discrete or eutectic phase problem when using the fixed grid finite element formulation. It is suggested that secant operator be used instead of the Newton Raphson tangent operator for those elements that are experiencing eutectic phase change. This should enable convergence using a steeper and more realistic approximation to the slope of the discontinuity in enthalpy. Therefore using the fixed grid finite element formulation a fine mesh must be used coupled with a more effective solution technique to model the eutectic or discrete phase change accurately. For Example I there is no difference in the results between the local equilibrium based model and the local non-equilibrium based model, the main reason being that most of the phase change takes place

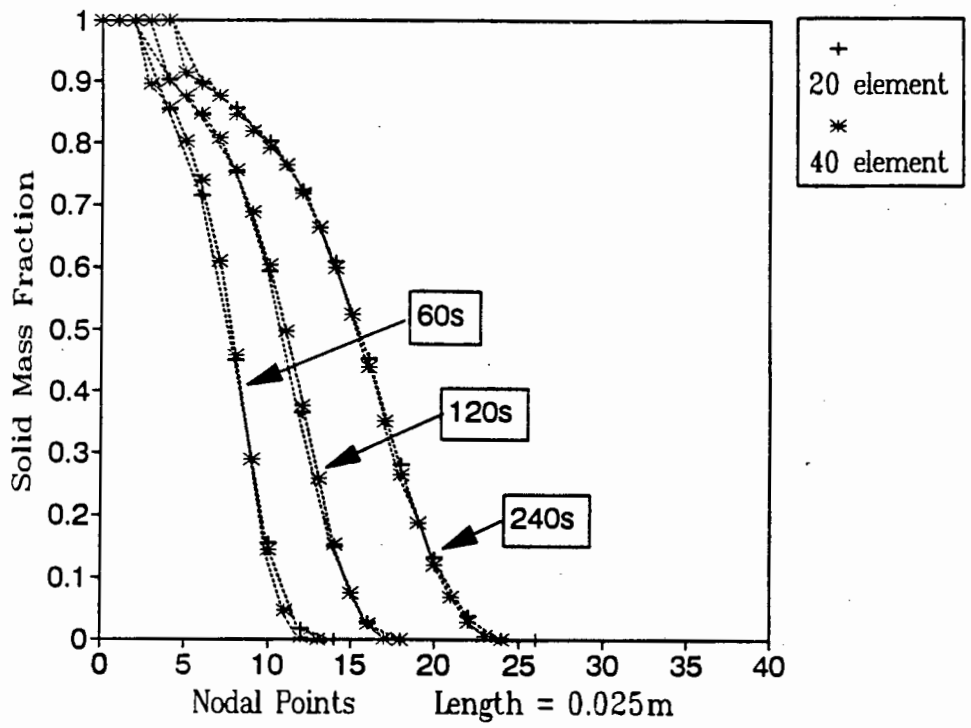


Figure 5.10: Mesh study of the variation in solid mass fraction at t = 60s, t = 120s and t = 240s.

at the eutectic. The results obtained in Example I show trends similar to those obtained by Bennon and Incropera [33] using a local equilibrium based finite difference model, even though some of the thermophysical data is different.

For Example II there is a clear difference in the evolution in mass fraction between the local equilibrium and local non-equilibrium based models. The equilibrium based model solidifies at a higher temperature than the non-equilibrium based model as more solute is rejected into the liquid for the non-equilibrium case lowering the freezing temperature. This results in all the solidification being dendritic for the equilibrium case and approximately 90 % being dendritic, with the remainder being eutectic, for the non-equilibrium case. Even though the maximum change in average solute concentration from $\bar{C}_0$ is of the order of 1%, the variations in $\bar{C}$ for the local non-equilibrium based model were greater than for the local equilibrium based model. Therefore, for Example II, greater segregation occurs when using the local non-equilibrium based model.

For both examples there is clearly little difference between results obtained using the 40 element mesh as opposed to the 20 element mesh except for a more defined approximation at the eutectic. Using enthalpy together with the average solute concentration as the field variables ensured energy conservation in both examples.

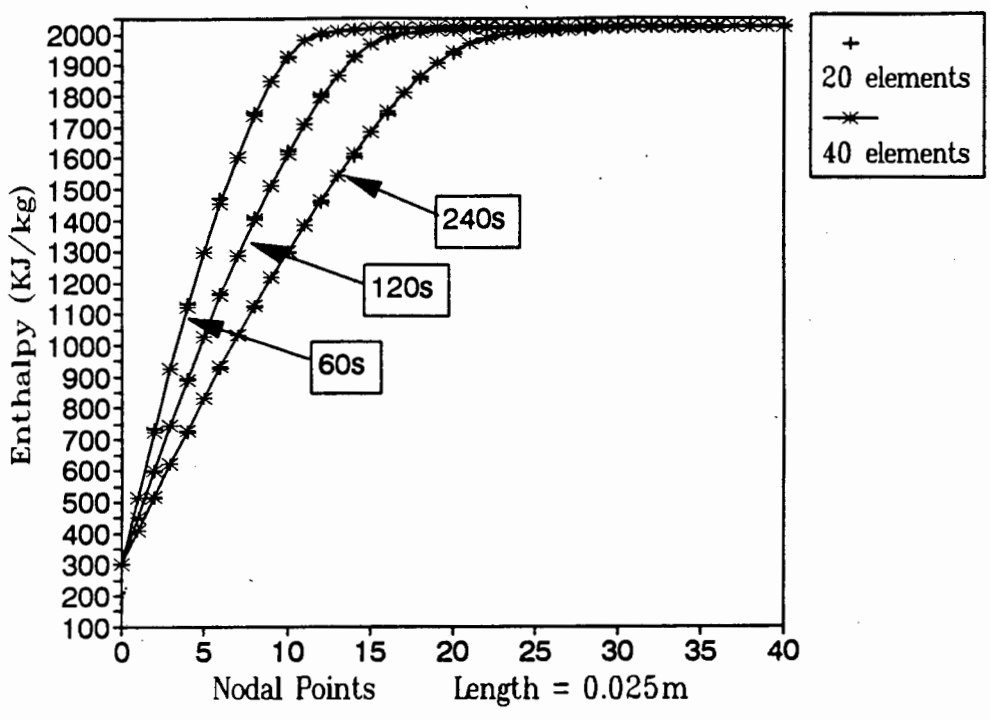


Figure 5.11: Mesh study of the variation in enthalpy at t = 60s, t = 120s and t = 240s.

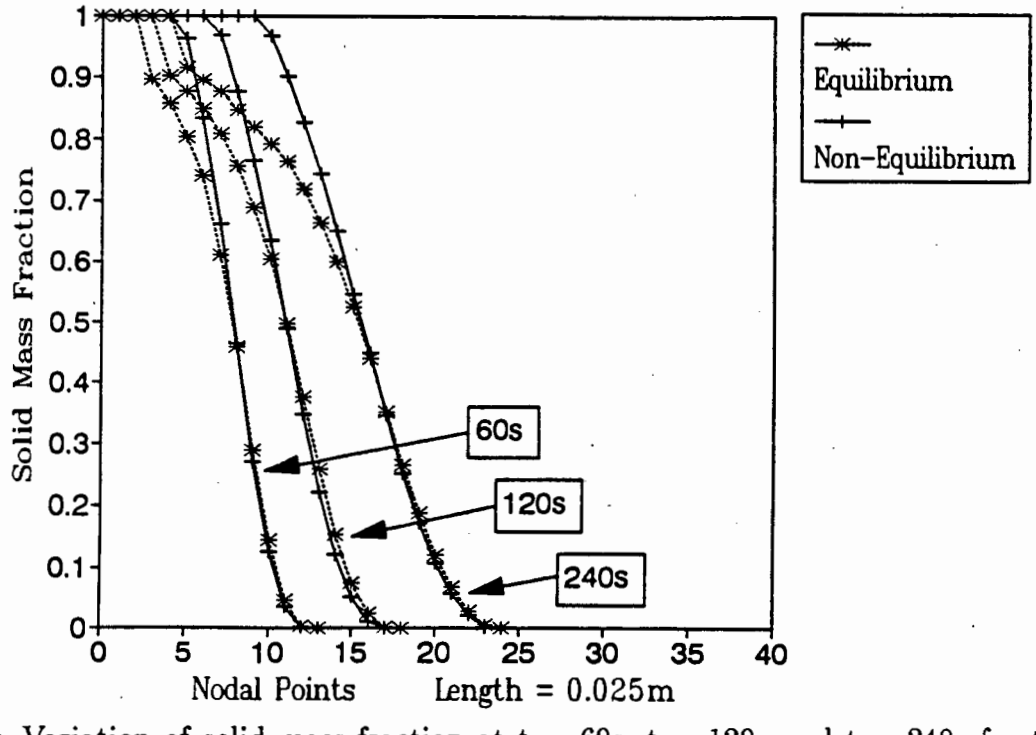


Figure 5.12: Variation of solid mass fraction at t = 60s, t = 120s and t = 240s for the local equilibrium and local non-equilibrium cases.

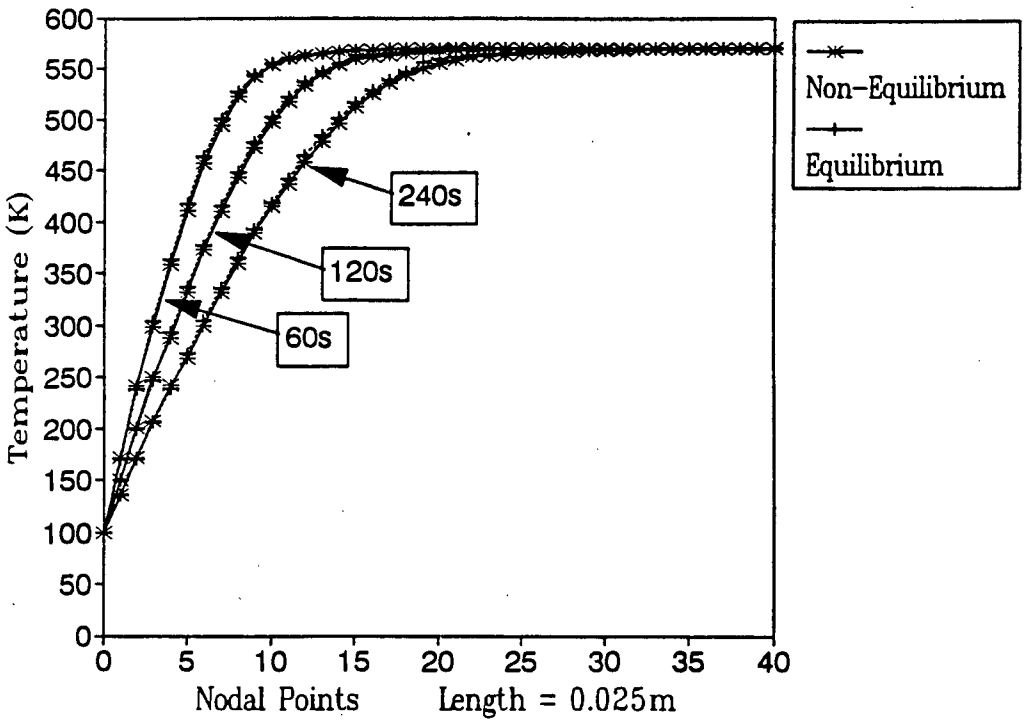


Figure 5.13: Variation in temperature at t = 60s, t = 120s and t = 240s for the local equilibrium and local non-equilibrium cases.

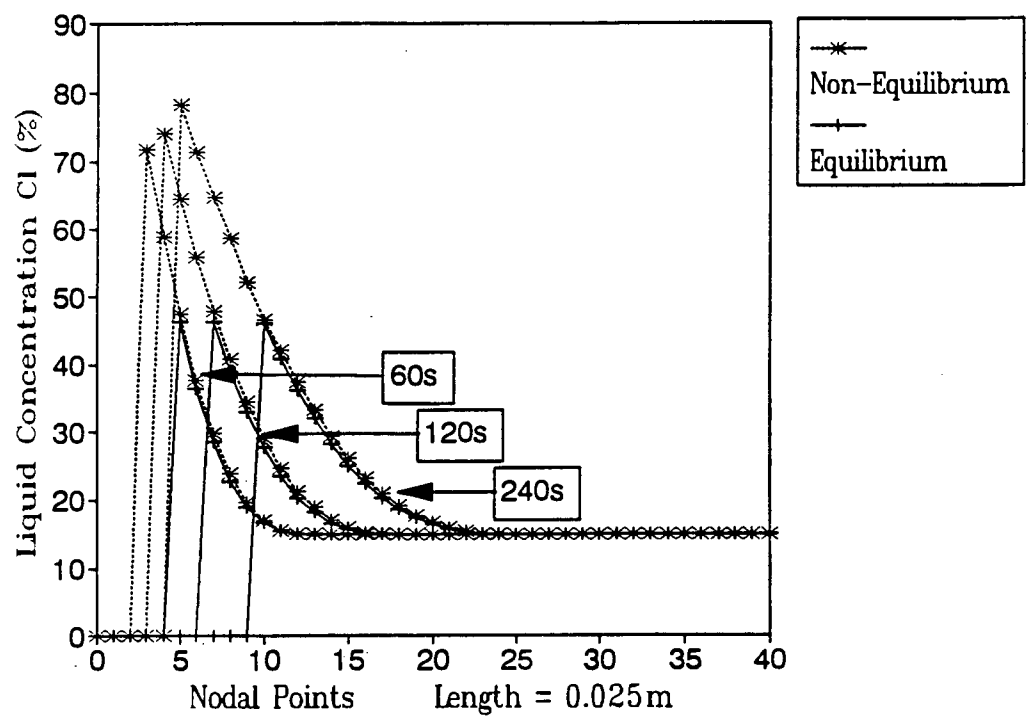


Figure 5.14: Variation in liquid solute concentration at t = 60s, t = 120s and t = 240s.

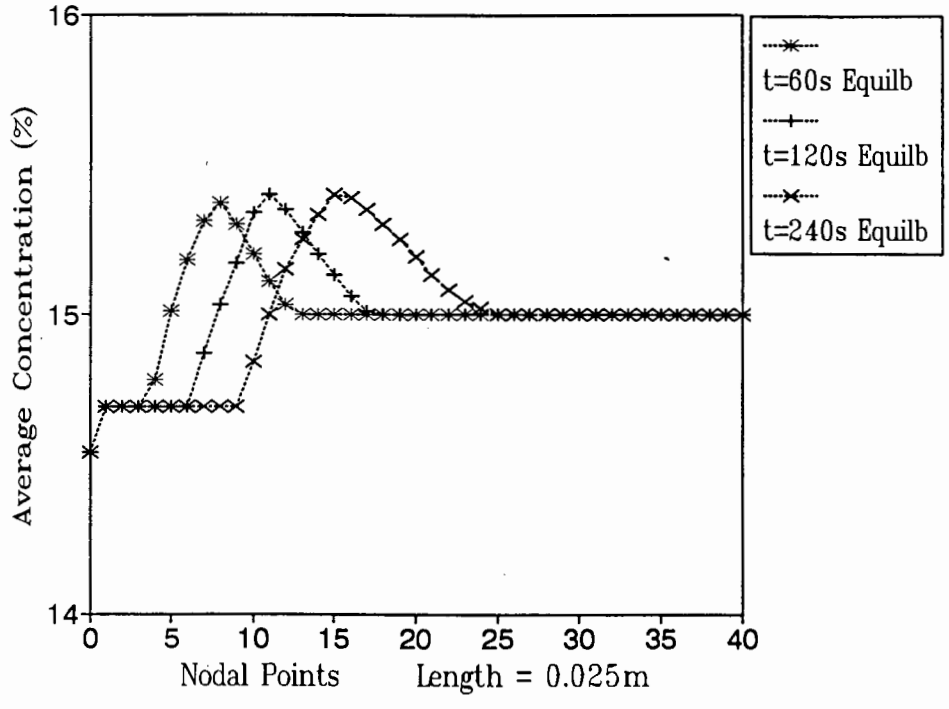


Figure 5.15: Variation in average solute concentration for the equilibrium based model at t= 60s, t = 120s and t = 240s.

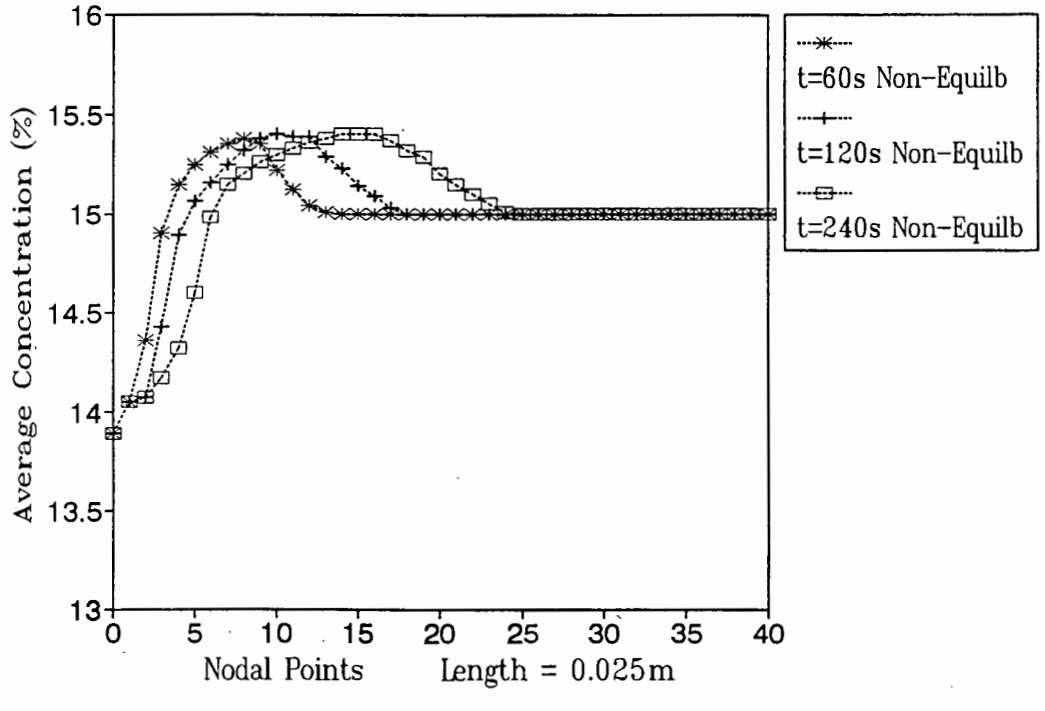


Figure 5.16: Variation in average solute concentration for the non-equilibrium based model at t= 60s, t = 120s and t = 240s.

# CHAPTER 6
# CONCLUSION

Thermodynamically consistent formulations for the solidification and melting of binary alloy systems, based on local non (quasi) - equilibrium and local equilibrium phase change, have been developed. These formulations have been incorporated into a global continuum based description of the solidification/melting process. This led to the formulation of a fixed grid finite element model. The finite element model, based on diffusion dominated binary alloy solidification/melting, has been implemented as a user element into the finite element program ABAQUS [16]. The complete alloy phase change process has been modelled where both dendritic and eutectic phase change are included. Numerical results for both local equilibrium and local non-equilibrium have been described and their effect compared locally and globally.

The local non-equilibrium description, like the local equilibrium description, is cast in terms of pressure, temperature and average solute concentration. This allows the local non-equilibrium formulation to be easily implemented into a global continuum model in a similar fashion to that presented in the literature for the local equilibrium case. The local non-equilibrium description includes the solute profile history which enables remelting of the solid particles to be modelled. Local phase interface equilibrium is assumed for solidification and remelting. For the remelting case, the assumption of Rappaz and Voller [20] is used, where it is assumed that an infinitely thin layer exists in the solid at the phase interface, which exhibits the equilibrium solute value, while the remaining solid retains its previous solute profile. Even though interface equilibrium is assumed for remelting, the new liquid solute concentration is calculated from the previous solid solute profile. A realistic description of the influence of the local solute redistribution on the dendritic solidification and melting processes is therefore provided. The incorporation of this model into the global continuum model thus enables a physically representative finite element model to be developed.

Two solidification examples were analyzed using the diffusion dominated finite element model. The first example was similar to that presented by Bennon and Incropera [33] where the initial solute concentration was close to the eutectic. The results obtained demonstrated similar trends to those obtained in [33] and differences in results for local equilibrium and local non-equilibrium cases were negligible. The second example illustrated the solidification of a binary alloy where the initial solute concentration was low. It was found that the local equilibrium based model experienced complete dendritic solidification, whereas for the model based on local non-equilibrium, solidification occured over a larger temperature range which resulted in a mixture of dendritic and eutectic crystals being formed.

These results illustrate that for near eutectic solidification, differences in the results from models based on the local equilibrium and local non-equilibrium cases are negligible, whereas for dilute solutions there are significant differences in the results from these two cases. Therefore, depending on the initial concentration of the alloy solution, the local solute modelling assumptions do

effect the global behaviour of the finite element model.

From the results obtained for the diffusion dominated solidification of a dilute binary alloy, it is seen that the choice of the local solute redistribution model affects the global segregation of solute. Even though the global solute segregation is small for the presented example, it is clear that when using the local non-equilibrium model the global solute segregation is greater than that obtained with the local equilibrium model. This effect should be significantly increased if interdendritic and bulk convection are included in the formulation. Note that even though fluid convection has been neglected the results presented in this thesis illustrate the importance of the effect of the local non-equilibrium solute redistribution on macro-segregation in the solidified product. It is proposed that in future work, fluid flow should be included in the present finite element formulation and the effect of the local solute redistribution on the global solute segregation be investigated.

When using the fixed grid, enthalpy based, finite element model the discrete eutectic phenomena are smeared over the element. This is in keeping with the continuum based formulation where the phase change phenomena are smeared over the sample element. Even though the discontinuities in enthalpy and solid mass fraction at the eutectic, are smeared over the element, the results obtained are reasonably representative of what occurs in reality. In reality, the common presence of impurities in alloys impede discrete eutectic phase change. Therefore smooth but steep changes in enthalpy and mass fraction, at the eutectic, are considered to be reasonable approximations of what occurs in practice.

The discrete phase change can be modelled accurately by refining the finite element mesh. Unfortunately the model is limited by the use of the Newton-Raphson global solution scheme which cannot cope with large sudden changes in the enthalpy at the eutectic resulting in an inaccurate handling of the eutectic phase change. To enable convergence at the eutectic and therefore a better approximation of the eutectic phase change, it is proposed that a secant approximation of the fully consistent Newton-Raphson Jacobian operator be investigated.

To improve the computational efficiency and speed in modelling the solidification or melting of a binary alloy adaptive mesh refinement methods similar to that developed by Huang and Lewis [39] should be investigated in future work. This should allow a course mesh to be used in the pure phase regions and a very fine mesh in the mushy region, thus enabling accurate predictions of the mushy and discrete phase change phenomena to be efficiently calculated.

# REFERENCES


1. Bennon, W.D. & Incropera, F.P., A continuum model for momentum, heat and species transport in binary solid-liquid phase change systems - 1. Model formulation, *International Journal of Heat Mass Transfer*, **30**, No. 10, 2161-2170, 1987.

2. Loper, D.E. & Roberts, P.H., On the motion of an Iron-Alloy Core Containing a Slurry. I. General Theory, *Geophysics, Astrophysics, Fluid Dynamics*, **9**, 289-321, 1978.

3. Hills, R.N. & Roberts, P.H., On the formulation of diffusive mixture theories for two-phase regions, *Journal of Engineering Mathematics*, **22**, 93-106, 1988.

4. Hills, R.N., Loper, D.E. & Roberts, P.H., A Thermodynamically Consistent Model of a Mushy Zone, *Quarterly Journal of Mechanics & Applied Mathematics*, **36**, Pt. 4, 1983.

5. Lynch, D.R. & Gray, W.G., Finite element simulation of flow in deforming regions, *Journal of Computational Physics*, May, 1980.

6. Lynch, D.,R. & O'Neill,K., Continuously deforming finite elements for the solution of parabolic problems, with and without phase change, *International Journal of Numerical Methods in Engineering*, **17**, 81-96, 1986.

7. Yoo, J. & Rubinsky, B., A finite element method for the study of solidification processes in the presence of natural convection, *Numerical Journal of Numerical Methods in Engineering*, **17**, 81-96, 1981.

8. Yoo, J. & Rubinsky, B., Numerical Computation using Finite Elements for the Moving Interface in Heat Transfer Problems with Phase Transformation, *Numerical Heat Transfer*, **6**, 209-222, 1983.

9. Muller, I.A., A thermodynamic theory of mixtures of fluids, *Archive for Rational Mechanics and Analysis*, **28**, 1-39, 1968.

10. Bowen, R.M., Toward a thermodynamics and mechanics of mixtures, *Archive for Rational Mechanics and Analysis*, **24**, 370-403, 1967.

11. Drumheller, D.S., The theoretical treatment of a porous solid using a mixture theory, *International Journal of Solids and Structures*, **14**, 441-456, 1978.

12. Nunziato, J.W., A multiphase mixture theory fr fluid-particle flows, In *Theory of Dispersed Multiphase Flow*, 191-226, Academic Press, New York, 1983.

13. Green, A.E. & Naghdi, P.M., A Theory of Mixtures, *Archive for Rational Mechanics and Analysis*, **24**, 243-263, 1967.

14. Burchardt, M.D. & Bowley, W.W., Sublimation in a porous continuum developed from non-equilibrium thermodynamics, *Journal of Heat Transfer*, **96**, 319-323, 1974.

15. Prandtl, V.C. & Dawson, P.R., Application of mixture theory to continuous casting, In *Transport Phenomenon in Materials Processing*, (Editors Chen, M.M, Mazumder, J. & Tucker, T.C.1), ASME HTD, **29**, 47-54, 1983

16. Hibbit, Karlson and Sorenson, Inc., ABAQUS Users Manual, Version 4.9, Providence, Rhode Island, USA.

17. Loper, D.E. & Roberts, P.H., On the motion of an Iron-Alloy Core Containing a Slurry. II A Simple Model, *Geophysics, Astrophysics, Fluid Dynamics*, **16**, 83-127, 1980.

18. Voller, V.R., Brent, A.D. & Prakash, C., The modelling of heat, mass and solute transport in solidification systems, *International Journal of Heat Mass Transfer*, **32**, No. 9, 1719-1731, 1989.

19. Bennon, W.D. & Incropera, F.P., A continuum model for momentum, heat and species transport in binary solid-liquid phase change systems - II. Application to solidification in a rectangular cavity, *International Journal of Heat Mass Transfer*, **30**, No. 10, 2171-2187, 1987.

20. Rappaz, M. & Voller, V., Modelling of Micro-Macrosegregation in Solidification Processes, *Metallurgical Transactions A*, **21A**, 749-753, 1990.

21. Hills, R.N. & Roberts, P.H., A generalized Schiel-Pfann equation for a dynamical theory of a mushy zone, *International Journal of Non-Linear Mechanics*, **23**, No. 4, 327-339, 1988.

22. Rao, Y.K., Stoichiometry and Thermodynamics of Metallurgical Processes, Cambridge University Press, Cambridge, 1985.

23. Thomas, D.R., PhD Thesis, *University of Witwatersrand*, Johannesburg, RSA., 1987.

24. Smithells, C.J., Metals Reference Book, *4th Ed.*, Butterworths, London, **1,2,3**, 1978.

25. Gray, W.G., A derivation of the equations for multiphase transport, *Chemical Engineering Science*, **30**, 229-233, 1975.

26. Gray, W.G. & O'Neil, K., On the general equations for flow in porous media and their reduction to Darcy's law, *Water Resources Research*, **12**, 148-154, 1976.

27. Gray, W.G., General conservation equations for multiphase systems: 4. Constitutive theory including phase change, *Advances in Water Resources*, **6**, 130-140, 1983.

28. Beckerman, C. & Viskanta, R., Double-diffusive convection during dendritic solidification of a binary mixture, *Physico Chemical Hydrodynamics*, **10**, 195-213, 1988.

29. Landau, L.D. & Lifshitz, E.M., Fluid Mechanics, *Volume 6 of Course of Theoretical Physics*, Pergamon Press, Oxford, 1959.

30. Hills, R.N. & Roberts, P.H., On the use of Fick's law in regions of mixed phase, *International Communications in Heat and Mass Transfer*, **15**, 113-119, 1988.

31. Prescott, P.J., Incropera, F.P. & Bennon, W.D., Modeling of dendritic solidification systems: reassessment of the continuum momentum equation, *International Journal of Heat and Mass Transfer*, **34**, No. 9, 2351-2359, 1991.

32. Ganesan, S. & Poirier, D.R., Conservation of mass and momentum for the flow of interdendritic Liquid during solidification, *Metallurgical Transactions B*, **21B**, 173-181, 1990.

33. Bennon, W.D. & Incropera, F.P., Numerical analysis of binary solid-liquid phase change using a continuum model, *Numerical Heat Transfer*, **13**, 277-296, 1988.

34. Prakash, C.& Voller, V., On the numerical solution of continuum mixture model equations describing binary solid-liquid phase change, *Numerical Heat Transfer*, **15**, Part B, 171-189, 1989.

35. Poirier, D.R., Permeability for flow of interdendritic liquid in columnar-dendritic alloys, *Metallurgical Transactions B*, **18B**, 245-255, 1987.

36. Kececioglu, I. & Rubinsky, B., A Continuum model for the propagation of discrete phase-change fronts in porous media in the presence of coupled heat flow, fluid flow and species transport processes, *International Journal of Heat and Mass Transfer*, **32**, 1111-1130, 1989.

37. Bonnerot, R. & Jamet, P., Numerical computation of the free boundary for the two dimension Stefan problem by space time finite elements, *Journal of Computational Physics*, **25**, 163-181, 1977.

38. Lewis, R.W., Huang, H.C., Usmani A.,S. & Tadayon M.R., Solidification in castings by the finite element method, *Internal report*, Institute for Numerical Methods in Engineering, University of Wales, University College of Swansea.

39. Huang, H.C., & Lewis, R.W., Adaptive analysis for heat flow problems using error estimation techniques *Internal report* , Institute for Numerical Methods in Engineering, University of Wales, University College of Swansea, **CR/635/89**, 1989.

40. Thevoz, Ph., Rappaz, M. & Desbiolles, J.-L., 3-MOS: A general FEM code for the prediction of microstructures in castings, *1990 TMS-AIME Conference Proceedings, Anaheim, California*, 1990.

41. Rappaz, M., Modelling of microstructure formation in solidification processes, *International Materials Reviews*, **34**, No. 3, 93-123, 1989.

42. Lewis, R.,W. & Roberts, P., Finite element simulation of solidification problems, *Applied Scientific Research*, **44**, 61-92, 1987.

43. Samonds, M., Morgan, K, & Lewis, R.,W., Finite element modelling of solidification in sand castings employing an implicit-explicit algorithm, *Applied Mathematical Modelling*, **9**, 170-174, 1985.

44. Comini, G., Del Guidice, S., Lewis, R.,W. & Zienkiewicz, O.C., Finite element solution of non-linear heat conduction problems with special reference to phase change, *International Journal for Numerical Methods in Engineering*, **8**, 613-624, 1974.

45. Morgan, K., Lewis, R.,W. & Zienkiewicz, O.C., An improved algorithm for heat conduction problems with phase change, *International Journal for Numerical Methods in Engineering*, **13**, 1191-1195, 1978.

46. Morgan, K., A numerical analysis of freezing and melting with convection, *Computer Methods in Applied Mechanics and Engineering*, **28**, 275-284, 1981.

47. Carslaw, H.S. & Jaeger, J.C., Conduction of Heat in Solids, Oxford University Press, Oxford, 1959.

48. Hughes, T.J.R., The Finite Element Method: Linear Static and Dynamic Finite Element Analysis, Prentice-Hall, New Jersey, 1987.

49. Mitchell, A.R. & Wait, R., The Finite Element Method in Partial Differential Equations, Wiley, New York, 1977.

50. Strang, G.& Fix, G.J., Analysis of the Finite Element Method, Prentice-Hall, New Jersey, 1973.

51. Hughes, T.J.R.& Pister, K.S., Consistent Linearization in mechanics of Solids, *Computers and Structures*, **8**, 391-397, 1978.

52. Minkowycz, W.J., Sparrow, E.M., Schneider, G.E. & Pletcher, R.H., Handbook of Numerical Heat Transfer, John Wiley & Sons, INC., New York, 1988.